ROBOTIC PEG-HOLE INSERTION OPERATION ANALYSIS

HONG QIAO Ph.D

ROBOTIC PEG-HOLE INSERTION OPERATION ANALYSIS

HONG QIAO, B.Sc, M.Sc, M.Phil

Department of Mechanical and Manufacturing Engineering

School of Mechanical Engineering

A thesis submitted in partial fulfilment

of the requirements of De Montfort University

for the degree of Doctor of Philosophy

April, 1994

De Montfort University

ACKNOWLEDGEMENTS

I am deeply indebted to my supervisors Professor R. M. Parkin and Professor J. A. G. Knight for their guidance, support and encouragement. Thanks for giving me so much.

Special thanks to Mr. B. S. Dalay for his guidance, cooperation and great understanding. It would have been difficult to complete the work without his help. Thanks for helping me so much.

Thanks to all the friends and scientists who made this work possible. Thanks for believing in me.

Finally, I would like to thank my family ZouLiang Qiao, ZheNan Xiong and Bo Zhang, for all the love they gave me.

ABSTRACT

Assembly operation plays an important role in the industry due to the fact that:-

(a) it accounts for a substantial proportion of production cycle time and,

(b) it requires high precision.

Recently, the replacement of the human function in assembly operation by robots has been considered, since:-

(a) it is difficult for human being to perform high precision and high speed assembly operation,

(b) the cost of human labour is increasing rapidly,

(c) due to the automation of other production steps, reliable and automated assembly operation is necessary and,

(d) people need to be librated from this repetitive work.

Because of the above, research into precise and fast robotic assembly operations is becoming an important subject. Furthermore the peg-hole insertion operation, which is the widest used simplified industrial application model, has special prominence. The basic research includes hardware design, control method, geometric analysis and strategy analysis. In terms of the hardware, various complex six-component force sensors, passive compliance and vibration systems have been designed for this purpose. In the control area, a disturbance filter and real-time control have been applied to the system to enhance performance. Techniques using geometric concepts such as pre-images and back-projections, models of contact configurations, pattern recognition and fine motion analysis have been studied. Based on this research, the assembly operation can be achieved with a clearance varying from 0.01 mm to 0.5 mm. The operational time is 2 seconds to 5 seconds.

The remaining basic problems are:-

(a) whether it is reliable to achieve the assembly operation with the current hardware design such as force sensors or RCC (Remote Centre Compliance) and,

(b) whether there is any possibility to simplify the hardware design.

In this thesis, an important problem of interpretation of the contact configuration between the peg and the hole is presented. It is pointed out that it is difficult to use the signals from the force sensors to present the positional relationship between the peg and the hole and to guide the adjustment of the system. One set of the signals from the force sensor can present various positional relationships between the peg and the hole. It can be concluded from this that the assembly operation with a force sensor is not always possible. It is also found that, if the peg is in a certain area, information can be obtained from the signals of the force sensor which can probably be used to achieve one step adjustment. Based on this analysis, a strategy to perform a precise assembly operation, with the ambiguity of the contact configuration through the force sensors, is provided. Furthermore it is found that it is possible to achieve the assembly operation without force sensors or RCC. As a conclusion, the general principles to investigate the strategies are provided. To prove the reliability of the strategies, a simulation of the assembly operation is also presented. The focus of this thesis is the presentation of a strategy for reliable, fast and precise robotic peg-hole insertion operation. The experiments using UMI-RTX robot are carried out with the clearance of 0.02 mm and the operational time of 2.5 seconds.

CONTENTS

NOTATION

The notation in this thesis can be divided into five sections, see Fig. I and Fig. II:

(a) **The basic parameters of the system:** for example, the dimensions of the peg and hole, the mass and inertia of the peg, etc. These should be prior knowledge.

(b) **The designed parameters:** the input forces (including torques) to the peg and their duration for every step. These should be designed according to the known basic parameters (a).

(c) **The parameters for the movement of the peg:** the velocities and accelerations of the peg during each step.

(d) **The parameters for the contact forces and errors between the peg and hole:** the parameters which indicate the state of the process. In this paper, they can be predicated and analyzed according the first two types of parameters.

(e) **The parameters for the equations concerning about the pre-images.**

For the sake of distinguishing, in what follows, letters with a subscript "*h*" and "*p*" refer to as the parameters measured in the coordinate system of the hole and peg respectively. Letters with a subscript "*hw*" and "*pw*" refer to the parameters along the "W_h"-axis and "W_p"-axis, respectively, where $w=x, y, z$ and $W=X, Y, Z$. Letters with a subscript "*i*" (i= 1, 2, 3, 4, 5, 6) refer to parameters at the *ith* event for the peg-hole insertion process. Letters with the subscript "*n*" and "*m*" refer to their minimum and maximum values, respectively. The definitions for the letters can be divided into:

Definitions for the basic parameters of the system:

$O_hX_hY_hZ_h$ is the frame fixed with the hole, where O_h is defined as the centre of the upper surface of the hole, O_hY_h is defined as the line from O_h to the base of the robot, O_hZ_h is along the axis of the hole upwards, and

O_hX_h is perpendicular to O_hY_h and O_hZ_h,

$O_pX_pY_pZ_p$ is the frame fixed with the peg, where O_p is the centre of the end-surface of the peg, O_pY_p is parallel to the projection of the O_hY_h on the end surface of the peg, O_pZ_p is along the axis of the peg upwards, and O_pX_p is perpendicular to O_pY_p and O_pZ_p,

$O_{pp}X_{pp}Y_{pp}Z_{pp}$ is the frame formed by the rotation of $O_pX_pY_pZ_p$ around Z_p axis with angle $arctan(\theta_{hy}/\theta_{hx})$,

$O_{hp}X_{hp}Y_{hp}Z_{hp}$ is the frame formed by the rotation of $O_hX_hY_hZ_h$ around Z_h axis with angle $arctan(\theta_{hy}/\theta_{hx})$

R_p is the radius of the peg (mm),

R_h is the radius of the hole (mm),

L_g is the length of the peg (mm),

m is the mass of the peg (Kg),

I is the inertia of the peg ($Kg.m^2$),

c_p is the centre of the peg,

μ is the frictional coefficient,

θ_1 is the angle between force sensor system and the system according to the locations of the strain gauges in tube-design force sensor (rad),

e_i ith output from the force sensors,

Definitions for the designed parameters:

t is the specified time (s),

F is the force acting on the peg (N),

M is the torque acting on the peg (Nm),

B is a damping matrix,

Definitions for the Movement of the Peg:

w is the rotational velocity of the peg (*rad/s*),

v is the velocity of the centre of the mass of the peg (*m/s*),

a is the acceleration of the centre of the mass of the peg (m/s^2),

ΔX_2 is the translational movement along the X_h axis during the first step (*m*),

ΔY_2 is the translational movement along the Y_h axis during the first step (*m*),

$\Delta \theta_{hx2}$ is the rotational movement around the X_h axis during the first step (*rad*),

Y_0 is the translational movement along the Y_h axis caused by the rotation around the X_h axis (*m*),

s_i is a node in state space, $s_i = (P, C, I, Q)$, where P is the position of the peg in the configuration space, C is a set of contact points, S is a set of potential motion, I is qualitative signal based on the associated physical situations, and Q is a heuristic assessment of the "quality" of the conatct situations,

Definitions for the Contact States and Errors Between the Peg and Hole:

θ is the angle between the axes of the peg and the hole which can be considered as a vector whose direction is defined by the right hand law (*rad*),

θ_{hx}, θ_{hy} are the projections of vector θ along X_h and Y_h axes, respectively. These are in the $Y_hO_hZ_h$ and $X_hO_hZ_h$ planes, respectively (*rad*),(*rad*),

(O_hO_p) is the directed line segment from O_h to O_p (*m*),

U is the directed line segment from the axis Z_h axis to the centre of the

upper surface of the peg (m),

ε is the constant used to define the ranges of $(O_hO_p)_{hx}$ and $(O_hO_p)_{hy}$ (m),

θ_{h1} is the constant used to define the ranges of θ_{hx1} and θ_{hy1} (rad),

K_1 is the value used to define the ranges of U_{hx1} and U_{hy1},

F_c is the contact force acting on the peg (N),

cc is the centre of contact points,

co is the centre of overlap of the contact surfaces,

C is contact point when there is one contact point between the peg and hole,

C_1, C_2 are two contact points respectively when there are two contact points between the peg and hole,

G is the projection of the lowest point of the end-surface of the peg on the $X_hO_hY_h$ plane,

α is the angle between the X_h axis and the projection of O_hO_p on the $X_hO_hY_h$ plane (rad),

α_1 is the angle between the X_h axis and O_hC_1 (rad),

α_2 is the angle between the X_h axis and O_hC_2 (rad),

z_{d5} is the distance between the side-surface contact point to end-surface of the peg (mm),

ϕ_1 is the angle between the Y_h axis and the projection of O_hO_p on the $X_hO_hY_h$ plane (rad),

β_{m1} is the angle between projection of O_hO_p on the $X_hO_hY_h$ plane and O_hC_1 (rad)

A is the point whose projection is on the overlap between the projections of the contact surfaces,

α_a is the angle between the projection of vector θ on the $X_hO_hY_h$ plane and θ_{hx} (*rad*),

θ_{min} is the maximum θ for the insertion (*rad*),

$f_1(\beta)$ is the distance between O_h and C (m),

β, β_1, β_2 are the angles in triangle O_hO_pC (*rad*),

β_m, β_n are the angles from O_hO_p to O_hC_1 and O_hC_2, respectively (*rad*),

O are the contact forces and the direction of their sum is $\otimes$ or $\odot$ (*rad*),

-O- are the contact forces and the direction of their sum is one of following cases: $\leftarrow\otimes$, $\otimes\rightarrow$, $\leftarrow\odot$, $\odot\rightarrow$ (N),

l is the distance between O_h and any point in the sectioned area (m),

S is the area of the overlap of the end-surface of the peg and the area surrounding the hole (m^2),

e_i is the output from the one of eight groups of the strain gauges of the sensor,

pp is the coefficient between the maximum angle between the axes of the peg and the hole in the initial state and the rotational angle in the first step,

Parameters in the equations concerning the pre-images:

| is the connection between a variable and its description,

ϵ is the description of the relationship between an element and a subset which the element belongs to,

$\forall$ is a symbol which denotes "arbitrary",

$P_b(a)$ is the pre-image of goal a related to set b,

$P_{b,c}(a)$ is the pre-image of goal a related to a set b and nominal velocity v_c^*,

$P_b(a)$ is the back-projection of goal a related to set b,

$P_{b,c}(a)$ is the back-projection of goal a related to a set b and nominal velocity v_c^*,

$F_b(a)$ is the forward projection of a with commanded velocity v_b^*,

E is used to denote the polyhedral environment,

$T_p(t)$ is the trajectory of the moving object versus time t,

$T_v(t)$ is the velocity of the moving object versus time t,

T is the vector including $T_p(t)$ and $T_v(t)$, and $T = [T_p(t)^T, T_v(t)^T]$,

τ is the set of all the possible vectors T,

πX is the projection of vector X on the positional space,

G is the goal of whole procedure operation,

$P^*_\theta(G)$ is the weak pre-image which is the set of points which could possibly enter the goal recognizably, given sensing and control event,

H_0 is the set difference of the forward projection minus the weak pre-image,

H_s are all regions where sticking is possible in the weak minus strong pre-images,

$Z(H_s)$ is the zero velocity over H_s,

H is the error detect and recovery range,

G_i is the sub-goal with i steps to G,

R_i is the pre-image of G_{i-1},

t_i is the time for the end of the ith step in the procedure.

$v_{\theta,1}^*$ is the commanded velocity to achieve G from G_1,

$v_{\theta,i+1}^*$ is the commanded velocity to achieve G_i from G_{i+1},

α_{hpzm} is the angle between the contact force and m axis in $Z_{hp}O_{hp}M_{hp}$ plane,

where $m = x$ *or* y, and $M = X$ *or* Y,

Δx is the displacement of the variable x,

x^* is the nominal value of x,

c_i is the ith contact point which the peg-hole system obtains between the bottom of the peg and the upper-surface of the hole,

sc_i is the ith side-surface which the peg-hole system obtains on the side-surfaces of the peg and hole

f_c is the frictional force on the peg from the hole,

F_c is the contact force acting on the peg,

θ_1 is the angle between the commanded velocity $v_{\theta 1}$ and X_h axis,

θ_i is the angle between the commanded velocity $v_{\theta i}$ and X_h axis,

S_1 is the set including all the commanded velocities $v_{\theta 1}$ to achieve G from G_1,

S_i is the set including all the commanded velocities $v_{\theta i}$ to achieve G_{i-1} from G_i,

X^* is the nominal value of variable X,

X^T is the transpose of the vector X,

F_s^* are force sensor signals and $F_s^* = [F_x^*, F_y^*, F_z^*, M_x^*, M_y^*, M_z^*]^T$,

p is actual position,

$B_{ep}(p)$ is the positional uncertainty ball with p as the centre of the ball,

n is an integer that a sequence of n motions can be found such that each motion terminates by the utilization of the environment or the force signals, and the final motion terminates in the goal,

j_a is the unitary vector j along the Y_a axis in the a coordinate system,

i_a is the unitary vector i along the X_a axis in the a coordinate system.

$\angle a_b$ is an unitary vector which is along the projection of the vector a on the plane b,

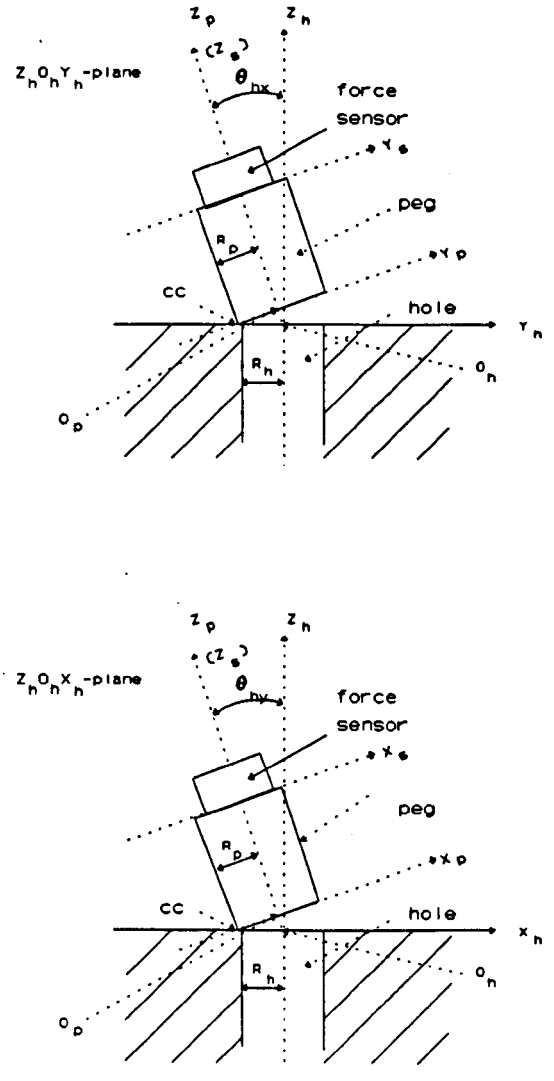

Fig. I General Peg-hole configuration

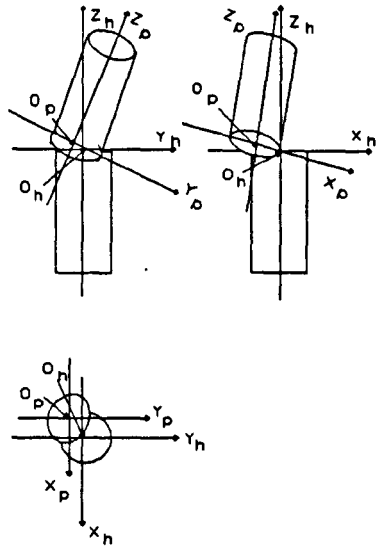

Fig. II The frames $O_hX_hY_hZ_h$ and $O_pX_pY_pZ_p$

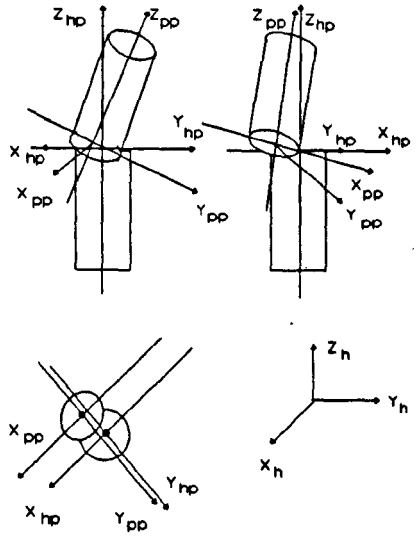

Fig. IV The frames $O_{hp}X_{hp}Y_{hp}Z_{hp}$ and $O_{pp}X_{pp}Y_{pp}Z_{pp}$

LIST OF TABLES

LIST OF FIGURES

CHAPTER 1 INTRODUCTION

1.0 Introduction

Robots play an important role and are widely used in industry. They can be used to replace people in dangerous or hard environments and to liberate people from repetitive work. From an industrial point of view, robots can also be used to increase production quality, reduce operation time, make a process reliable and reduce manufacturing prices. However in most cases, it is difficult to achieve all of these demands in one go.

For example, it is common to think that the use of robots reduces the number of jobs for people. However to liberate people from hard physical and mental work is one of the purposes of science and technology and is one important sign of the development of a society. As science and technology develop, the labour prices increase allowing people to have more freedom in life and spend more time on research and less time on essential work. Since the use of human labour in dangerous areas such as nuclear power plants is immoral and the use of human labour in the repetitive situations in the long run brings a lowering of morale, the use of robots is a vital part of the society's development and is widely accepted.

The high precision provided through the use of robots instead of humans is widely acknowledged and warmly welcomed. In most cases, a new technology like robotics which provides lower operation times, high quality and high reliability leads to high costs to begin with. To achieve a wider application, it is necessary to reduce costs to a range which can be accepted by industry.

In almost all manufacturing processes, the assembly is an essential step and also one of the most difficult. Manual assembly operation increases the operation time, reduces the reliability and prohibits the process of automation. So machinery or robotic assembly operation research is widely needed. The robotic peg-hole insertion

operation is the most widely used assembly operation model and heavily researched. If a precise peg-hole insertion operation can be achieved through cheap robots, many practical assembly problems can be solved.

Robotic assembly can provide high reliability and high precision in the manufacturibng process and liberate people from repetitive and sometimes dangerous work.

In this chapter, the following problems are addressed:-

(a) what is the purpose of robotic peg-hole insertion?

(b) what are the basic current research directions?

(c) what is the extent of this research?

(d) what is the contribution of this thesis?

The applications of assembly operation in life and industry is described in Section 1.1. The basic research directions including hardware design, control input design, geometrical analysis and strategy investigation through pre-image and back-projection concepts are studied in Section 1.2. The current extent of major research areas are presented in Section 1.3. The organization of this thesis is shown in Section 1.4.

1.1 Application and motivation

So far the most advanced level of robotic assembly operates with clearance of 0.02-0.06 mm, while the accuracy of the end-effector of the robot is about 0.2-0.4 mm. Some people are trying to increase the accuracy of the robot to achieve this more precise assembly operation, but at the same time, the price is also increased. Basically, the objective is to achieve high accuracy assembly operations with limited cost increase.

The importance of this project can be seen in several ways. Firstly, from the logical

point of view, it can be found that almost everything is a unit which needs to be assembled by bringing different pieces together. For example, tables, chairs, indeed any items which are not single parts. If a worker is manufacturing a table, he manufactures pieces which can be used to be assembled into a table rather than making a table in one go. So assembly operations are an essential step for industrial processes.

In industry worldwide plenty of assembly robots are used. There are 16 thousand robots in Japan, and 8 thousand robots in America (1-4). These robots are widely used. In Japan, there are some associations from which companies can rent very expensive assembly robots. In America, IBM, for example, has used assembly robots to replace people and obtain 100 percent success in the quality requirements.

In research the robotic peg-hole insertion operation is very interesting and challenging. It is considered as the most difficult robotic task due to its high requirement on accuracy. MIT takes the leading role in the world (1-4).

1.2 Research issues

The current research can be divided into four parts:-

(a) The basic research is about hardware design. Assuming there is a person who is trying to insert a key into a lock:-

   (i) Firstly he would determine the neighbourhood of the lock,

   (ii) Secondly he would move the key to touch the neighbourhood of the lock, and

   (iii) Thirdly he would sense the forces acting on his hand rather than bending over to stare at the lock, and adjust the state of the key to achieve the insertion according to the force signals.

At the same time, it can be found that no one would insert the key with a stiff wrist. People relax the wrist in the insertion procedure. So the hardware design includes two parts: the force sensor design and flexible wrist design, a typical design is Remote Centre Compliance. The problem in using a force sensor is that it is too expensive and easily damaged. The problem of the usage of RCC is that it can not be controlled like a human, and it decreases the accuracy of the end-effector of the robot. It would look like a weak person with a shaky hand.

(b) In practice, people can open the door just by randomly moving the key (Fig. 1). So vibration can be considered as one method in the assembly operation. People in the control area are studying the best vibration trajectories and frequencies.

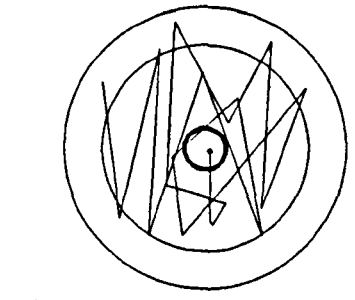

Fig. 1 A trajectory of a key in the approach operation

(c) The symbolic presentation of the contact parts and the contact configuration have been obtained and can be used to efficiently present the system.

(d) In strategy investigation, concepts such as pre-images and back-projections have been provided (Fig. 2).

How to structure the pre-images which eventually include the initial area is a very complex problem.

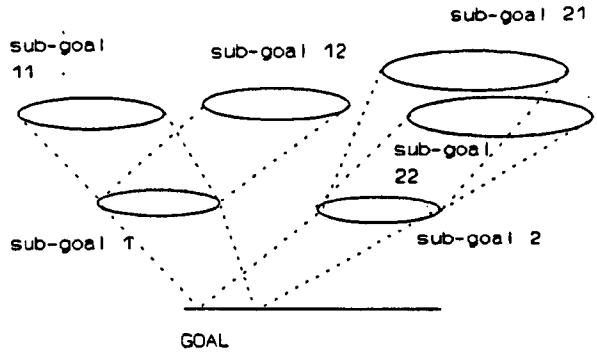

Fig. 2 Basic idea for the pre-image concept

1.3 Review of previous work

During the last twenty years, a great deal of attention has been focused on robotic peg-hole insertion (**1-4**). Recently, there are four major research parts:-

(a) passive accommodation used in the robotic peg hole insertion operation (**5-23**)

  (i) compliant wrist and work station (**5-14**)

  (ii) vibratory motion (**15-19**)

  (iii) air and gas steam (**20-21**)

  (iv) magnetic force (**22-23**)

(b) active accommodation used in the robotic peg-hole insertion operation (**24-54**)

  (i) position feedback based upon force information (**24-47**),

  (ii) learning control algorithm (**48-52**), and

  (iii) a nullifying strategy (**53-54**)

(c) Contact dynamics analysis (**55-67**)

  (i) The generalized damper models with sliding (**55-59**)

  (ii) Friction (**60-61**)

  (iii) Compliant Motion (**62-67**)

(d) Fine motion strategies (**68-100**)

(i) Pre-images (**68**)

(ii) back-projection and forward-projection (**69**)

(iii) error-recovery-detection (**70**)

(iv) sensorless (**71-75**)

1.3.1 Passive accommodation used in the robotic peg hole insertion operation (5-23)

A number of methods have been developed using the passive accommodation concept. These can be divided into the four different categories (**1**):

(a) Compliance method (**5-14**)

A degree of compliance can be put into the assembly system which deforms under the influence of the assembly forces, thus reducing the misalignment (**30**). Early devices developed to assist the alignment of components used 'floating heads'. Several authors (**2, 3, 5, 9, 10** and **12**) at the Carles Stark Draper Labs (USA) have proposed the utilization of passive compliance in parts mating applications. They used the peg-in-hole operation to model a typical assembly task and advocated the use of chamfers to reduce the accuracy required to position a peg over a hole. This work led to the development of a device called the Remote Centre of Compliance (RCC), which was the first commercially available and most successful passive device for peg-into-hole type assembly operation.

The RCC strategy can be summarised schematically as in Fig. 3:

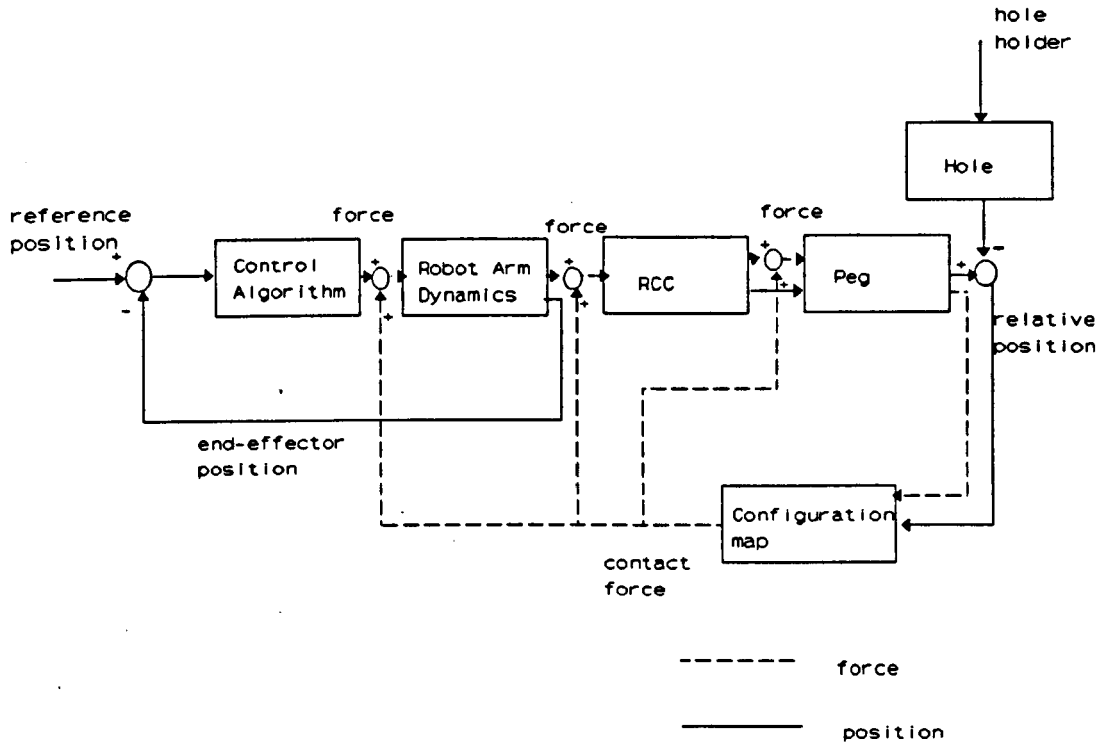

Fig. 3 The block diagram of assembly system using Remote Centre Compliance (RCC)

However, the use of RCC can cause some problems (**1, 20**):

(a) RCC would cause vibration of the peg,

(b) RCC would cause large displacements to be generated by a small force,

(c) Permitted initial position error of the peg would be restricted by the width of the chamfer,

(d) The robot must produce great power to press the peg into the hole,

(e) RCC would cause some uncertainty in the positioning of the peg and

(f) The approaches using RCC do not consider the effects of uncertainty on the resulting assembly strategies.

The assembly of the chamfered peg-hole has been performed using an RCC device, most successfully when the peg is in, or partly in, the hole (48). When the peg approaches the chamfer of the hole, the contact forces make RCC provide the

necessary displacement and rotation of the peg for insertion. In this case, RCC can be regarded as a mechanically executed mapping which transfers the force/moments signals to the desired motion.

(b) Vibratory motion method (15-19)

The idea of utilizing vibratory equipment to absorb the positional error between the peg and hole, by giving one of them a planar random movement, has been exploited. Since the robot holding the peg has limited sensing ability, the direction of the vibration cannot be prior knowledge. Correct insertion is thus difficult to obtain in a short process time (1).

1.3.2 Active accommodation used in the robotic peg-hole insertion operation (24-54)

The sensors most often used for this accommodation include visual sensors, force or torque sensors and proximity sensors (1 and 35). The typical hardware used in the robotic insertion system includes HI-T-HAND EXPERT robot (26, 27 and 28), programmable force controlled wrist and active sensory table.

Along with the hardware developments a variety of insertion strategies have been proposed. These include position feedback based upon force information (24-47), learning control algorithm (48-52), and a nullifying strategy (53-54).

Among all the software methods, position feedback based upon force information is the most popular. In this field, only a few methods have been successfully applied. The technique block diagram can be summarised as Fig. 4:

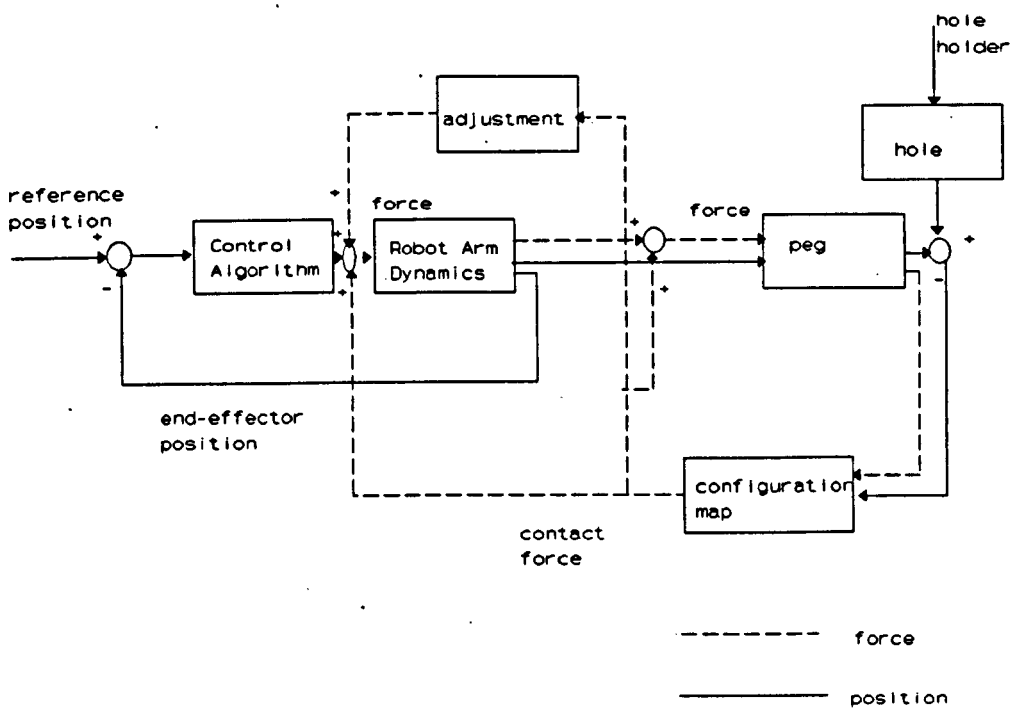

Fig. 4 The block diagram of assembly system using a force sensor

This method also has some constraints (1):

(a) The hardware is very expensive.

(b) It takes a long time to collect the data.

(c) The measurement devices are easily damaged.

(d) It is difficult to achieve fine position control due to the high inertia of the robot.

1.3.3 Contact dynamics analysis (55-67)

The basic study includes generalized dampers (55), compliance and force hybrid control (56 and 57) and stiffness control (58 and 59). The complete exploration is proposed (66).

(a) The generalized damper models with sliding:(55-59) The generalized damper, proposed by Whitney (55), is the model of sliding motion:

$$F = B(v - v^*) \quad (1)$$

where:-

F: is the vector of forces and torques acting on the moving object relative to its reference point,

v^*: is the commanded velocity vector,

v: is actual velocity, and

B: is a damping matrix.

(b) Friction: **(60-61)** A constant representation of friction in the real space is the frictional cone which defines the range of reaction forces.

(c) Compliant Motion: **(62-67)** There are three basic contact motions in the assembly operation: sensor based motion, pushing motion and compliant motion. Compliant motion occurs when the trajectories of an object are modified by contact forces or tactile stimuli. In practice, every element in a robot is compliant to some extent and this compliance is in universal use **(66)**.

To avoid assembly states that cause premature termination of planned motion, the friction must be accounted for the compliant movement and guarded movement strategies. There are several viewpoints **(11, 53, 54** and **67)** on the state where jamming and wedging can be avoided. The impact on RCC methods **(11, 53** and **54)** have also been examined.

1.3.4 Fine motion strategies (68-100)

(a) Pre-images: **(68)** The pre-images, which were proposed by Lozano, Mason and Taylor **(68)**.

(i) Non-directional pre-images: A pre-image of a collection of goals $\{G_a\}$ related to a set R is:

$$P_R(\{G_\alpha\}) = \{p \in R \mid \forall p_0^* \in B_{ep}(p),\ S(p_0^*, R, \{G_\alpha\}) \neq 0\} \quad (2)$$

where

$\forall$ is a symbol which denotes "aribtrary",

p is the actual position,

p_0^* is the measured position,

$B_{ep}(p)$ is the positional uncertainty ball with p as the centre,

$\{G_\alpha\}$ is a collection of goal sets,

$S(p_0^*, R, \{G_\alpha\})$ is the set of all commanded control velocities v_0^*, such that the termination predicate is guaranteed to signal success of operation, knowing that the initial measured position p_0^* corresponds to actual position p in R, .

The strategy recursively constructs pre-image collections until one pre-image includes the initial area of the process.

(ii) Directional pre-images: A pre-image of a collection of goals $\{G_\alpha\}$ relative to a set R and nominal control velocity v_θ^* (where θ is the angle between the velocity and x axis) is:

$$P_{\theta,R}(\{G_\alpha\}) = \{p \in R \mid \forall p_0^* \in B_{ep}(p),\ v_\theta^* \in S(p_0^*, R, \{G_\alpha\})\} \quad (3)$$

Here v_θ^* is the velocity vector that in the planar case making angle θ with the x-axis.

(b) Back-projection and forward-projection: (69)

(i) Back-projection:

The back-projection concept was firstly used by Erdmann (69). The basic difference between pre-images and back-projections is the use of termination predicates. A back-projection region should be a zone from which any motion

commanded along the desired direction is certain to satisfy the goal. The simple non-directional back-projection of a collection of goal sets $\{G_\alpha\}$ related to a set R is given by:

$$\bar{P}_R(\{G_\alpha\}) = \{p \in R \mid \bar{S}(p,R,\{G_\alpha\}) \neq 0\} \tag{4}$$

The simple directional back-projection of a collection of goal sets $\{G_\alpha\}$ under the commanded velocity v_θ^* is given by:

$$\bar{P}_{R,\theta}(\{G_\alpha\}) = \{p \in R \mid v_\theta^* \in \bar{S}(p,\{G_\alpha\})\} \tag{5}$$

$S(p, R, \{G_\alpha\})$ is the set of all commanded control velocities v_θ^* that are guaranteed to move any point in the pre-image R into one of the goal sets $\{G_\alpha\}$. These definitions capture the notion that a back-projection should consist of those points which are guaranteed to satisfy the positioning goal.

(ii) Forward-projection:

For a measured position p_0^*, which is known to correspond to an actual position p in the set R, the forward-projection at time t under the command velocity v_{θ^*} is given by:

$$F_\theta(R) = \{(T_p(t), T_v(t)) \mid T \subseteq \tau(v_\theta^*) \cap T_p(0) \subseteq R\} \tag{6}$$

where $T_p(t)$ and $T_v(t)$ are trajectories and velocities which satisfy the damper equations with uncertainties relative to the commanded velocity v_θ^*. τ is the set of all vectors T which include $T_p(t)$ and $T_v(t)$. In practice, the back projection can be used to choose the subgoals, and the forward projection can be used to judge the achievement.

(c) Error detection and recovery (EDR): (69)

The weak pre-image is the set of points which possibly enter the goal

recognizably, given sensing and control events. H_0 is the set difference of the forward projection minus the weak pre-image. Then H_0 can be presented as follows:

$$H_0 = F_\theta(R) - P*_\theta(G) \tag{7}$$

H_s can be defined as all regions where sticking is possible in the difference of weak pre-image minus strong pre-image:

$$H_s = \{x \in P*_\theta(G) - P_\theta(G) | \textit{sticking is possible at } x\} \tag{8}$$

Then error detect and recovery range can be defined as:

$$H = \pi(H_0) \bigcup Z(H_s) \tag{9}$$

where $Z(H_s)$ denotes the zero velocities over H_s. $\pi(H_0)$ denotes the projection of H_0 in the positional state space.

(d) Sensorless motion: (71-75)

The possibility for the robot to plan and execute some simple tasks without sensors was analysed. The motion strategy is, in most cases, simpler and faster than the sensing strategies.

So the remaining tasks are:

(a) to see if the existing methods for the robotic peg-hole insertion operation are reliable and,

(b) based on the understanding of the feature of presently existing force sensors and passive accommodation and the understanding of the contact dynamics, using pre-image, back-projection, forward-projection and error-detection recovery, to develop a fast and reliable strategy for the precise robotic peg-hole insertion operation.

1.4 Organization of this thesis

Here is an outline of the remainder of this thesis. The force sensors which are being widely used in others work on robotic assembly operations are analysed in Chapter 2. The common features in the design of force sensors are identified. Assembly operations can be divided into two parts: the identification of the positional relationship between the peg and the hole, and the adjustment of the peg-hole system. The positional relationship can be obtained from the contact configuration. The presentation of the contact configurations between the peg and hole are also described in Chapter 2. If one piece of equipment can be used to present the contact configuration, it can be used to obtain the positional relationship between the peg and the hole, the correct adjustment can be obtained. The question is, what kind of information the force sensors can provide. Is it possible to identify the contact configuration, or at least the positional relationship through the signals from the force sensors? Uncertainties caused by sensory errors, model errors and control errors are presented in Chapter 3. Also, an important, but widely ignored problem in the interpretation of the force sensory signals in the positional space is proposed. This practical problem is due to the fact that the two concepts -the centre of the contact area and the centre of the overlap between the contact surfaces- are different because of the angle between the axes of the peg and hole and the defects between the contact surfaces. This implies that it is difficult to identify the peg-hole configuration by the signals from the force sensors. A strategy to perform the peg-hole insertion, overcoming the difficulties caused by the angle between the axes of the peg and hole and the defects of the contact surfaces, is proposed in Chapter 4. A strategy to perform the precise robotic peg-hole insertion without force sensors is proposed in Chapter 5. This method makes clever use of the environment. The

systematic development of the strategies for the precise robotic peg-hole insertion, based on the fine motion theory, is addressed in Chapter 6. To prove the feasibility of the strategies, simulations of the assembly operations are provided in Chapter 7. The experiments with clearance of 0.02 mm are described in Chapter 8. Conclusions and suggestions for further work are contained in Chapter 9.

The main achievements of this thesis can be presented as follows:

(a) The current six-component force sensors have been analysed and common features of the six component force sensors have been found, which can be used to guide new force sensor design.

(b) The ambiguities in the presentation of the peg-hole contact configurations using force sensors are analysed. These ambiguities exist widely and greatly influence the judgement of the relative positions of the peg and the hole, so it is not always possible to identify the positional relationship through the signals from the force sensors.

(c) It is firstly pointed out that in certain areas, the force sensor can partly provide some information about the peg and the hole, which can be used in the adjustment to some extent.

(d) A strategy to overcome the difficulty caused by ambiguous presentation of the contact configuration of the peg-hole system is provided.

(e) A strategy to achieve precise assembly operation without force sensors or RCC is provided.

(f) The allowed initial range and the applied force design are analysed.

(g) The assembly operation is simulated, and does not require specific robot to be used.

(l) The experiments with a clearance of 0.02 mm without force sensors are carried

out by UMI-RTX robot.

From this chapter it is clear:-

(a) why robotic peg-hole insertion operation should be analysed,

(b) what the major current work is,

(c) how about the extent of the major research and,

(d) what will be reported in this thesis.

To begin with, it is necessary to analyse six-component force sensors which are the most used as pieces of hardware in the robotic peg-hole insertion operations. There are several questions raised by six-component force sensor design:

(a) whether the force sensors used in the robotic peg-hole system can be used to measure six-component forces and what are the features of the six-component force sensors,

(b) how should six-component force sensors be designed?

(c) whether six-component force sensors can provide the positional relationship between the peg and the hole in the assembly operation and,

(d) what kind of information the six-component force sensor can provide?

The first two questions will be studied in Chapter 2.

CHAPTER 2 FORCE SENSORS AND PRESENTATION OF CONTACT CONFIGURATIONS BETWEEN PEG AND HOLE

2.0 Introduction

As mentioned before, the six-component force sensors play an important role in robotic peg-hole insertion operations. The major feature of these sensors is that they can measure the forces and moments in three directions. In Sections 2.1 and 2.2, the working principles of the force sensors are analysed through two typical force sensors which were designed by other people. In Section 2.3, common aspects of six-component force sensors are studied. In Section 2.4, the basic problems in six-component force sensor design is studied. Sections 2.1 and 2.2 are the analysis of others' work, Sections 2.3 and 2.4 are new work in this thesis.

In general, the assembly operation can be divided into two steps: identifying the states of the peg-hole system, and adjusting the peg to achieve the insertion operation. If feedback hardware, such as force sensors, can provide the identification of the contact configuration, the right adjustment can be obtained. This raises the question: what is the contact configuration between the peg and hole system? The contact configurations can be presented by:

(a) the rotational and translational errors which can be directly used to design the adjustment movement of the end-effector of the robot, or

(b) the locations of the contact points.

The general presentation of the contact configuration between the peg and the hole is analysed in Section 2.5.

2.1 Tube-design six-component force sensor

There are several popular six-component force sensor configurations. The tube design six-component force sensor is presented in Fig. 5 (24).

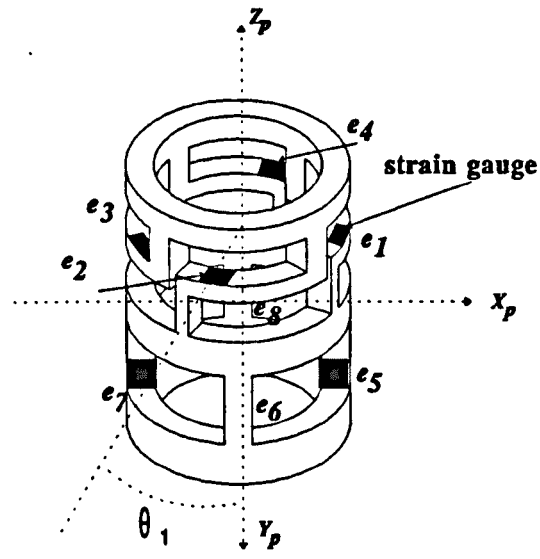

Fig. 5 The tube-design six-component force sensor

For this sensor:

(a) θ_1 the angle as shown in Fig. 5,

(b) e_i (i=1,2,...,8) outputs from the eight groups of the strain gauges of the sensor, respectively.

This sensor is very complex in structure providing sensitivity. The relationship between the forces, torques exerted on the sensor and the outputs of the force sensors can be shown as follows:

Forces or torques to be measured	location of main corresponding deformed strain gauges	measured process
F_{sx}	e_8, e_6	average of deformation is proportional to F_x
F_{sy}	e_7, e_5	average of deformation is proportional to F_y
F_{sz}	e_1, e_2, e_3, e_4	average of deformation is proportional to F_z
M_{sx}	e_3, e_4	difference of deformation is proportional to M_x
M_{sy}	e_3, e_1	difference of deformation is proportional to M_y
M_{sz}	e_9, e_0, e_7, e_8	average of deformation is proportional to M_z

Table 1 Forces, torques and locations of corresponding deformed strain gauges in the tube-design six-component force sensor

2.2 Celular-design six-component force sensor

The sensor, shown in the Fig. 6 is a direct force sensor, i.e., the forces and torques can be calculated directly from the outputs of the force sensors (28).

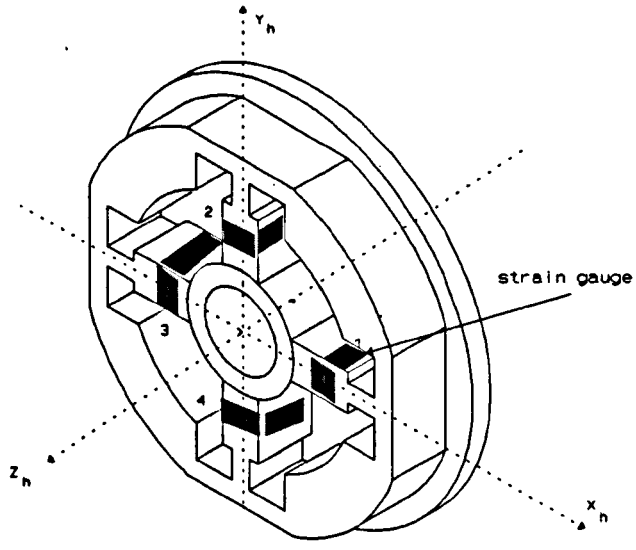

Fig. 6 The celular-deign six-component force sensor

The forces, torques and the deformation of corresponding strain gauges can be shown in the following table:

Forces or torques to be measured	location of corresponding deformed strain gauges	measured process
F_{sx}	side surfaces of 2 and 4	average of deformation is proportional to F_x
F_{sy}	side surfaces of 3 and 1	average of deformation is proportional to F_y
F_{sz}	upper and end surfaces of 1, 2, 3 and 4	average of deformation is proportional to F_z
M_{sx}	upper and end surfaces of 2 and 4	difference of deformation is proportional to M_x
M_{sy}	upper and end-surfaces of 3 and 1	difference of deformation is proportional to M_y
M_{sz}	upper and end-surfaces of 1, 2, 3 and 4	average of deformation is proportional to M_z

Table 2 Forces, torques and locations of corresponding deformed strain gauges in the celular six-component force sensor

There are also other six-component force sensors shown in Fig. 7.

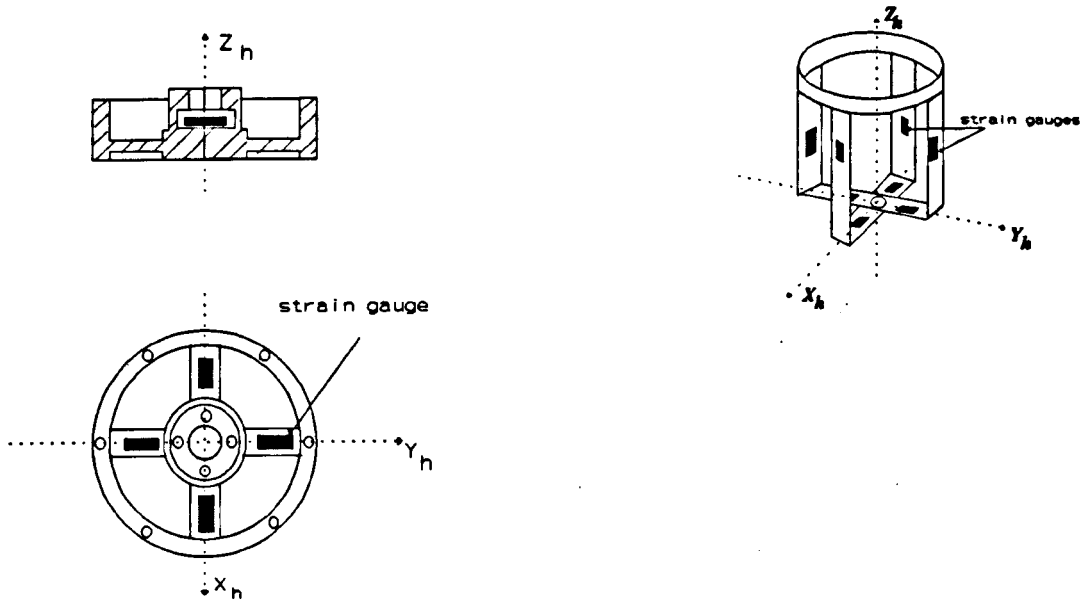

Fig. 7 Other six-component force sensors

2.3 Common aspects of six-component force sensor design

In general, the coordinate system for the force sensors can be established as shown in Fig. 8:

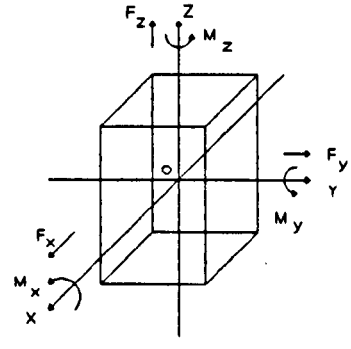

Fig. 8 General coordinate system for the force sensor

It is found that for the six-component force sensors, the strain gauges are always distributed in the planes which are parallel to the coordinate planes, $X_sO_sY_s$, $Y_sO_sZ_s$ and $X_sO_sZ_s$ if the coordinate system is established in a suitable way. The result is that forces in three directions can be measured. To measure the torques in different directions, the strain gauges must be used in pairs. To measure M_{SI} (I=X, Y, Z), the distribution of the pair of the strain gauges must satisfy the following conditions:

(a) The pair of strain gauges should be in planes parallel to the coordinate plane $I_sO_sJ_s$ (I can be X, Y, or Z, and J is not equal to I),

(b) The strain gauges should be distributed in the line which is parallel to J and symmetric to the corresponding centre.

The location of the strain gauges to measure the torques acting on the force sensor can be shown as follows:

The torques to be measured	The connection line of the corresponding strain gauges is parallel to	The plane in which the strain gauges located is parallel to
M_{sx}	Y_s axis or X_s axis	$X_sO_sY_s$ plane $X_sO_sZ_s$ plane
M_{sy}	X_s axis or Z_s axis	$X_sO_sY_s$ plane $Z_sO_sY_s$ plane
M_{sz}	X_s axis or Y_s axis	$X_sO_sZ_s$ plane $Y_sO_sZ_s$ plane

Table 3 The general locations of strain gauges with corresponding torques

Using the table, a variety of six-component force sensors can be designed.

2.4 New Practical Force Sensor Design

Two force sensor concepts shown in Fig. 9 satisfy these requirements.

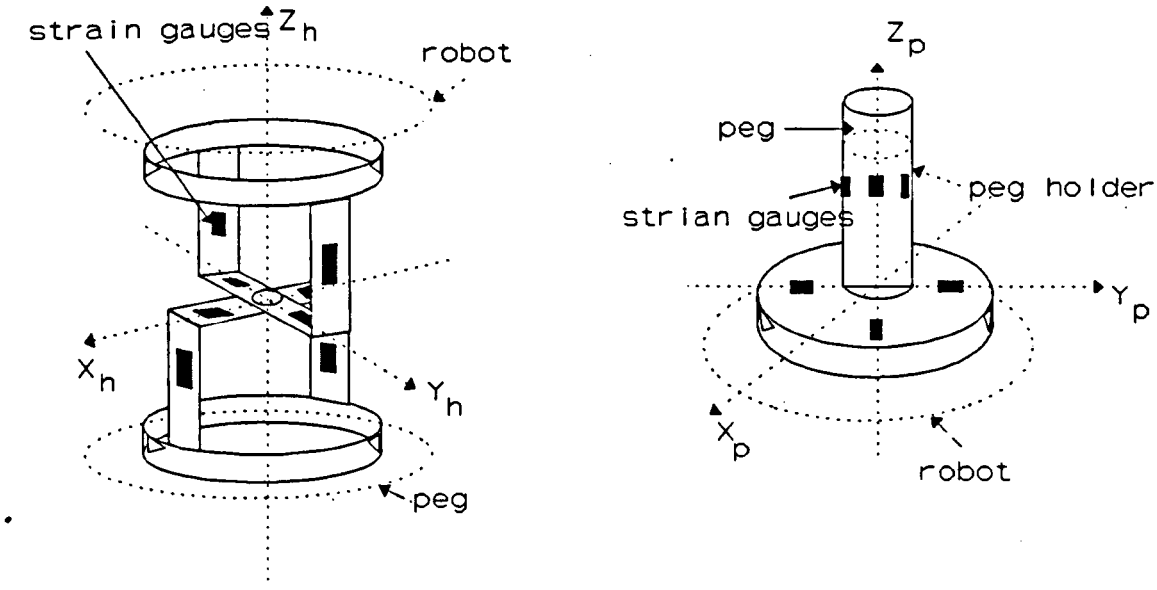

Fig. 9 New practical force sensor designs

These force sensors were only based on the design rule described in §2.3. Other factors, such as, strength, sensitivity, rigitidy, weight, accuracy, nonlinearity, hysteresis, conformance, resolution, repeatibility and scatter, were not considered.

2.5 Presentation of contact configurations between the peg and hole

The presentation of the peg-hole contact configurations, which is based on Luh, J.Y S. and Krolak, R. J. (64) will be discussed here. For a complete description of the contact configuration, the node concept can be used. A node $s_i=(P, C, S, I, Q)$, where P is the position of the peg in the configuration space, C is a set of contact points, S is a set of potential motion, I is qualitative signal based on the associated physical situations, and Q is a heuristic assessment of the "quality" of the contact situations.

(a) If the hole is fixed, the contact configuration of the peg-hole system is determined by the configuration of the peg, which can be denoted by a six-component vector *P*. In this case, the contact configuration can also be represented by the angular and translational errors which are needed for the direct adjustment of the peg.

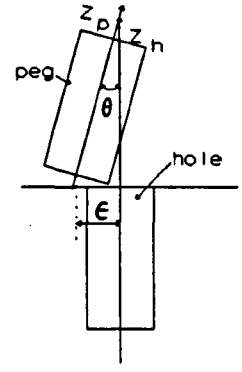

Fig. 10 Translational and angular errors between the peg and hole

where:

θ is the angle between the axes of the peg and hole,

ϵ is the deviation between the centres of the end-surface of the peg and the upper-surface of the hole.

The aim of the assembly motions is to reduce the translational and angular errors.

(b) If the translational and rotational errors are known exactly, the assembly operation can be translated through motion control. In practice, the signals which are used to detect the configurations are those from force sensors. The force signals are related to the contact configuration, rather than the translational and angular errors. These contact points can be divided according to the contact elements, i.e. the contact modes (vertex, edge or

plane):

Contact elements	Degree of contact elements	Contact types	Degree of contact types
vertex/vertex	(1)/(1)	point	(1)
vertex/edge	(1)/(2)	point	(1)
vertex/plane	(2)/(3)	point	(1)
edge/vertex	(2)/(1)	point	(1)
edge/edge	(2)/(2)	point line	(1) (2)
edge/plane	(2)/(3)	point line	(1) (2)
plane/vertex	(3)/(1)	point	(1)
plane/edge	(3)/(2)	point line	(1) (2)
plane/plane	(3)/(3)	point line plane	(1) (2) (3)

Table 4 Contact types and contact elements

The maximum contact degree corresponds to minimum degree of contact type, such as the maximum contact degree of the Edge/Plane is two and the minimum degree of the contact type is two.

For the peg-hole system, the basic contact configurations can be presented as follows:

Contact element	Peg-hole contact types	Peg-hole contact diagrams

edge/edge	edge of peg contacts edge of hole	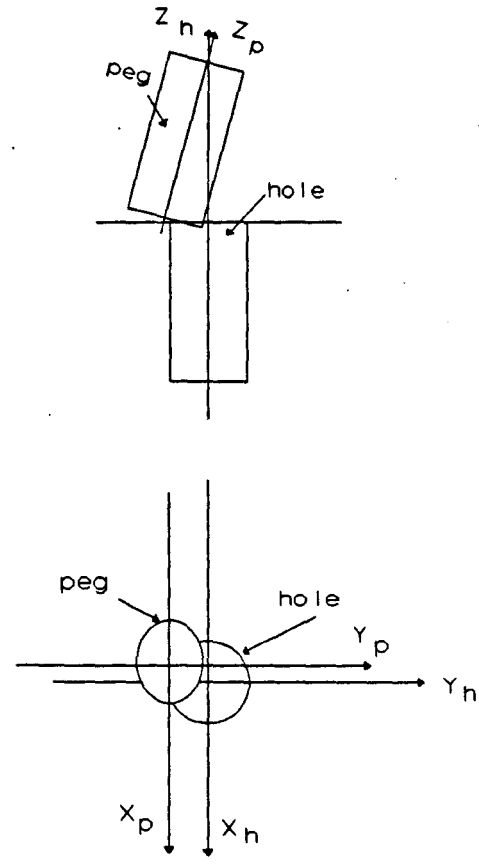

edge/plane	edge of the peg contacts the upper-surface of the area surroundin g the hole	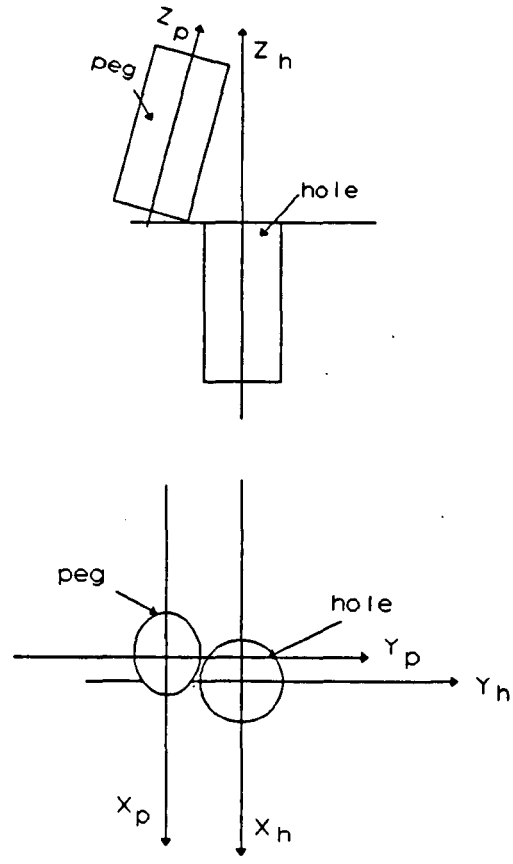

	edge of the peg contacts the side-surface of the hole	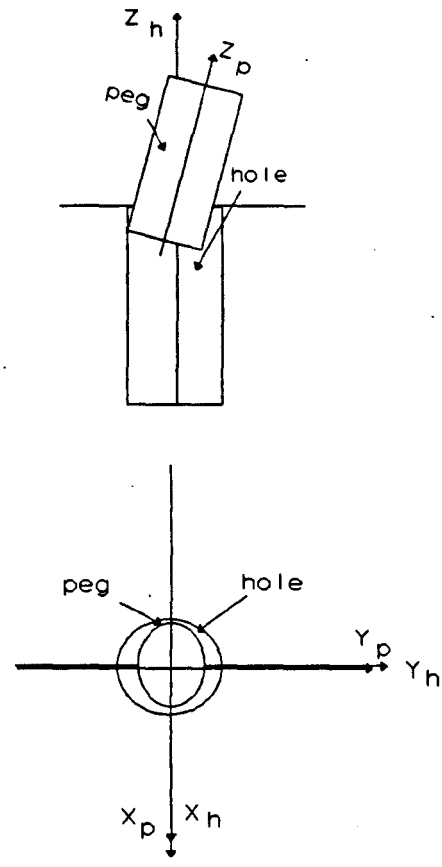

	edge of the peg contacts bottom of the hole	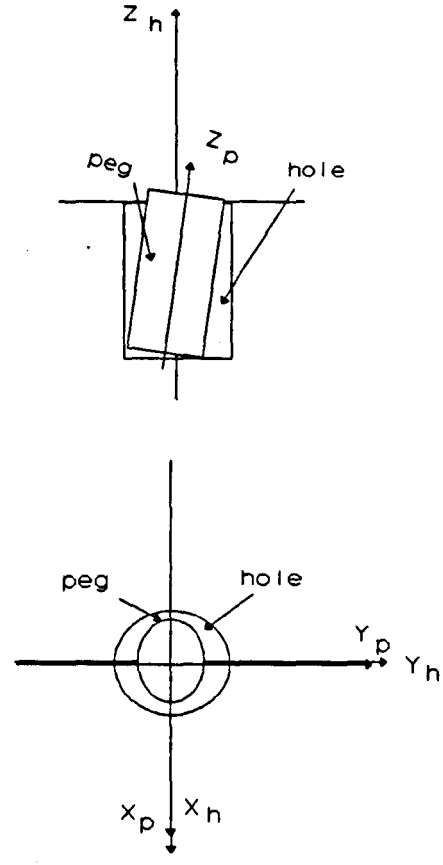

plane/edge	side-surface of the peg contacts the edge of the hole	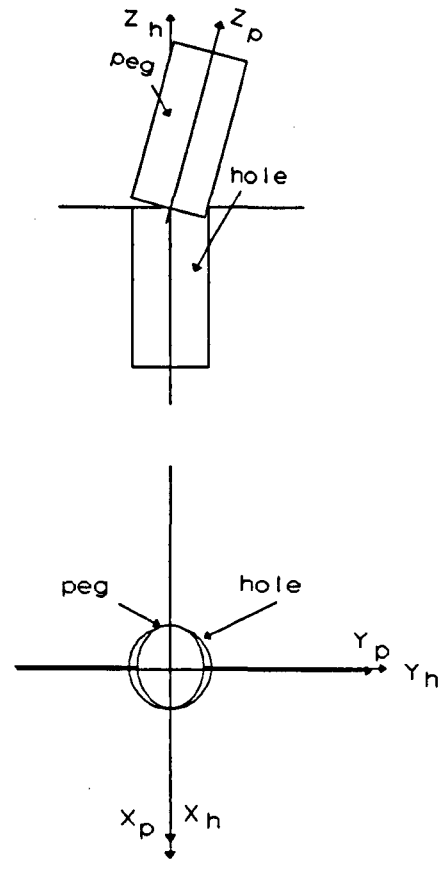

plane/plan e	bottom-surface of the peg contacts upper-surface of area surroundin g the hole	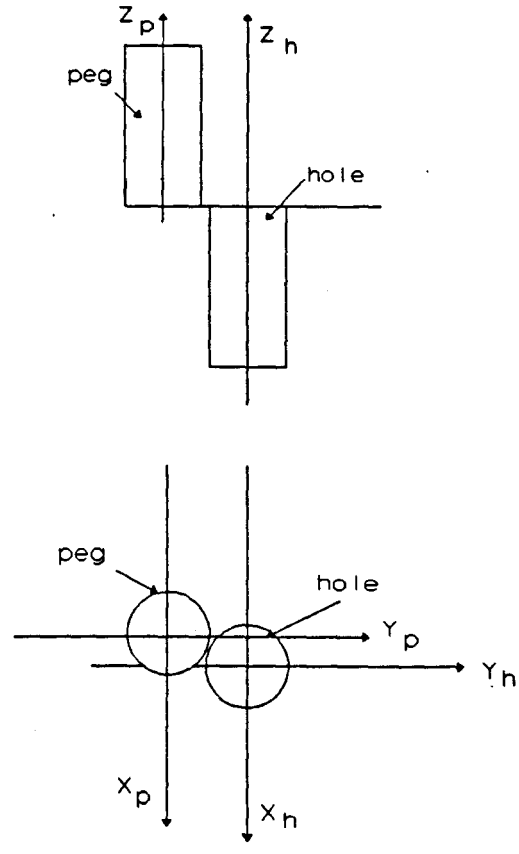

	bottom surface of the peg contacts upper-surface of area surroundin g the hole and edge of the hole	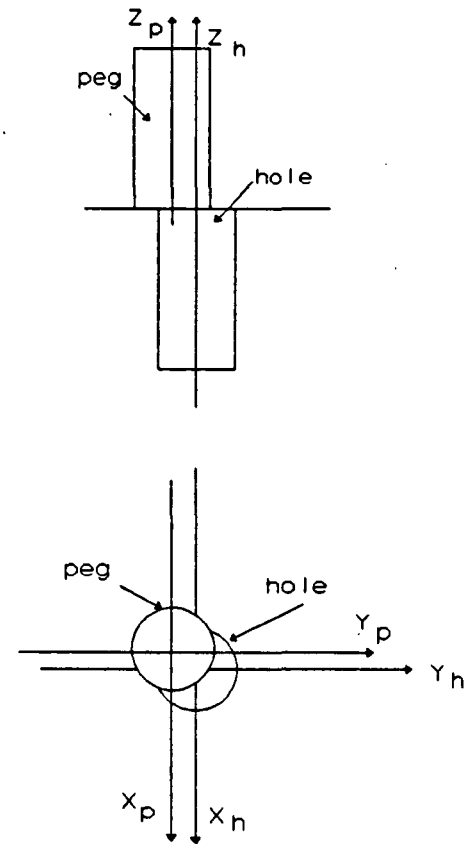

	side-surface of the peg contacts side-surface of the hole	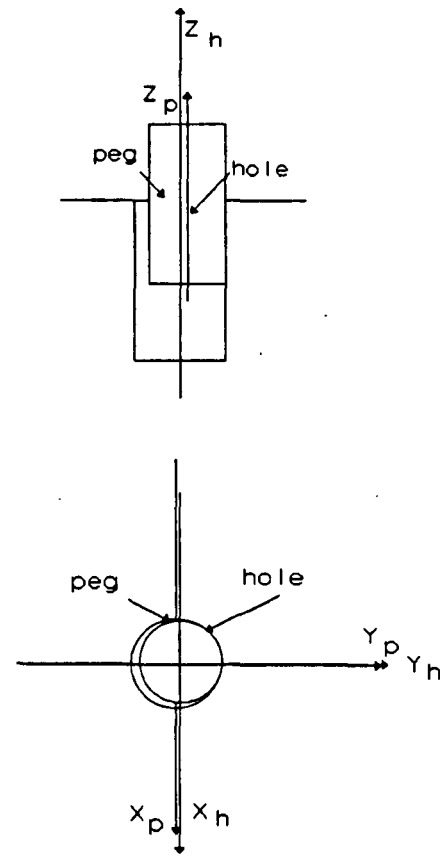

Table 5 Peg-hole basic contact configurations

(c) Potential motion S

Sometimes, a contact configuration can only be identified by its possible potential motions. Two types of translation motion, namely separation motion and compliance motion are defined. Any differential motion that results in breaking the contact between the objects is referred to as separation motion. Any differential motion that does not result in breaking the contact between the objects is termed compliant motion. Both motions are permitted. The separation cone of a contact is defined as the set of all separation motions for

that contact mode. The compliance cone of a contact is defined as the set of all compliance motions for that contact mode.

This chapter can be divided into two parts. The major aim of the first part including Sections 2.1, 2.2, 2.3 and 2.4, is the analysis of the common aspects of six-component force sensors. According to these common features, it would be easy to design any form of six-component force sensor.

The second part, Section 2.5, shows the application of the contact configuration concept to the peg-hole system. From that, it is clear how many contact configurations the peg-hole system can have. The next question to be addressed is what kind of information six-component force sensors can provide in the presentation of the contact configuration of the peg-hole system.

CHAPTER 3 THE USE OF FORCE SENSORS IN THE ROBOTIC PEG-HOLE SYSTEM

3.0 Introduction

The uncertainty in the robotic peg-hole system is analysed in Section 3.1. The major problem of using force sensors in the robotic peg-hole insertion operation is explained in Sections 3.2-3.5. Since the purpose of using the force sensor in the robotic peg-hole system is to identify the positional relationship between the peg and hole, the problem is whether the positional relationship can be obtained through the signals from the force sensor. In Section 3.3, through two examples, it is found that the force sensor cannot provide the information needed to identify the contact configuration. It cannot even provide the information to identify the positional relationship between the peg and hole which is often needed for the adjustment. In these examples, the positional relationships are different, while the force sensory signals are the same. In Section 3.3, two concepts are provided, one is the centre of contact area and the other is the centre of overlap area. It is found that:

(a) the force sensor can only provide information about the centre of the contact area,

(b) the positional relationship can be only obtained from the location of the centre of the overlap.

In most cases, the centre of contact area is different from the centre of the overlap. So in theory this explains why the positional relationship can not be obtained from the force sensory signals. In Section 3.4, through the motion analysis, the contact configurations which share one set of signals from the force sensors are analysed.

3.1 Uncertainty in the robotic peg-hole system

3.1.1 Sensor errors

Due to the structure of the sensors and the noise in the system, the nominal physical value may be different from the actual value. The actual and nominal force signals can be presented as an error sphere:

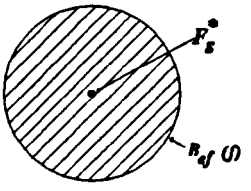

Fig. 11 Sensor error ball

where $B_{ef}(f)$ represents the sensory error zone which represents the range of actual physical values, and F_s^* denotes the nominal physical value. For a six-component force sensor, the nominal and actual forces can be presented as follows:

$$F_s^* = [F_{sx}^*, F_{sy}^*, F_{sz}^*, M_{sx}^*, M_{sy}^*, M_{sz}^*]^T \tag{10}$$

$$F_s = [F_{sx}, F_{sy}, F_{sz}, M_{sx}, M_{sy}, M_{sz}]^T \tag{11}$$

3.1.2 Model errors

The insertion can only be completed when the diameter of the peg is smaller than that of the hole.

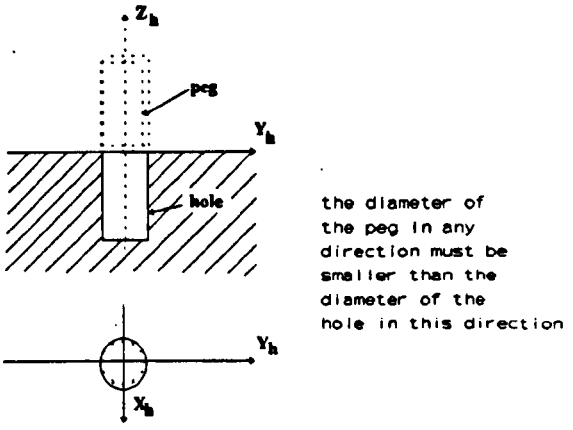

Fig. 12 The tolerance between the peg and hole

3.1.3 Control cone

The actual velocity may be different from the nominal velocity on both direction and magnitude. The actual velocity of the centre of the peg will then be in a velocity cone with the nominal velocity as the axis of the cone.

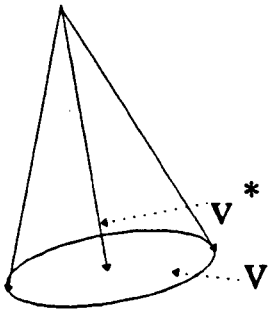

Fig. 13 The control cone for the peg centre velocity

3.2 Two practical problems

(a) In the case of the wrist force sensor and non-zero θ (see Fig. 14)

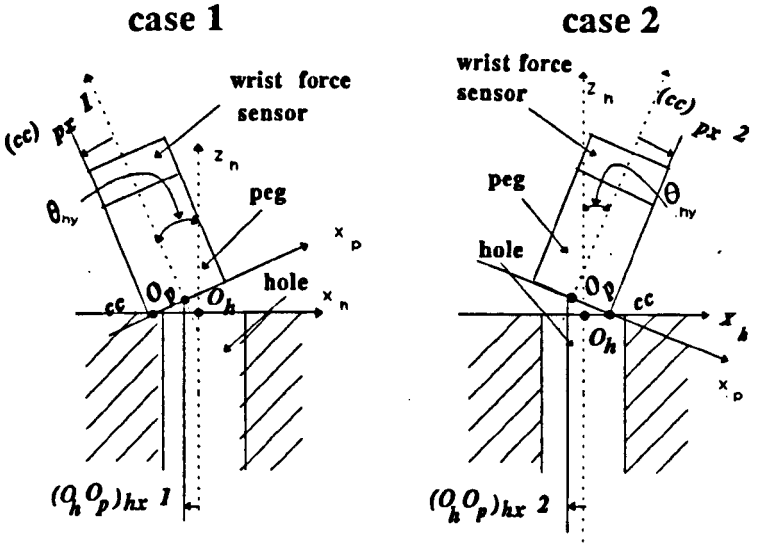

Fig. 14 Contact configuration with wrist force sensor and non-zero $|\theta|$

The letters with subscript "1" refer to that in case 1 configuration, and the letters with subscript "2" refer to that in case2. It follows that:

$$\begin{aligned} (cc)_{px}1 &< 0 \\ (cc)_{px}2 &> 0 \end{aligned} \tag{12}$$

while

$$(O_hO_p)_{hx}1 = (O_hO_p)_{hx}2 \tag{13}$$

(b) In the case of the table force sensor and non-zero θ (see Fig. 15)

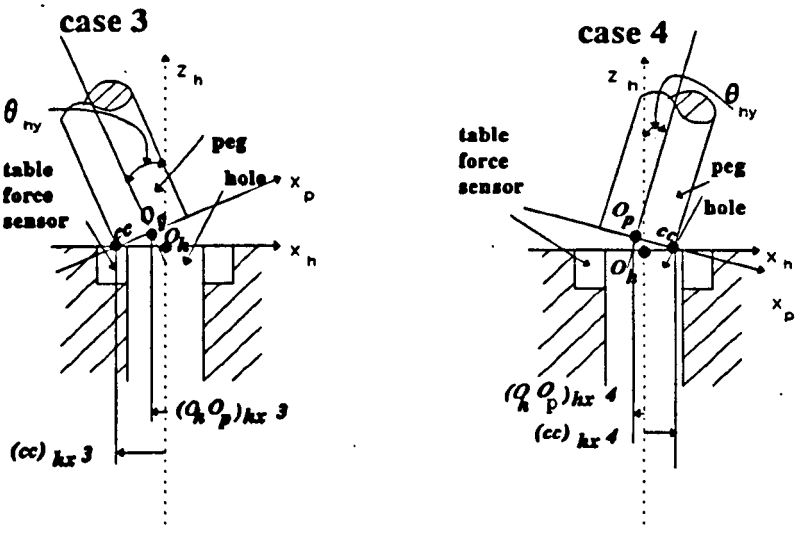

Fig. 15 Contact configuration with table force sensor and non-zero $|\theta|$

Similarly, the letters with subscript "3" refer to the letters in case 3 configuration and the letters with subscript "4" refer to the letters in case 4 configuration. It follows that:

$$\begin{aligned} (cc)_{hx}3 &< 0 \\ (cc)_{hx}4 &> 0 \end{aligned} \tag{14}$$

while

$$(O_hO_p)_{hx}3 = (O_hO_p)_{hx}4 \tag{15}$$

Here the angle between the axes of the peg and the hole makes the centres "co" and "cc" misaligned.

In Fig. 16 and Fig. 17, the two centres, the centre of the overlap of the projections of the end-surface the peg and the area surrounding the hole on the $X_hO_hY_h$ and the centre of the contact area do not coincide due to the defects of the contact surfaces.

In the case of wrist force sensors (see Fig. 16),

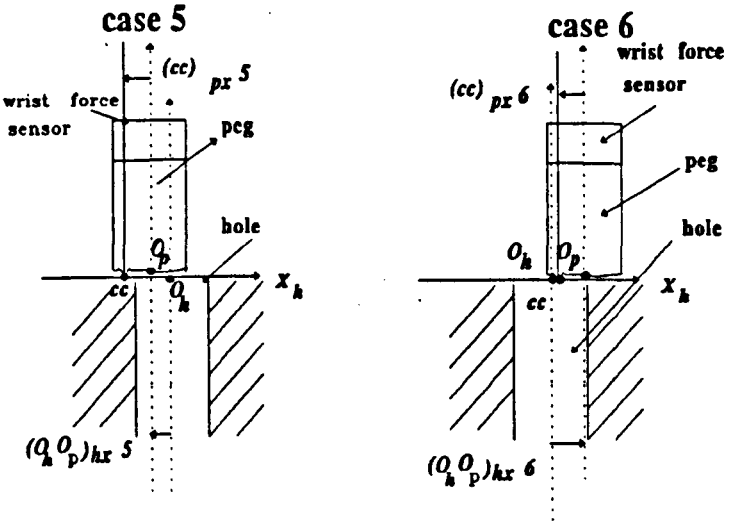

Fig. 16 Contact configuration with wrist force sensor and defects of contact surfaces

$$(cc)_{px}5 = (cc)_{px}6 \tag{16}$$

while

$$(O_hO_p)_{hy}5 \neq (O_hO_p)_{hy}6 \tag{17}$$

Likewise, in the case of table force sensors (see Fig. 17),

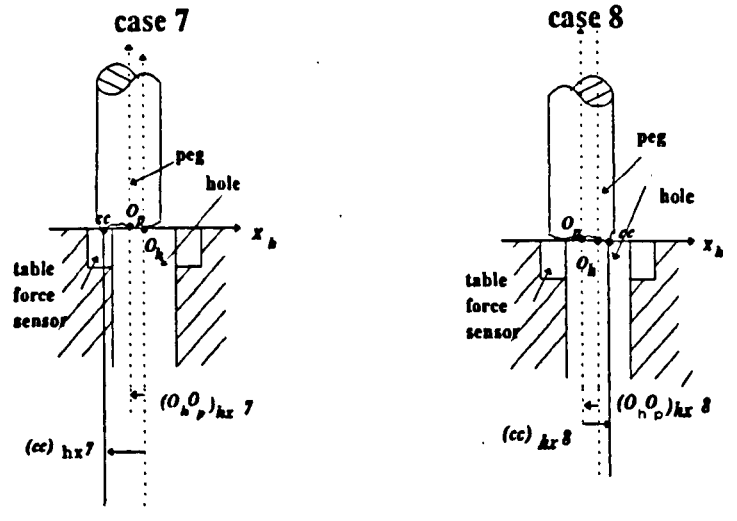

Fig. 17 Contact configuration with table force sensor and defects between the contact surfaces

$(cc)_{hx}7 < 0$, $(cc)_{hx}8 > 0$, while $(O_hO_p)_{hx}7=(O_hO_p)_{hx}8$.

3.3 Relationship among "*co*", "*cc*" ,"O_hO_p" and force sensory signals

3.3.1 Relationship between "O_hO_p" and location of "co"

It is found that the projections of a deviation "O_hO_p" between the peg and the hole on $X_hO_hY_h$ can be calculated from the coordinates of the centre of the overlap "*co*" of the projections of the end-surface of the peg and the area surrounding the hole. This is shown in Fig. 18,

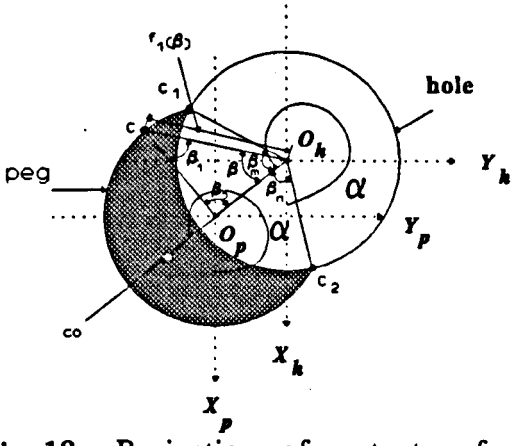

Fig. 18 Projections of contact surfaces on $X_hO_hY_h$ plane

in which

"*C*" is the point on the circumference of the end-surface of the peg outside the hole,

"C_1", "C_2" are the common points of the projections of the circumference of the end-surface of the peg and the upper-surface of the hole,

$f_1(\beta)$ is the distance between O_h and C,

β, β_1 and β_2 are the angles in triangle O_hO_pC,

β_m, β_n are the angles from O_hO_p to O_hC_1 and O_hC_2, respectively.

The location of "*co*" is established through very complex calculation. It should be located on the line through both O_p and O_h, and,

$$|O_h(co)| = \frac{\iint l dS}{S} = \frac{\int_{\beta_n}^{\beta_m}\int_{R_h}^{f_1(\beta)} l^2 dl d\beta}{\int_{\beta_n}^{\beta_m}\int_{R_h}^{f_1(\beta)} l dl d\beta} \tag{18}$$

where l is the distance between O_h and any point in the sectioned area, S is the area of the overlap of the end-surface of the peg and the area surrounding the hole, $|O_h(co)|$ is the length of the directed line $O_h(co)$, and limits for integration are given as below.

$$\beta_n = -\arccos\frac{|O_hO_p|}{2R_h}$$
$$\beta_m = \arccos\frac{|O_hO_p|}{2R_h} \tag{19}$$

If the angle between the axes of the peg and hole is zero,

$$f_1(\beta) = \frac{R_p \sin\beta_2}{\sin\beta} \tag{20}$$

$$\frac{\sin\beta_1}{\sin\beta} = \frac{|O_hO_p|}{R_p} \tag{21}$$

$$\beta_1 = \arcsin(\frac{|O_pO_h|}{R_p}\sin\beta) \tag{22}$$

$$\beta_2 = \pi - \beta - \beta_1 \tag{23}$$

Then:

$$f_1(\beta) = \frac{R_p \sin[\beta + \arcsin(\frac{|O_h O_p|}{R_p}\sin\beta)]}{\sin\beta} \tag{24}$$

where β_1, β_2, β_n, β_m and $f_1(\beta)$ are expressed in Fig. 18.

Similarly, the location of "*co*" can also be obtained with a known angle between the axes of the peg and hole. The point "*co*" can be considered to be approximately at the centre of the projections of the circumferences of the end-surface of the peg and the upper-surface of the hole. Then the relationship between the deviation of the peg and hole and the projection of the centre of the overlap "*co*" can be determined. The angle between X_h and $O_h O_p$ satisfies:

$$\begin{aligned} \tan\alpha &= \frac{[(co)O_h]_{hy}}{[(co)O_h]_{hx}} \\ &= \frac{[(co)O_p]_{py}}{[(co)O_p]_{px}} \end{aligned} \tag{25}$$

The magnitude of the deviation can be calculated according to $|(co)O_p|$:

$$|O_h O_p| \approx R_h + R_p - 2|O_p(co)| \tag{26}$$

or according to $|(co)O_h|$:

$$|O_h O_p| \approx 2|O_h(co)| - R_p - R_h \tag{27}$$

3.3.2 Relationship between force signal and location of "*cc*"

The general equations for the force sensor can be expressed as follows:

$$\begin{aligned} M_{sx} &= F_{sx} \times cc_{sz} - F_{sz} \times cc_{sy} \\ M_{sy} &= -F_{sx} \times cc_{sz} + F_{sz} \times cc_{sx} \\ M_{sz} &= -F_{sy} \times cc_{sx} + F_{sx} \times cc_{sy} \end{aligned} \tag{28}$$

So cc_{si} can be obtained from F_{si} and M_{si}, where i=x,y, and z. F_{si} and M_{si} can be obtained

from the signals from the force sensor. If the angle between the axes of the peg and the hole is zero, then the location of the centre of the contact surfaces can be easily obtained as shown in Fig. 19 and the relationship among them can be expressed as follows:

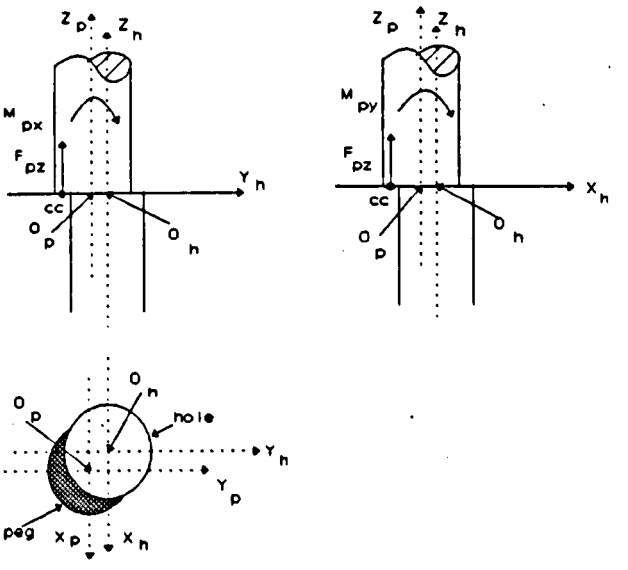

Fig. 19 cc and force sensor signals

$$(cc)_{sx} = \frac{M_{sy}}{F_{sz}}$$
$$(cc)_{sy} = \frac{M_{sx}}{F_{sz}} \qquad (29)$$

3.3.3 Relationship between force signals and O_hO_p

The deviation between the peg and hole can be calculated from the outputs of a six-component force sensor if the relationship between the centre of the overlap "co" and the centre of the contact surfaces "*cc*" can be obtained. These two concepts are often oversimplified and treated as one. It is found that if and only if :

(a) the angle between the axes of the peg and the hole is zero,

(b) and the contact surfaces are absolutely smooth,

will these two measures coincide (see Fig. 20):

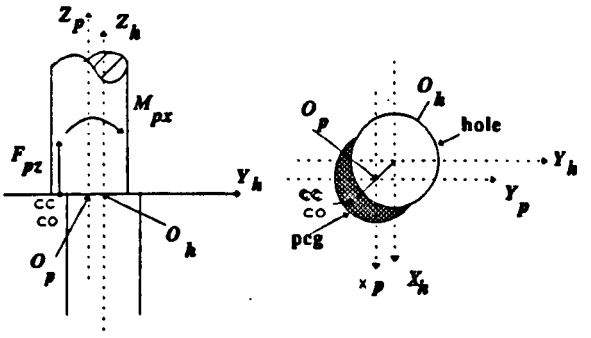

Fig. 20 Configuration when angular error is zero and contact surfaces are smooth

In these cases, the deviation between the peg and hole can be obtained from the signal of the force sensor (for example, a wrist force sensor):

$$\begin{aligned}(O_hO_p)_{px} &= [R_h + R_p - 2|(co)O_p|]\cos\alpha \\ &= [R_h + R_p - 2|(cc)O_p|]\cos\alpha = [R_h + R_p]\cos\alpha - 2\frac{M_{py}}{F_{pz}} \\ (O_hO_p)_{py} &= [R_h + R_p - 2|(co)O_p|]\sin\alpha \\ &= [R_h + R_p - 2|(cc)O_p|]\sin\alpha = [R_h + R_p]\sin\alpha - 2\frac{M_{px}}{F_{pz}}\end{aligned} \tag{30}$$

If there is an angle error (Fig. 21) or defects on the contact surfaces, then the deviation has an unclearly defined relationship with the force sensor signals:

$$(O_hO_p)_{px} = [R_h+R_p - 2|(co)O_p|]\cos\alpha$$
$$\neq [R_h+R_p-2|(cc)O_p|]\cos\alpha \neq [R_h + R_p]\cos\alpha - 2\frac{M_{py}}{F_{pz}}$$
$$(O_hO_p)_{py} = [R_h + R_p - 2|(co)O_p|]\sin\alpha \tag{31}$$
$$\neq [R_h + R_p - 2|(cc)O_p|]\sin\alpha \neq [R_h + R_p]\sin\alpha - 2\frac{M_{px}}{F_{pz}}$$

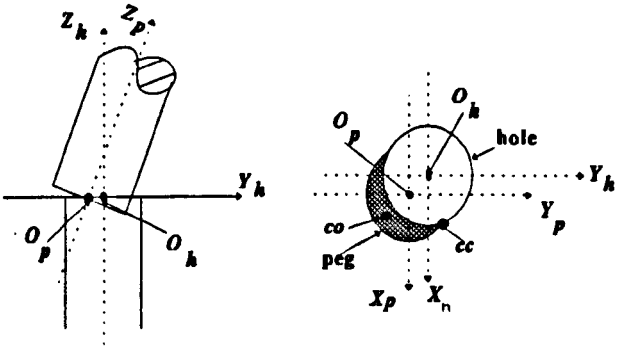

Fig. 21 Configuration when angular error is not zero

In the peg-hole insertion operation, the force signal is used to judge the state of the peg which is in five degrees of freedom if the peg is considered to be symmetric about Z_p axis. The location of the centre of the contact points in the peg coordinate system can be written as:

$$(O_pcc)^* = [(cc)_{px}^*, (cc)_{py}^*, (cc)_{pz}^*]^T \tag{32}$$

The mapping between the location of the contact point centre in the peg coordinate frame and the signals from the force sensor can be presented as follows:

$$(O_pcc)^* = [FC]F_s^* \tag{33}$$

where $[FC]$ is the mapping matrix from F_s^* to $(O_pcc)^*$.

The key problem is to obtain the map between the deviation of the peg and hole and

the force signals or the location of the contact point in the sensor coordinate frame. Here the situations before insertion, i.e., $c_{hz} = 0$ are analysed.

3.3.3.1 In single point contact

The only contact point c should be on the end-surface of the peg and the upper-surface of the hole:

$$c = \{c_{px}, c_{py} | c_{px}^2 + c_{py}^2 \leq R_p^2 \cap c_{hx}^2 + c_{hy}^2 \geq R_h^2\} \tag{34}$$

Furthermore, it can be proven that the contact point must be on the circumference of the end-surface of the peg (38), so:

$$c = \{c_{px}, c_{py} | c_{px}^2 + c_{py}^2 = R_p^2 \cap c_{hx}^2 + c_{hy}^2 \geq R_h^2\} \tag{35}$$

The contact point must be a point on the top-surface of the hole, so:

$$c = \{c_{px}, c_{py}, c_{pz} | c_{px}^2 + c_{py}^2 = R_p^2 \cap c_{hx}^2 + c_{hy}^2 \geq R_h^2 \cap c_{hz} = 0\} \tag{36}$$

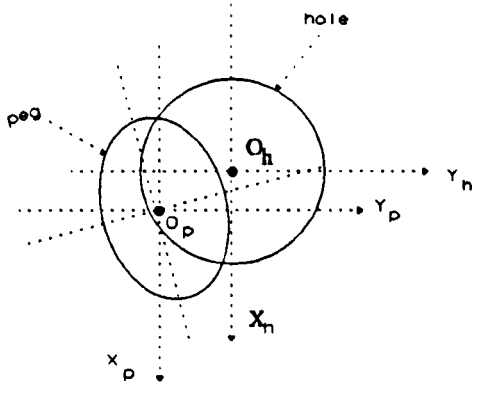

Fig. 22 Projections of the end-surface of the peg and the upper-surface of the hole with one point contact

The location of the contact point in the peg coordinate frame can be presented by the deviation and angle between the axes of the peg and the hole.

$$|O_hc| = |O_hO_p + R_p\cos\theta_c \angle\theta_{X_hO_hY_h} + R_p\sin\theta_c\sin\theta_{hx}\angle(\theta+90^0)_{X_hO_hY_h}| = R_h \quad (37)$$

where θ_c is the angle between O_hc and the direction of the projection of θ on $X_hO_hY_h$ plane. $\angle\theta$ is the unitary vector along the direction of the projection of the vector θ on the $X_hO_hY_h$ plane and $\angle(\theta+90^0)$ is obtained through 90^0 rotation of the unitary vector $\angle\theta$ in $X_hO_hY_h$ plane. In practice, the location of the contact point in the peg coordinate frame (for the wrist force sensor), rather than the relationship between the contact point c and θ, can be clearly obtained from the force signals. So the above equation can be further presented as follows:

$$|O_hc| = |O_hO_p + R_p\cos(\theta_{cx} - \alpha_\theta)i_{X_hO_hY_h} + R_p\sin(\theta_{cx} + \alpha_\theta)\sin\theta_{hx}j_{X_hO_hY_h}| = R_h \quad (38)$$

where O_hO_p is the vector from O_h to O_p, α_θ is the angle between the direction of θ and Y_h axis, which can be presented as follows:

$$\alpha_\theta = \arctan(\frac{\theta_{hx}}{\theta_{hy}}) \quad (39)$$

The mapping relationship from θ_{cx} to O_hO_p can be presented according to Equ. (38):

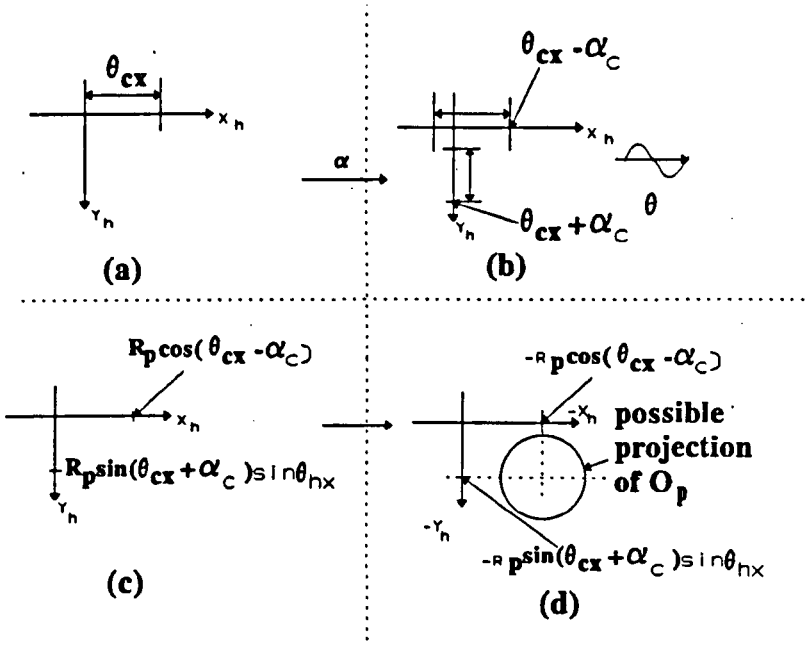

Fig. 23 Mapping relation between θ_{cx} and O_hO_p

The conclusion of the relationship between the force signals and deviation is:

(a) From Equ. 38, it can be obtained that θ_h has a nonlinear influence over the mapping projection. The direction of θ, which is defined by α_θ, plays a substantial role. The magnitude of θ would only influence one projection of force signal which is normal to that of θ (see Fig. 23(c)),

(b) From Equ. 38, it can be obtained that, for the same θ_{cx} and θ, only the magnitude of O_hO_p is determined. So O_p is on the circle with the centre related to θ_{cx}, θ_{cy} and θ and the radius R_h. This means that even with the same force signal and same angle between the axes of the peg and hole, the locations of the centre of the end-surface of the peg can be different (see Fig. 23(d)).

3.3.3.2 In two point contact

The general projection of the end-surface of the peg and the upper-surface of the hole with two contact points on the $X_hO_hY_h$ plane can be presented as follows:

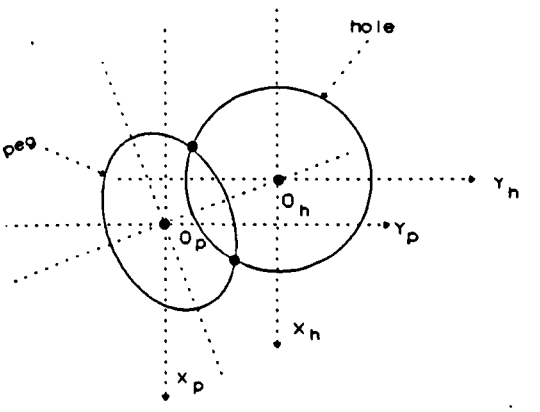

Fig. 24 General projections of the end-surface of the peg and the upper-surface of the hole on $X_hO_hY_h$ plane with two point contact

It has been proven that (37):

(a) the projection of the end-surface of the peg on the $X_hO_hY_h$ plane is an ellipse, and

(b) the short axis of this ellipse would go through the point O_h.

$$\angle O_pO_hY_h = \pi - \arctan\frac{\theta_{hx}}{\theta_{hy}} = \pi - \alpha_\theta \tag{40}$$

and

$$|O_hO_p|_{X_hO_hY_h} \approx |O_pcc|(1 + \cos|\theta|) \tag{41}$$

It is clear that in two point contact situation, the mapping between the force sensor signals and the contact state is more straight forward.

3.3.3.3 In side-surface contact

The direction of the contact force is opposite to that of O_pc. O_pc is normal to the direction of θ.

3.4 Classification of the fine motion

The movements can be classified according to their influences on the positions of the

contact points. These influences would be detected by force sensors. According to the combination of the contact movement on each object, the contact motion can be categorised into four types (97):

(a) The contact positions on both mobile part and immobile part keep their positions,

(b) Only the contact points on the mobile part maintain their positions,

(c) Only the contact points on the immobile part maintain their positions and,

(d) The contact points on both objects move.

For the robotic peg-hole system, the motion to maintain the position of the contact point static in hole are rotations about the contact point on the hole and the translation along a specified feature of the peg:

Contact configurations of the peg hole system	Motions to maintain the static contact point on the hole	
edge of the peg contacts the edge of the hole	rotation around the contact point on the hole	rotate the peg to make each point on the edge of the peg to contact the same point of the hole
edge of the peg contacts the upper-surface of the area surrounding the hole	as above	as above
edge of the peg contacts side-surface of the hole	as above	as above
edge of the peg contacts the bottom of the hole	as above	as above
side-surface of the peg contacts of the edge of the hole	as above	rotate and move the peg to make each point on the side-surface of the peg to contact the same point of the hole

bottom of the peg contacts upper-surface of the area surrounding the hole	as above	rotate around the axis of the peg
bottom of the peg contacts upper-surface of the hole	as above	
bottom of the peg contacts bottom of the hole	as above	rotate around the axis of the peg
side-surface of the peg contacts side-surface of the hole	as above	rotate the peg to make each straight line on the side-surface of the peg to contact the same position of the hole

Table 6 The motion to maintain a static contact point on the hole

The motion to make the contact point static on the peg can be presented as follows:

Contact configurations of the peg hole system	Motions to maintain the static contact point on the peg	
edge of the peg contacts the edge of the hole	rotation around the contact point on the hole	move the peg around the surface of the hole with the same contact point on the edge of the peg
edge of the peg contacts the upper-surface of the area surrounding the hole	as above	as above
edge of the peg contacts side-surface of the hole	as above	as above
edge of the peg contacts the bottom of the hole	as above	as above
side-surface of the peg contacts of the edge of the hole	as above	rotate around the edge of the hole with the same point on the side-surface of the hole

bottom of the peg contacts upper-surface of the area surrounding the hole	as above	rotate around the axis of the peg
bottom of the peg contacts upper-surface of the hole	as above	rotate around the upper-surface of the hole to make same part of the bottom surface of the peg contact the upper-surface of the hole
bottom of the peg contacts bottom of the hole	as above	rotate around the axis of the peg
side-surface of the peg contacts side-surface of the hole	as above	rotate the peg with same straight line on the side-surface of the peg

Table 7 The motion to maintain a static contact point on the peg

In this chapter:-

(i) From Section 3.2, it is found that the force sensor cannot provide the positional relationship between the peg and hole which is necessary in general robotic assembly operations.

(ii) From Sections 3.2 and 3.3, it is found that there are two concepts, one being the centre of the contact area, the other being the centre of the overlap area. They do not coincide with each other. This explains why the relationship between the peg and the hole cannot be provided by the force sensory signals.

(iii) based on the others' researching work in fine motion analysis, the contact configurations which share one set of signals from the force sensors are analysed.

This chapter pointed out that the force sensor cannot provide the total information

to identify the positional relationship between the peg and the hole. The information necessary in the assembly operation may not be as much as that necessary to identify the positional relationship. This means that even though the force sensor cannot provide the information necessary to identify the positional relationship, it is still possible for it to provide the information necessary to guide the adjustment. The question now is whether the force sensor can provide sufficient information to the robotic assembly operation.

CHAPTER 4 ASSEMBLY OPERATION STRATEGY WITH AMBIGUOUS INTERPRETATION OF FORCE SIGNALS

4.0 Introduction

In Chapter 3, it was pointed out that the force sensor can not provide the information with which to judge the contact configurations. The problem is whether the force sensor can provide sufficient information for robotic peg-hole insertion operation.

The information that the force sensor can provide is the location of the contact point. The location of the contact point depends on the positional error, the angular error between the peg and the hole and the defects of the contact surfaces. As analysed in Chapter 3, even if the angle between the axes of the peg and the hole and the defects on the contact surfaces are known, the positional error can not be obtained from the signals from the force sensors. Additionally it is difficult to know how large the rotational error is.

In the approach step, the value of the force sensor provides sampled data. So, only the direction of the deviation, i.e. the signs of $(O_hO_p)_{hx}$ and $(O_hO_p)_{hy}$ are essential. The problem then is reduced to how to obtain these signs from the force signal.

If the sign of the rotational error θ_{hx} is known, the relationship between the sign of the positional error $(O_hO_p)_{hx}$ and the sign of the location of the contact point $(O_hc)_{hx}$ can be obtained. So it is possible to obtain the sign of $(O_hO_p)_{hx}$ from the sign of force sensory signals. The first step, therefore, is designed to rotate the peg to make the sign of the angle θ_{hx} unitary from any initial situation. The new θ_{hx} can also be used to eliminate the influence of the defects of the contact surfaces on the identification of the direction of the positional relationship. Since the direction of the projection $(O_hO_p)_{hx}$ of the positional error is known, the direction of the adjustment to eliminate the projection of the positional error is known. The state where the projection $(O_hO_p)_{hx}$ is eliminated can be identified by the force sensor.

Afterwards, the robot starts to eliminate the other projection $(O_hO_p)_{hy}$ of the positional error. In this chapter, a strategy is proposed to perform the precise robotic peg-hole insertion operation in the presence of ambiguous interpretations of force signals in the positional state.

The basic idea is to divide the insertion process into the following steps:

(a) Approach.

(b) Moving the peg into the new area.

(c) Obtaining $(O_hO_p)_{hx} = 0$, or eliminate the projection of the distance between the centre of the end-surface of the peg and the centre of the upper-surface of the hole along the X_h axis.

(d) Obtaining side-surface contact in the $Y_hO_hZ_h$-plane.

(e) Insertion adjustment.

(f) Insertion.

From the above analysis, it is clear that "*co*" and "*cc*" would not coincide if there is an angle between the axes of the peg and the hole or the contact surfaces are not absolutely smooth, no matter how small these quantities are. Axes alignment and surface defects cause severe practical difficulties in calculating the deviation between the peg and hole, and furthermore influence the insertion operation. In practice, the angle between the axes of the peg and hole and defects of the contact surfaces always exist in varying quantities. The magnitude and even direction of the deviation would be difficult to obtain from the outputs of the force sensors.

4.1 Definitions of the range for initial state of the peg

The initial range for the axis of the peg can be expressed as follows:

parameter	ranges in state 1
θ_{hx}	$[\theta_{hx1n}, \theta_{hx1m}]$
θ_{hy}	$[\theta_{hy1n}, \theta_{hy1m}]$
$(O_hO_p)_{hx}$	$[(O_hO_p)_{hx1n}, (O_hO_p)_{hx1m}]$
$(O_hO_p)_{hy}$	$[(O_hO_p)_{hy1n}, (O_hO_p)_{hy1m}]$

Table 8 An desired range for the initial state of the peg

Furthermore, because this envelope must be symmetric about the hole coordinate axes (X_h, Y_h and Z_h) and the projection of O_p on the hole surface can be defined as a circle, the following definition can be made:

$$\begin{gathered}(O_pO_h)_{hx1n} = (O_pO_h)_{hy1n} = -\epsilon_1 \\ (O_pO_h)_{hx1m} = (O_pO_h)_{hy1m} = \epsilon_1 \\ |O_pO_h| < \varepsilon_1 \\ U_{hx1n} = U_{hy1n} = -K_1 \\ U_{hx1m} = U_{hy1m} = K_1 \\ \theta_{hx1n} = \theta_{hy1n} = -\theta_{h1} \\ \theta_{hx1m} = \theta_{hy1m} = \theta_{h1}\end{gathered} \tag{42}$$

where ε_1, θ_{h1}, and K_1 are constants. The magnitudes of ε_1, θ_{h1} and K_1 depend on the location errors of the peg and the hole generated by the robot. For the insertion process to be successful, there is a requirement for these parameters to be constrained. The insertion can then be realized when the actual values are smaller than required values.

The peg-hole configuration at the initial state can be described in the $X_hO_hZ_h$ and $Y_hO_hZ_h$ planes:

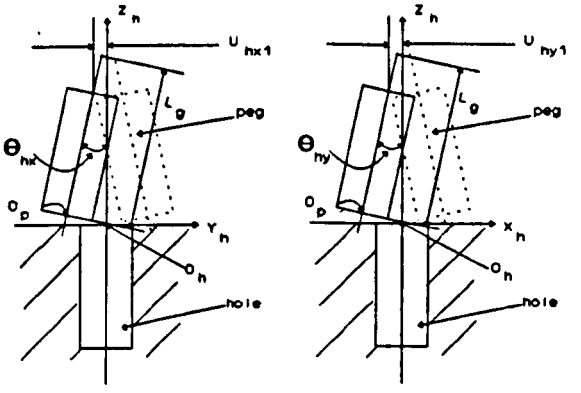

Fig. 25 Initial configuration of peg and hole system

The peg axis location envelope can be presented in 3_D space:

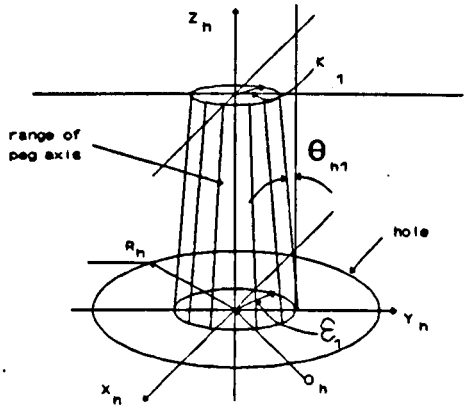

Fig. 26 Envelope of peg axis uncertainty in the initial state

4.2 Gross movement of the peg from the initial state to the second state

At this stage the peg is established as being close to the hole inside an envelope described by angular and lateral errors. The next step is to move and rotate the peg to a new area. Combining the conditions for the second state and the character of the first state, the conditions of the first state and the adjustment from the first state to the second state for successful assembly can be generated.

The general description for the second state is that:

(a) The end-surface centre of the peg must be in one quadrant of the coordinate which is fixed on the hole, no matter where it exactly is.

(b) The lowest point of the peg must be inside the hole.

If the projection of the lowest point of the peg in $X_hO_hY_h$ plane is defined as "G", then:

$$O_hG = O_hO_p' + \frac{\theta}{|\theta|}R_p\cos|\theta| \tag{43}$$

where O_hO_p', θ, and O_hG are three vectors and O_p' is the projection of O_p on the horizontal plane. If the length of O_hG is less than R_h, i.e.

$$|O_hG| < R_h \tag{44}$$

the lowest point must be inside the hole.

If the peg is rotated $\Delta\theta_{hx2}$ around X_h axis and satisfies:

$$\pi/2 > |\theta_{hx2}| > |\theta_{hy2}| \tag{45}$$

and

$$|O_pO_h|_2 \leq R_h \tag{46}$$

then there are two possibilities for the lowest point of the peg in the hole:

(a)

$$\begin{aligned} (O_pO_h)_{hx2} &\le 0, \\ \theta_{hx2} &\le 0 \end{aligned} \tag{47}$$

(b)

$$\begin{aligned} (O_pO_h)_{hx2} &\ge 0, \\ \theta_{hx2} &\ge 0 \end{aligned} \tag{48}$$

The relationship between the first and the second states can be presented as follows:

$$\begin{aligned} (O_pO_h)_{hx2} &= (O_pO_h)_{hx1} \\ (O_pO_h)_{hy2} &\approx (O_pO_h)_{hy1} + \Delta Y_2 + L_g \sin\Delta\theta_{hx2} \\ \theta_{hx2} &= \theta_{hx1} + \Delta\theta_{hx2} \\ \theta_{hy2} &= \theta_{hy1} \end{aligned} \tag{49}$$

where ΔY_2 is the translational movement along Y_h axes, and $\Delta\theta_{hx2}$ is the rotation around X_h axis. So the extreme values of the second state can be presented according the extreme value of the first state and the adjustment:

$$\begin{aligned} (O_pO_h)_{hx2n} &= -\epsilon_1 \\ (O_pO_h)_{hx2m} &= \epsilon_1 \\ (O_pO_h)_{hy2n} &\approx -\epsilon_1 + \Delta Y_2 + L_g \sin\Delta\theta_{hx2} \\ (O_pO_h)_{hy2m} &\approx \epsilon_1 + \Delta Y_2 + L_g \sin\Delta\theta_{hx2} \\ \theta_{hx2n} &= -\theta_{h1} + \Delta\theta_{hx2} \\ \theta_{hx2m} &= \theta_{h1} + \Delta\theta_{hx2} \\ \theta_{hy2n} &= -\theta_{h1} \\ \theta_{hy2m} &= \theta_{h1} \end{aligned} \tag{50}$$

If the first possibility of the peg location, described in Eq. 47, is selected, then:

$$\begin{aligned} (O_pO_h)_{hy2m} &= 0 \\ (O_pO_h)^2_{hx2} + (O_pO_h)^2_{hy2} &\le R_h^2 \\ -\pi/2 < \theta_{hx2n} &< -\theta_{h1} \\ \theta_{hx2m} &< 0 \\ \theta_{hy2n} &= -\theta_{h1} \\ \theta_{hy2m} &= \theta_{h1} \end{aligned} \tag{51}$$

The corresponding area for the peg axis is shown in Fig. 27 below:

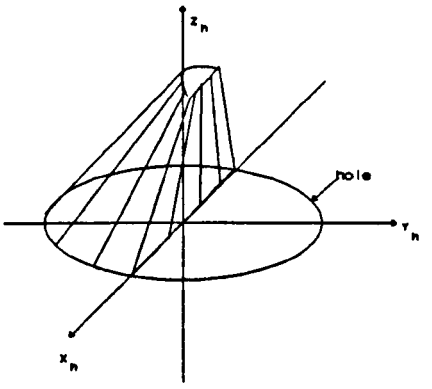

Fig. 27 Required range for the peg axis in the second state

The rotational angle $\Delta\theta_{hx2}$ (Eq. 49) is a designable parameter,

$$|\Delta\theta_{hx2}| = pp|\theta_{h1}| \tag{52}$$

where pp can be selected from a value around 10. Here pp is designed as 12, which causes the peg to lean at a great angle in the $Y_hO_hZ_h$ plane. If the initial state range of the projection of O_p on $X_hO_hY_h$ is assumed to be a circle with radius of ε_1 (see Fig. 26),

$$(O_hO_p)^2_{hx1} + (O_hO_p)^2_{hy1} \le \epsilon_1^2 \tag{53}$$

then the second state range is also a circle with the same radius, but different locations:

$$[(O_pO_h)_{hx2}]^2 + [(O_pO_h)_{hy2} - \Delta Y_2 - L_g\sin\Delta\theta_{hx2}]^2 \le \epsilon_2^2 \tag{54}$$
$$\epsilon_2 = \epsilon_1$$

The location of the centre of the end-surface of the peg O_p in the second state, shown in Fig. 27, must satisfy the quadrant identified in Fig. 28:

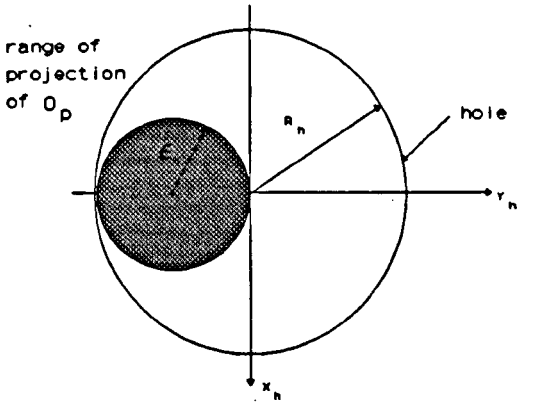

Fig. 28 Range of projection of O_p in the second state

So the maximum value of ϵ_2, is unchanged from the first state and, is related to the hole size:

$$\epsilon_{2m} = \epsilon_{1m} = \frac{R_h}{2} \tag{55}$$

This establishes the initial state conditions for successful assembly:

(a) The projection of the end-surface centre of the peg, O_p, must lie within a circle of radius:

$$\epsilon_{1m} = \frac{R_h}{2} \tag{56}$$

(b) The projection of the upper-surface centre of the peg must lie within a circle of radius:

$$K_{1m} \approx \epsilon_{1m} - L_g \sin\theta_{h1} \tag{57}$$

(c) θ_{h1} must satisfy the limits:

$$0 < \theta_{h1} < \pi/26 \tag{58}$$

where the angle is given by:

$$\theta_{hx2n} = -\theta_{h1} + \Delta\theta_{hx2} = -\theta_{h1} - 12\theta_{h1} = -13\theta_{h1}$$
$$\theta_{hx2n} < -\pi/2$$
$$\theta_{hx2m} = \theta_{h1} + \Delta\theta_{hx2} = \theta_{h1} - 12\theta_{h1} = -11\theta_{h1} \qquad (59)$$
$$\theta_{hx2m} < 0$$

The condition for the adjustment can be concluded as follows:

The translation along Y_h axis caused by the angle $\Delta\theta_{hx2}$ is:

$$Y_0 = L_g[\sin(\theta_{h1} + \Delta\theta_{hx2}) - \sin\theta_{h1}] \approx L_g \sin\Delta\theta_{hx2} \qquad (60)$$

The movements along X_h and Y_h axes to realize the second situation can be in a range of:

$$\epsilon_1 - L_g\sin\Delta\theta_{hx2} < -\Delta Y_2 < -\frac{R_h}{2} - L_g\sin\Delta\theta_{hx2} \qquad (61)$$

This can be concluded in the following figure:

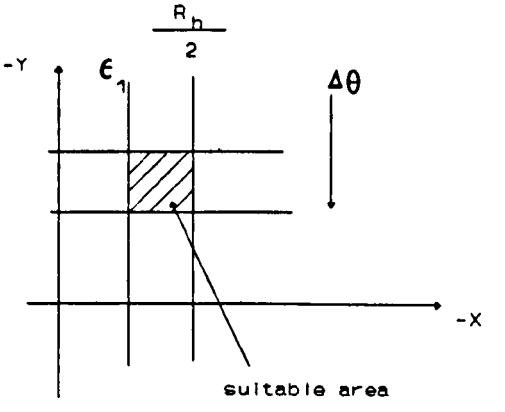

Fig. 29 Relation among R_h, ε_1, $\Delta\theta_{hx2}$, ΔX_2 and ΔY_2

So, the smaller ε_1 is, the greater is the range for ΔY_2. The general envelope for the peg axis in the second state can be presented as follows:

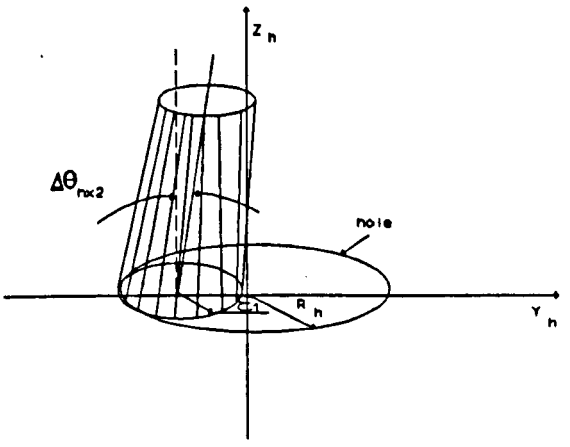

Fig. 30 Orientation of the peg axis envelope after the second state

4.3 The range for the second state of the peg

The range for the second state is in the following table:

	ranges in state 2
θ_{hx}	$[\theta_{hx2n}, \theta_{hx2m}]$
θ_{hy}	$[\theta_{hy2n}, \theta_{hy2m}]$
$(O_hO_p)_{hx}$	$[(O_hO_p)_{hx2n}, (O_hO_p)_{hx2m}]$
$(O_hO_p)_{hy}$	$[(O_hO_p)_{hy2n}, (O_hO_p)_{hy2m}]$

Table 9 A designed range for the second state of the peg

At this stage, the peg-hole configuration satisfies:

$$\begin{gathered} -\pi/2 < \theta_{hx2} < -\theta_{h1} \\ -\theta_{h1} < \theta_{hy2} < \theta_{h1} \\ |\theta_{hx2}| > |\theta_{hy2}| \\ (O_pO_h)_{hx}^2 + (O_pO_h)_{hy}^2 \le R_h^2 \\ (O_hO_p)_{hy2} < 0 \end{gathered} \tag{62}$$

The key problem reduces to identifying the sign of $(O_hO_p)_{hx}$ in the new situation. The projections of the end-surface of the peg and the area surrounding the hole on $X_hO_hY_h$ plane are shown in Fig. 31,

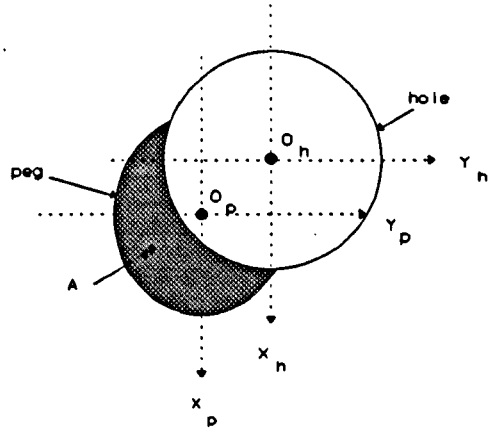

Fig. 31 Projection of contact surface on $X_hO_hY_h$ plane

The projection of the contact area of the end-surface of the peg and the area surrounding the hole must belong to the sectioned area. The equation for a point in the sectioned area is:

$$\begin{aligned} (A_{hx})^2 + (A_{hy})^2 &\geq R_h^2 \\ \sin^2\theta_{hx}(A_{hx} - (O_p)_{hx})^2 + (A_{hy} - (O_p)_{hy})^2 &\leq R_p^2\sin^2\theta_{hx} \end{aligned} \tag{63}$$

where "A" is the arbitrary point whose projection is in the sectional area, as presented in Fig. 31. Then:

$$A_{hz} - (O_p)_{hz} = A_{py}\sin\theta_{hx} \tag{64}$$

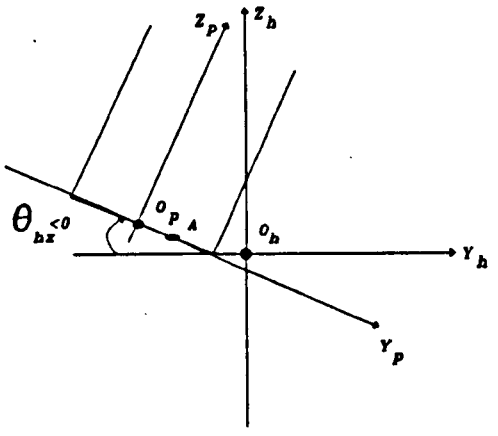

Fig. 32 Point whose projection in sectioned line area

The contact point must be the point in the sectioned area with the minimum projection along Z_h axis, i.e

$$(cc)_{hz} = \min A_{hz} \tag{65}$$

So the contact point must be the point in the sectioned area with the maximum projection along Y_p axis,

$$(cc)_{py} = \max A_{py} \tag{66}$$

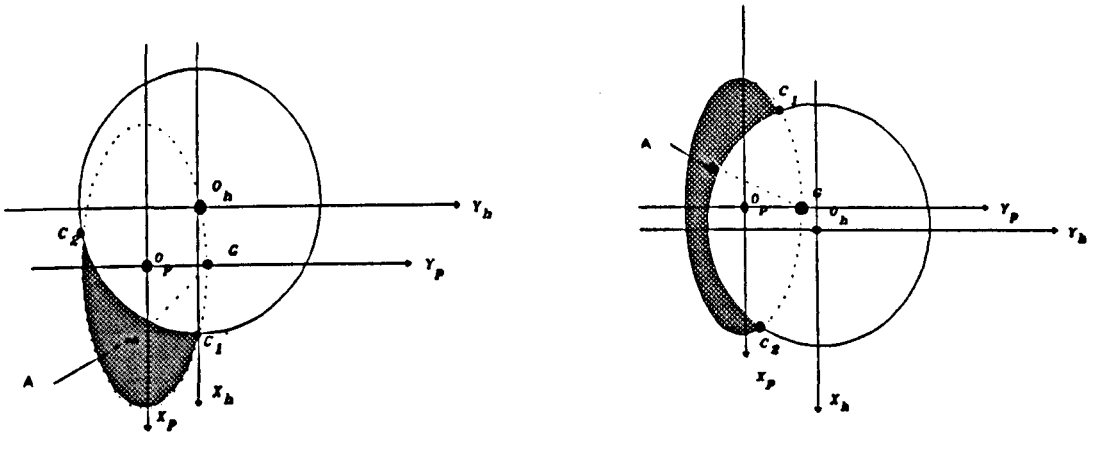

Fig. 33 The projections of the contact surfaces with different locations

For any point in the sectioned area and not along the circumference of the hole, the

line joining G and A, where G is the lowest point of the peg, must be through a point whose projection is on the circumference of the hole. This point must be lower than point A along the Z_h axis. So the contact point must be along the circumference of the hole. For the arc C_1C_2, because the lowest point is inside the hole, so the contact point must be points C_1 or C_2 or both of them.

If the peg is imagined as being rotated to make $\theta_{hx} = 0$, then the projections of the peg and the hole can be expressed as follows:-

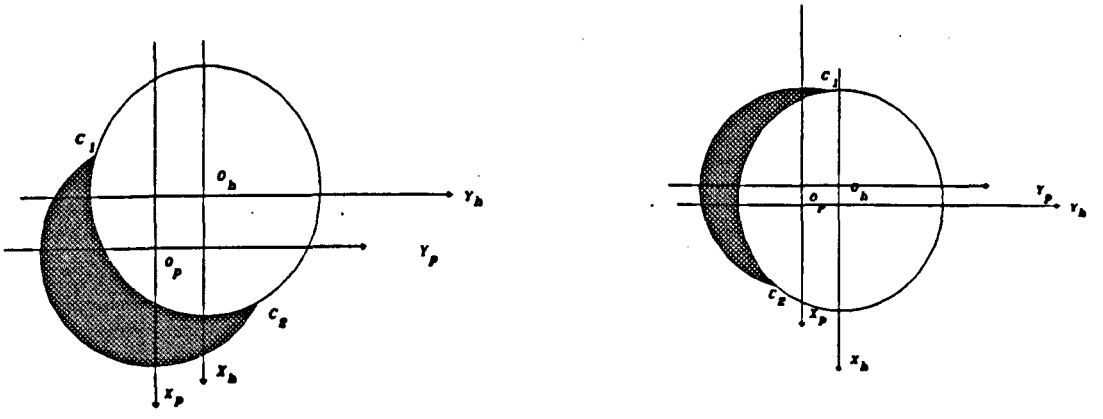

Fig. 34 The projections of the contact surfaces with imagined rotation

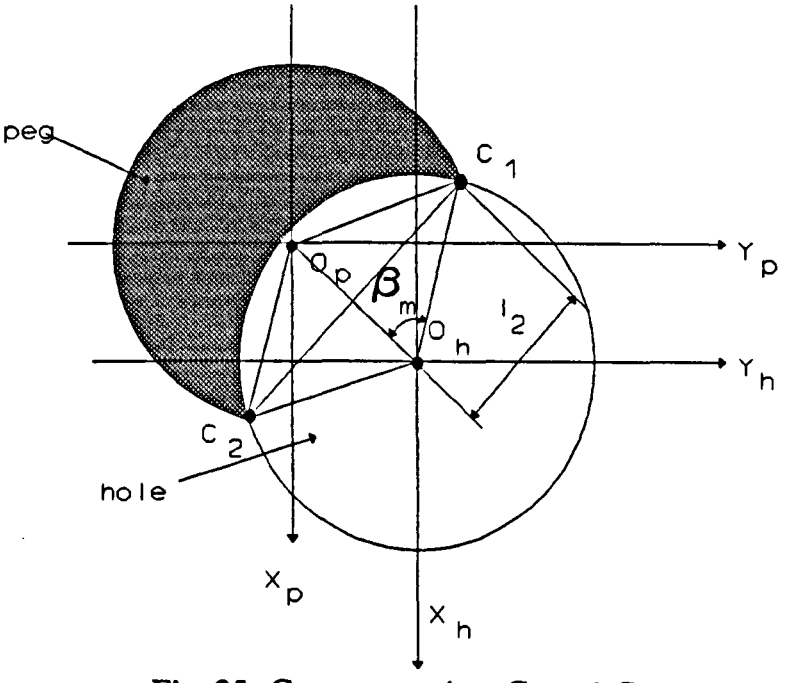

Fig. 35 Common points C_1 and C_2

Defining α, α_1 and α_2 as angles from X_h axis to O_hO_p, O_hC_1 and O_hC_2, respectively, then:

$$\begin{aligned} \alpha_1 &= \alpha - \beta_m \\ \alpha_2 &= \alpha + \beta_m \end{aligned} \tag{67}$$

where β_m is the angle between O_hO_p and O_hC_1 and $\beta_m \in [0, \pi/2]$.

The coordinates of C_1 and C_2 along Y_p axis can be obtained as follows:

$$\begin{aligned} (C_1)_{py2} &= (C_1)_{hy2} - (O_p)_{hy2} = R_h\sin\alpha_1 - (O_p)_{hy2} \\ &= R_h(\sin\alpha\ \cos\beta_m - \cos\alpha\ \sin\beta_m) - (O_p)_{hy} \\ (C_2)_{py2} &= (C_2)_{hy2} - (O_p)_{hy2} = R_h\sin\alpha_2 - (O_p)_{hy2} \\ &= R_h(\sin\alpha\ \cos\beta_m + \cos\alpha\ \sin\beta_m) - (O_p)_{hy2} \end{aligned} \tag{68}$$

Because

$$(O_p)_{hy2} < 0 \tag{69}$$

If $(O_p)_{hx2} < 0$,

$$\begin{aligned} \pi < \alpha < \frac{3}{2}\pi \\ \cos\alpha < 0 \end{aligned} \tag{70}$$

Then $(C_1)_{py2} > (C_2)_{py2}$. So, C_1 is the contact point.

If $(O_p)_{hx2} > 0$,

$$\begin{aligned} \frac{3}{2}\pi < \alpha < 2\pi \\ \cos\alpha > 0 \end{aligned} \tag{71}$$

Then $(C_2)_{py2} > (C_1)_{py2}$. So, C_2 is the contact point. Because O_p must be in the following circle,

$$x^2 + (y + \frac{R_h}{2})^2 \le \frac{R_h^2}{4} \tag{72}$$

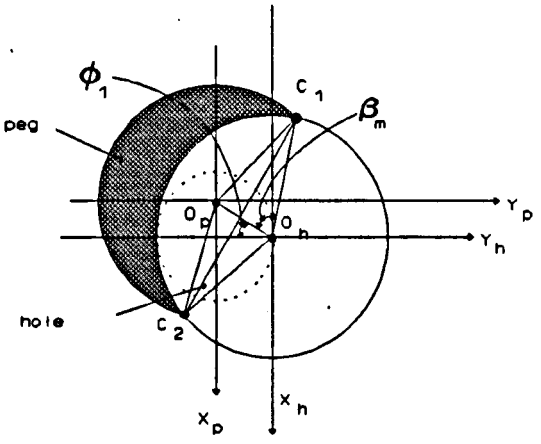

Fig. 36 ϕ_1 and β_m

If the angle between Y_h axis and O_hO_p is defined as ϕ_1, then:

$$\cos\phi_1 < = \frac{|O_hO_p|}{R_h}$$
$$\cos\beta_m = \frac{|O_hO_p|}{2R_h} \tag{73}$$

so $cos\phi_1 > cos\ \beta_m$.

Due to,

$$0 < \phi_1 < \pi/2$$
$$0 < \beta_m < \pi/2 \tag{74}$$

ϕ_1 is always smaller than β_m. So the following equation is always satisfied that:

$$(C_1)_{hx2} < (O_p)_{hx2} \tag{75}$$

or

$$(C_1)_{px2} < 0 \tag{76}$$

Similarly, it can be proven that:

$$(C_2)_{px2} > 0 \tag{77}$$

So, if $(O_p)_{hx2} < 0$,

$$(cc)_{px} = (C_1)_{px} < 0 \tag{78}$$

If $(O_p)_{hx2} > 0$,

$$(cc)_{px} = (C_2)_{px} > 0 \tag{79}$$

Because the rotation around the X_h axis does not change the coordinates along X_h and X_p axes and the orders of the coordinates along Y_p and Y_h axes, all the conclusions are true in the case when $\theta_{hx} \neq 0$.

4.4 Two point contact between the peg and hole

The next step is to move the peg parallel to X_h-axis. The movement begins with one contact point and ends when there are two. Two point contact configuration can be depicted as follows:

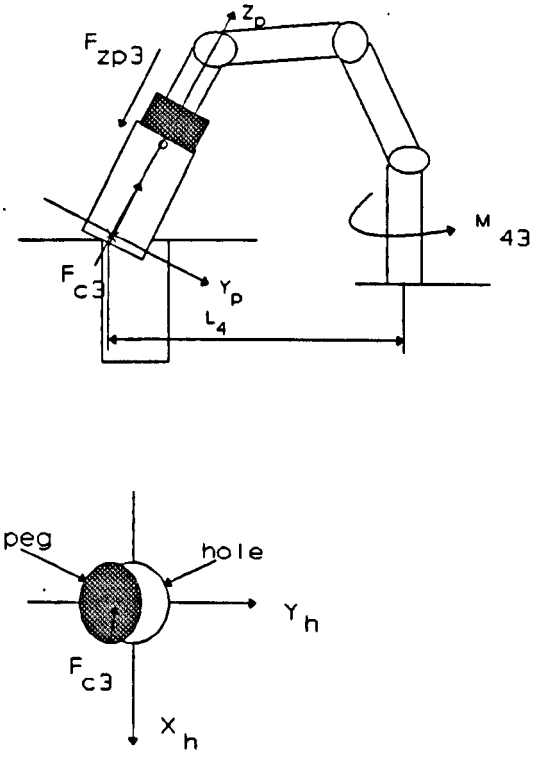

Fig. 37 Two point contact configuration

where F_{c3} is the contact force between the peg and hole, L_4 is the projection of connection line joining the contact point and the base of the robot parallel to the Y_h axis and M_{43} is the torque developed by the robot base actuator. F_{zp3} must be provided by a combination of linkages which may influence the peg location.

This motion can be accomplished in two steps:

Step 1: The base of the robot is rotated to move the centre of the peg towards Y_h axis.

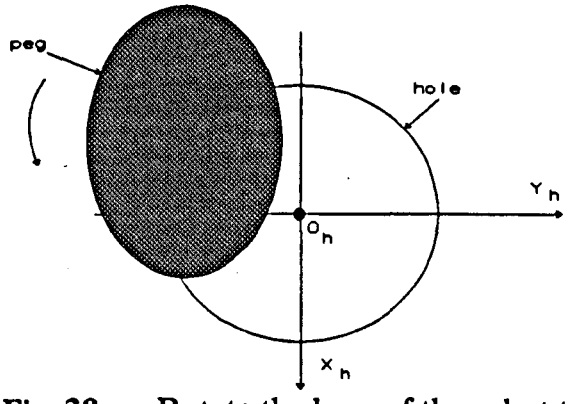

Fig. 38 Rotate the base of the robot to approach to Y_h axis

The sign of the $(O_hO_p)_{hx}$, which is same as that of $(cc)_{px}$ can be obtained from the force sensor. Then the control to make $(O_hO_p)_{hx}$ small is available.

When $|(O_hO_p)_{hx}|$ gets small, the absolute value of the torque M_{py} exerted through the centre of the force sensor would get bigger. This phenomenon arises when the centre of the end-surface of the peg moves to Y_h axis, the contact point on the end-surface of the peg moves a great distance from Y_p.

Step 2: Rotation would cease when there are two contact points,

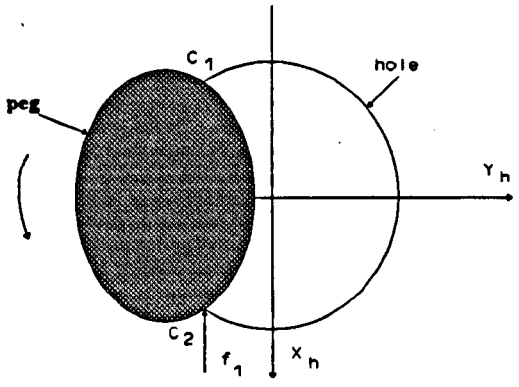

Fig. 39 Rotation ceases when there are two contact points

where C_1 and C_2 are two contact points between the end-surface of the peg and upper-surface of the hole. When the two contact points C_1 and C_2 are symmetric to Y_h axis, the torque exerted through the wrist force sensor would drop to zero. The robot is then controlled to be fixed at that point.

The goal of this step is to move O_p towards the Y_h axis. The problem is the size of $(O_hO_p)_{hx}$ when there are two contact points. If $\theta_{hy} = 0$, and θ_{hx} is not equal to zero, O_p touches the Y_h axis in this step. In most cases, θ_{hy} is not zero. If projections of θ on the $X_hO_hZ_h$ and $Y_hO_hZ_h$ planes θ_{hy} and θ_{hx} are presented as vectors, the angle θ can be expressed as:

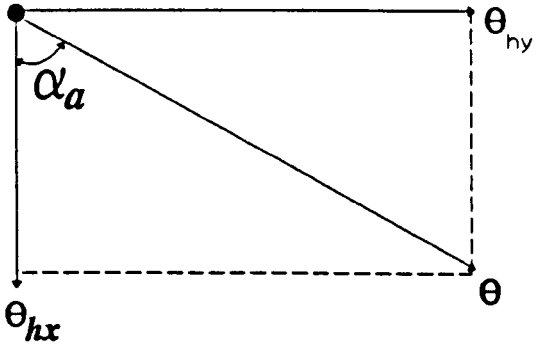

Fig. 40 Angle between contact surfaces

The angle between the vector θ and θ_{hx} is

$$\alpha_a = \arctan\frac{\theta_{hx}}{\theta_{hy}} \tag{80}$$

The magnitude of angle θ is

$$|\theta| = \sqrt{\theta_{hx}^2 + \theta_{hy}^2} \tag{81}$$

The projections of the end-surface of the peg and the upper-surface surrounding the hole with an angle of θ can be expressed as follows:

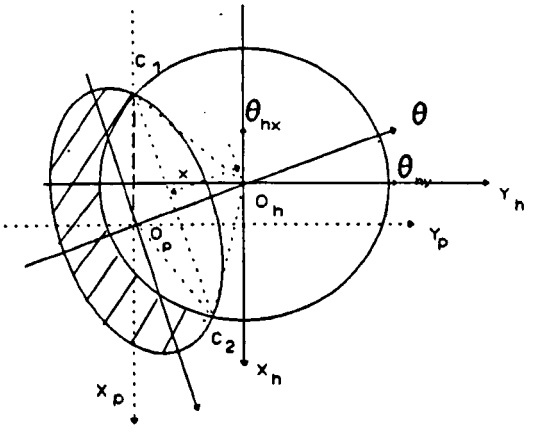

Fig. 41 Projections of contact surfaces with two point contact

where x is the distance between O_h and line segment C_1C_2. The projection of the end-surface of the peg is an ellipse, where the major axis is along the direction of θ with length of $2R_p$, and the length of the minor axis is $2R_p \cos\theta$. The key feature of the two-contact point state is that, the minor axis of the ellipse must pass through the upper-surface hole centre. This conclusion can be explained as follows. Both of C_1 and C_2 are on the $X_hO_hY_h$ plane, so

$$(C_1)_{hz} = (C_2)_{hz} \tag{82}$$

or

$$(C_1C_2) \;//\; plane\; X_hO_hY_h \tag{83}$$

On the other hand, (C_1C_2) belongs to $X_hO_hY_h$ plane, which can be obtained from Eq. 83 that:

$$(C_1C_2) \;//\; major\; axis \tag{84}$$

So C_1 and C_2 are symmetric about the minor axis of the ellipse. They are also symmetric about one radius of the hole. As a result, the minor axis of the ellipse coincides with a radius of the hole. The minor axis of the ellipse is through the upper-surface centre of the hole.

If the distance between the line joining C_1, C_2 and O_h is defined as x, then:

$$\begin{aligned}(O_pO_h)_{hx3} &= [x\cos\theta + x]\cos(\arctan\frac{\theta_{hx3}}{\theta_{hy3}}) \\ (O_pO_h)_{hy3} &= [x\cos\theta + x]\sin(\arctan\frac{\theta_{hx3}}{\theta_{hy3}})\end{aligned} \tag{85}$$

Expressing these as a ratio:

$$\frac{(O_pO_h)_{hx3}}{(O_pO_h)_{hy3}} = \frac{1}{\tan(\arctan\frac{\theta_{hx3}}{\theta_{hy3}})} = \frac{\theta_{hy3}}{\theta_{hx3}} \tag{86}$$

Since

$$|\theta_{hx3}| > |\theta_{hy3}| \tag{87}$$

and

$$|(O_pO_h)_{hx3}| < |(O_pO_h)_{hy1} + \Delta Y_2 + L_g\sin\Delta\theta_{hx2}| \tag{88}$$

then the range for the deviation of the centre of end-surface of the peg can be expressed as follows:

$$(O_pO_h)_{hx3} = \frac{\theta_{hy3}}{\theta_{hx3}}(O_pO_h)_{hy3} \tag{89}$$

$$[(O_pO_h)_{hy3} - \Delta Y_2 - L_g \sin\Delta\theta_{hx2}]^2 + [(O_pO_h)_{hx3}]^2 \le \epsilon_1^2$$

The range for the centre of the end-surface of the peg can be shown in the following figure:-

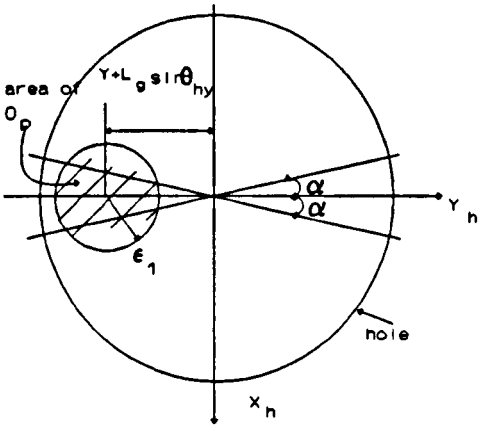

Fig. 42 Area of O_p in $X_hO_hY_h$-plane with two contact points

Here

$$\begin{aligned} \alpha &= \arctan[\max(\frac{|\theta_{hy3}|}{|\theta_{hx3}|}] \\ &= \arctan(\frac{\max|\theta_{hy3}|}{\min|\theta_{hx3}|}) \end{aligned} \tag{90}$$

and

$$\theta_{hx3} = \theta_{hx1} + \Delta\theta_{hx2} \tag{91}$$

$$-\theta_{h1} \le \theta_{hy3} \le \theta_{h1} \tag{92}$$

where

$$\begin{aligned} -\theta_{h1} \le \theta_{hx1} \le \theta_{h1} \\ \Delta\theta_{hx2} = 12\theta_{h1} \end{aligned} \tag{93}$$

Substituting Eq. 93 into Eq. 91, then:

$$-13\theta_{h1} \leq \theta_{hx3} \leq 11\theta_{h1}$$
$$13\theta_{h1} \geq |\theta_{hx3}| \geq 11\theta_{h1} \tag{94}$$

Substituting Eq. 94 and Eq. 92 into Eq. 90:

$$\alpha = \arctan(\frac{1}{11}) \tag{95}$$

4.5 Achievement of side-surface contact between the peg and hole

At this stage in the process, $(O_hO_p)_{hx3}$ is nearly zero and $(O_hO_p)_{hy3}$ is uncertain. Achieving peg side surface contact in $Y_hO_hZ_h$ plane with the edge of the hole, by moving along the Y_h-axis, will enable the final insertion to be completed.

This can be depicted in Fig. 43:

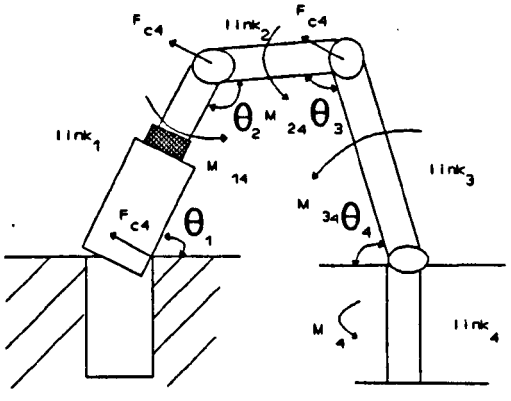

Fig. 43 Side surfaces contact

where: the angles between the links are given by:

- θ_1 the link 1 and the hole surface,
- θ_2 axes of link 1 and link 2,
- θ_3 axes of link 2 and link 3,
- θ_4 link 3 and hole surface.

and:

M_{14}, M_{24}, M_{34} and M_{44} are the moments supported by link 1, link 2, link 3 and link 4, respectively.

F_{c4} is the contact force between the peg and the hole.

When $|(O_hO_p)_{hy}|$ gets small, the two contact points between the peg and hole, which are symmetric to the axis Y_p, would drift away from the centre of the hole O_h, so the torque around the X_h axis is increased. The torque around X_h axis drops to zero when a third contact point C_3 is created.

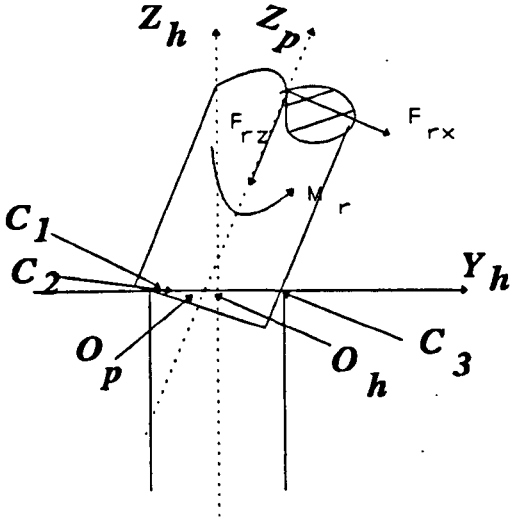

Fig. 44 Configuration of the peg and hole when there are three contact points

The most suitable adjustment is to rotate the last link of the robot to reduce $|\theta_{hx}|$ and leave other links free from the control. Small forces F_{rz} and F_{rx} are necessary to maintain the three contact points. When $|\theta_{hx}|$ is small enough, F_{pz} drops to zero. At this time, insertion starts.

4.6 Peg-hole insertion operation

After the peg is inside the hole, the way to realize the insertion is to push down the

peg and at the same time rotate the peg around X_h axis in $Y_hO_hZ_h$ plane according to the signal from the force sensors.

In this chapter, a strategy with a limited initial state was achieved, which was based on the Cartesian coordinate system. The strategy was to move the initial envelope of the axis of the peg into a new area where the signal from the force sensor is related to the deviation of the peg and the hole. There are several points in common with other researcher's method. However it was shown for the first time that the force sensor can not provide the positional relationship between the peg and the hole due to the influences of the rotational errors and the contact surface defects. It was also the first time that the initial rotation was set up to eliminate the influences of the initial rotational error and the defects. Finally, it was the first time that $(O_hO_p)_{hx} = 0$ was achieved by using two point contact state. The first part of this thesis has now been completed.

CHAPTER 5 ASSEMBLY OPERATION STRATEGY WITHOUT FORCE SENSORS

5.0 Introduction

In the first part of this thesis:-

(1) the problem in the presentation of the positional relationship between the peg and the hole using force sensors was pointed out,

(2) the factors which influence the identification of the positional relationship between the peg and the hole using force sensors were provided, while

(3) a strategy which performs precise assembly operation with the problem in using force sensors was provided. The allowed initial range for the peg was obtained and the applied forces and moments from the robot to the peg were designed.

If the first strategy is analysed deeply, it can be found that the force sensor was seldom used:-

(a) It was used at the beginning of the second step to identify the sign of the projection $(O_hO_p)_{hx}$ of the displacement between the peg and the hole along the X_h axis,

(b) It was used to identify whether the system is in the state where $(O_hO_p)_{hx} = 0$ where M_{hy} changes to be zero,

(c) It was used to identify whether the side-surface of the peg touches that of the hole where M_{hx} changes to be zero and,

(d) It was used to identify if the peg has been inserted into the hole.

If all of these functions can be replaced through the use of the environment and time, it is possible to perform precise insertion operation without force sensor or RCC. In this chapter, a strategy to achieve the precise assembly operation without force senors or RCC is provided.

The basic strategy can be divided into the following states (see Fig. 45):

(a) Initial inherited state,

(b) Moving the peg towards one quadrant where the lowest point of peg must be in the hole,

(c) Obtaining two contact points and O_p close to $Y_hO_hZ_h$ plane,

(d) Moving to get side-surface contact in $Y_hO_hZ_h$-plane,

(e) Insertion adjustment,

(f) Final insertion.

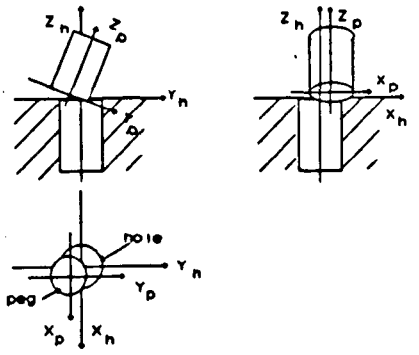

Step 1: Initial inherited state

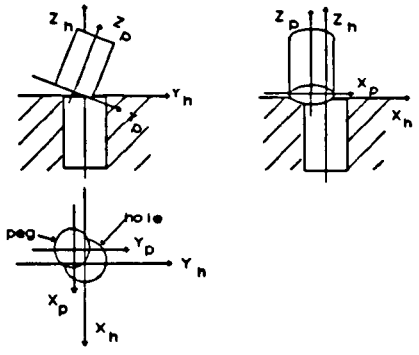

Step 2: New area

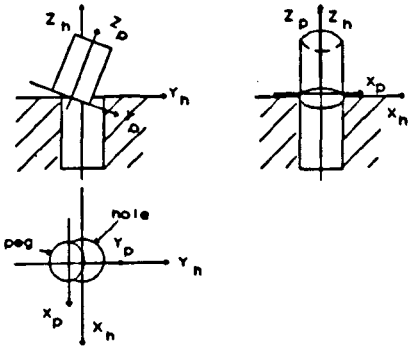

Step 3: Two point contact

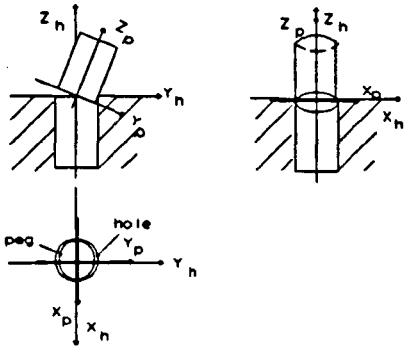

Step 4: Side contact

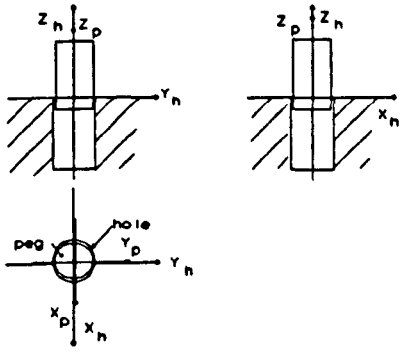

Step 5: Insertion adjustment

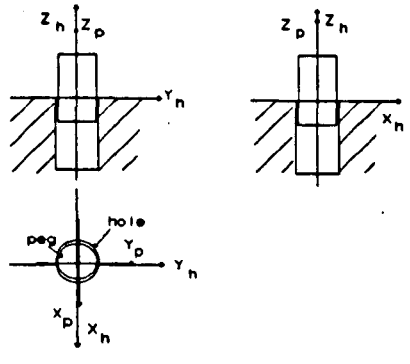

Step 6: Final insertion

Fig. 45 States in the strategy without force sensors

The initial inherited state expressed in Fig. 45 is only one of the many possibilities for the initial state.

5.1 Initial inherited state definition

The uncertain lateral and angular errors ($(O_hO_p)_1$, U_1, θ_{hx1} and θ_{hy1},) establish a 3-dimensional envelope for the peg axis in the initial state which can be defined as follows:

$$\begin{aligned} |(O_hO_p)_1| &< \varepsilon_1 \\ |U_1| &< K_1 \\ \theta_{hx1} &\le \theta_{h1} \\ \theta_{hy1} &\le \theta_{h1} \end{aligned} \qquad (96)$$

where ε_1, θ_{h1}, and K_1 are constants, and where $(O_hO_p)_1$ is the directed line from O_h to O_p at the first step. The magnitudes of ε_1, θ_{h1} and K_1 depend on the initial location errors of the peg and the hole. For the insertion process to be successful, there is a requirement for these parameters to be constrained to predetermined limits. The insertion can then be achieved when the actual values are smaller than these values which are carefully selected to ensure success.

The envelope of the peg axis can be presented in 3_D space (see Fig. 46).

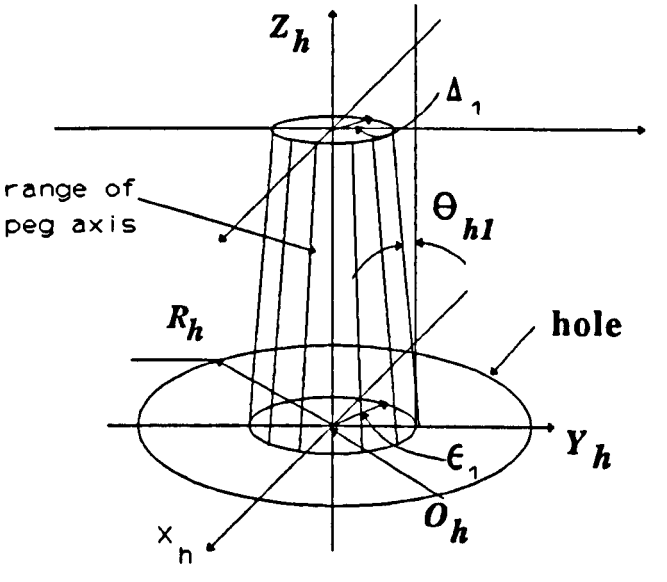

Fig. 46 Envelope of peg axis uncertainty in the initial state

5.2 Movement of peg to a new area

At this stage the peg is established as being close to the hole inside an envelope describing angular and lateral errors. The next step is to move and rotate the peg into a new area. The adjustments rely on the nature of the first state.

The demands for the second state can be described as follows:

$$\begin{gathered}(O_hO_p)_{hx2}\le 0\\(O_hO_p)_{hy2}\le 0\\|(O_hO_p)_2|\le R_h\\-\pi/2\le\theta_{hx2}\le-\theta_{h1}\\|\theta_{hy2}|\le\theta_{h1}\end{gathered}\qquad(97)$$

The corresponding area for the peg axis is shown in Fig. 47.

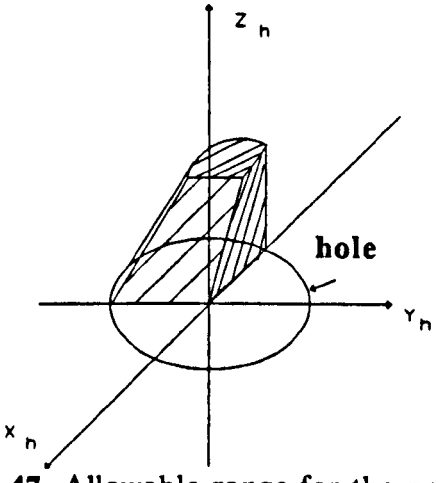

Fig. 47 Allowable range for the peg axis in the second state

The relationship between the first and the second states can be presented as follows:

$$\begin{gathered}(O_hO_p)_{hx2}=(O_hO_p)_{hx1}+\Delta X_{h2}\\(O_hO_p)_{hy2}\approx(O_hO_p)_{hy1}+\Delta Y_{h2}+L_g\sin\Delta\theta_{hx2}\\\theta_{hx2}=\theta_{hx1}+\Delta\theta_{hx2}\\\theta_{hy2}=\theta_{hy1}\end{gathered}\qquad(98)$$

where ΔX_{h2} and ΔY_{h2} are the translational movements along the X_h and Y_h axes, respectively, and $\Delta\theta_{hx2}$ is the rotation around the X_h axis. Substituting Equ. 98 into

Equ. 97 and using Equ. 96, the conditions for the adjustment (ΔX_{h2}, ΔY_{hy2}, $\Delta\theta_{hx2}$) and for the initial inherited state (ε_1, K_1, θ_{h1}) can be obtained as follows:

(1) The conditions for the first state:

(a) The projection of the end-surface centre of the peg, O_p, must lie within a circle of radius (see *Appendix 1*):

$$\varepsilon_1 \leq \frac{R_h}{\sqrt{2}+1} \tag{99}$$

(b) The projection of the upper-surface centre of the peg must lie within a circle of radius:

$$K_1 \leq \frac{R_h}{\sqrt{2}+1} - L_g \sin\theta_{h1} \tag{100}$$

(c) θ_{h1} must satisfy the inequality according to Equs. 96, 97 and 98:

$$0 < \theta_{h1} < \frac{\pi}{2(k_a+1)} \tag{101}$$

where k_a is an constant with $k_a >> 1$. k_a should be at least *4*, so,

$$0 < \theta_{h1} < \frac{\pi}{10} \tag{102}$$

The initial error range of this method which can achieve the peg-hole (diameters are about 32 mm) insertion with 6 mm initial error range compares favourably with other methods, utilizing RCC and force sensors, which offer between 0.2 mm and 3 mm (8).

(2) The condition for the adjustment:

(a) The rotational angle $\Delta\theta_{hx2}$ is a designable parameter, which can be:

$$-\frac{\pi}{2}+\theta_{h1}<\Delta\theta_{hx2}<-4\theta_{h1} \tag{103}$$

This causes the peg to tilt at a great angle in the $Y_hO_hZ_h$ plane.

(b) The movements along the X_h and Y_h axes to realize the second situation can be in a range of:

$$\begin{aligned} \varepsilon_1 &< -\Delta X_{h2} < \frac{R_h}{\sqrt{2}+1} \\ \varepsilon_1 + L_g \sin\Delta\theta_{hx2} &< -\Delta Y_{h2} < \frac{R_h}{\sqrt{2}+1} + L_g \sin\Delta\theta_{hx2} \end{aligned} \tag{104}$$

This can be summarised in Fig. 48.

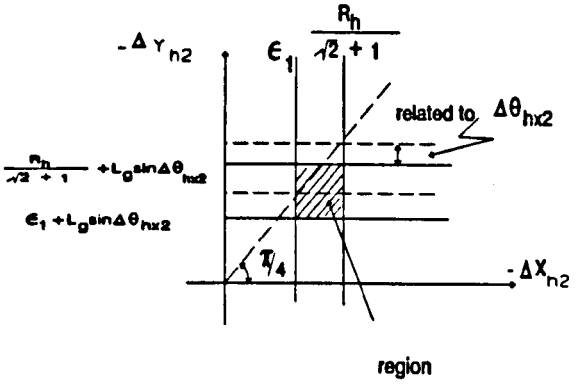

Fig. 48 Relation among R_h, ε_1, $\Delta\theta_{hx2}$, ΔX_{h2} and ΔY_2 giving the solution to ΔX_{h2} and ΔY_{h2}

So, the smaller θ_{h1}, K_1 and ε_1 are, the greater is the range for θ_{hx2}, ΔX_{h2} and ΔY_{h2}. The general envelope for the peg axis in the second state, which is inside the demands for the second state and has the same uncertainties as the first state, can be presented as in Fig. 49.

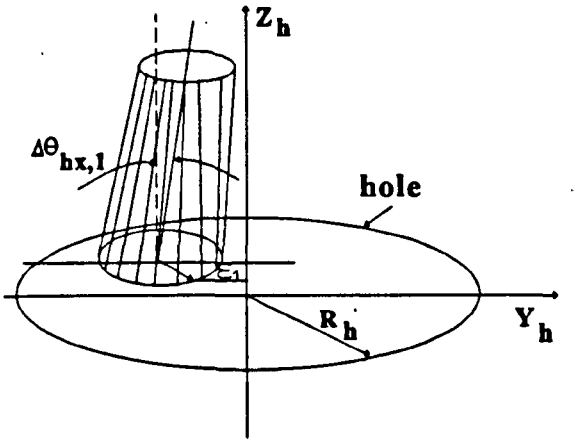

Fig. 49 Orientation of the peg axis envelope after the second state

5.3 Movement to the two point contact phase (moving the centre of the end-surface of the peg close to the Y_h axis)

At this stage, the peg-hole configuration satisfies:

$$\begin{gathered}(O_hO_p)_{hx2} < 0 \\ (O_hO_p)_{hy2} < 0 \\ [(O_hO_p)_{hx2} - \Delta X_{h2}]^2 + [(O_hO_p)_{hy2} - \Delta Y_{h2} - L_g \sin\Delta\theta_{hx2}]^2 \le \epsilon_2^2 \\ -\pi/2 < \theta_{hx2} < -\theta_{h1} \\ |\theta_{hy2}| < |\theta_{h1}|\end{gathered} \tag{105}$$

The next step is to move the peg parallel to X_h-axis to reduce $(O_hO_p)_{hy2}$. The movement begins with one contact point and ends when there are two. The angle between the axes of the peg and hole θ_{hx3} and $(O_hO_p)_{hy3}$ are held by the robot. A force F_{hz3} is supported by the robot to keep the peg in touch with hole. This step can be accomplished in two periods.

Period 1: The peg would be moved along the positive direction of X_h axis (see Fig. 50),

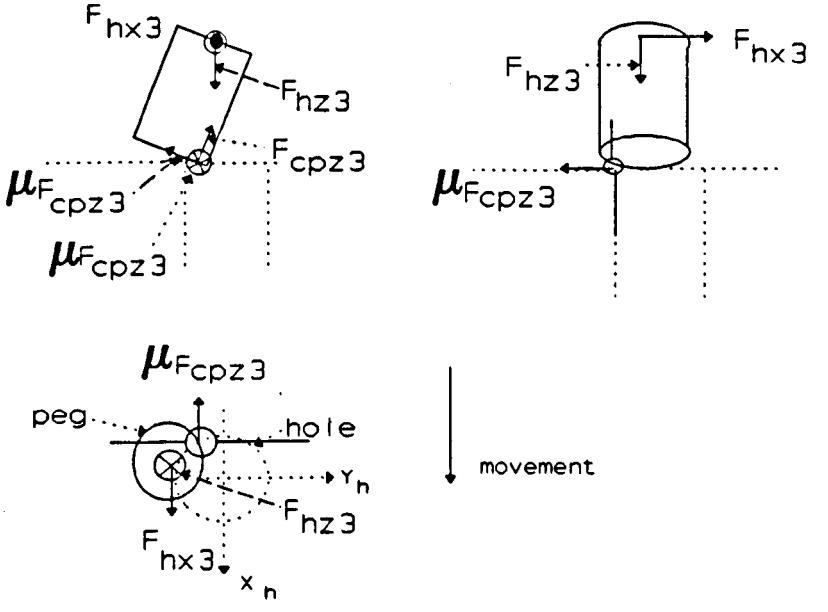

Fig. 50 Peg is moved along the positive direction of X_h axis

The forces along the X_h axis can be obtained as follows:

$$|F_{hx3}| - \mu |F_{pz3}| = m|a_{hx3}| \tag{106}$$

and forces along Z_h axis can be obtained as follows:

$$|F_{cpz3}|\cos|\theta_{cp3}| + \mu |F_{cpz3}|\sin|\theta_{hx3}| = |F_{hz3}| \tag{107}$$

Period 2: Movement would cease when there are two contact points (see Fig. 51),

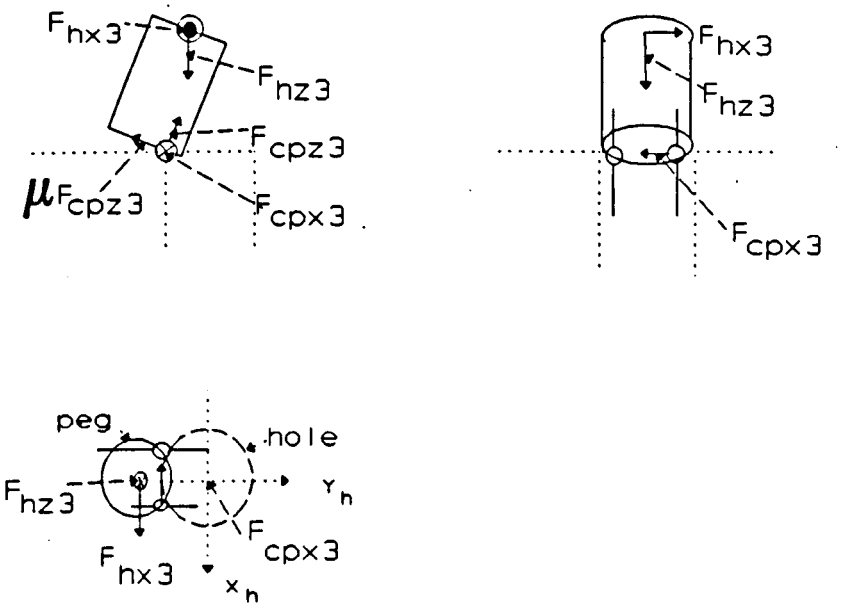

Fig. 51 Movement ceases when there are two contact points

Since

$$|\theta_{hx3}| > 0 \tag{108}$$

the provision of F_{cpx3} would inhibit further movement beyond that needed for two contact points. In the static situation,

$$|F_{cpx3}| = |F_{hx3}| \tag{109}$$

The contact force F_{cpx3} is used to compensate F_{hx3}, no matter what the size of F_{hx3}. The required force F_{hx3} and the time for this step, t_3, can be obtained from Eq. 106 and Eq. 107 as follows:

$$|F_{hx3}|>\frac{\mu}{\cos\theta_{hx3}+\mu\sin|\theta_{hx3}|}|F_{hz3}|$$

$$t_3>\sqrt{\frac{2mR_h}{|F_{hx3}|-\frac{\mu}{\cos\theta_{hx3}+\mu|\sin\theta_{hx3}|}|F_{hz3}|}} \tag{110}$$

where use has been made of the fact that:

$$|(O_hO_p)_{hx2}|<R_h \tag{111}$$

The range for the centre of the end-surface of the peg can be shown in the Fig. 52 (see *Appendix 2*):

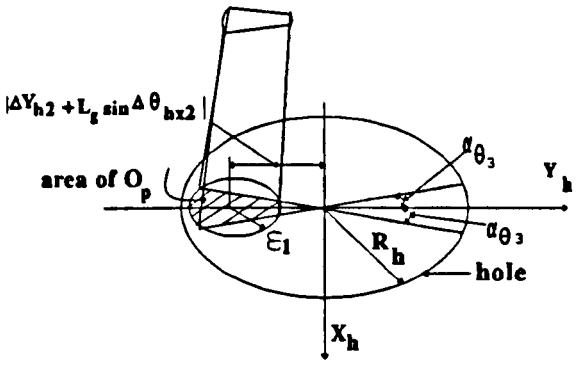

Fig. 52 Area of O_p in $X_hO_hY_h$-plane with two contact points

where

$$\alpha\theta_3=\arctan\frac{|\theta_{hy3}|}{|\theta_{hx3}|} \tag{112}$$

and the sectional area represents the area in which O_p may lie in the third state.

5.4 Obtain the peg side surface contact in $Y_hO_hZ_h$-plane (obtain three point contact)

At this stage in the process, $(O_hO_p)_{hx3}$ is nearly zero and $(O_hO_p)_{hy3}$ is uncertain. Achieving peg side surface contact in $Y_hO_hZ_h$ plane with the edge of the hole, by

moving along the Y_h-axis, will enable the final insertion to be completed. The angle θ_{hx4} is held by the robot. A force along Z_h axis F_{hz4} is applied to the peg to keep it in touch with the hole. The motion along the X_h axis and the rotation around the Y_h axis, θ_{hy4}, are free from the control of the robot and influenced by the contact force.

The applied forces acting on the peg from the robot can be shown in Fig. 53.

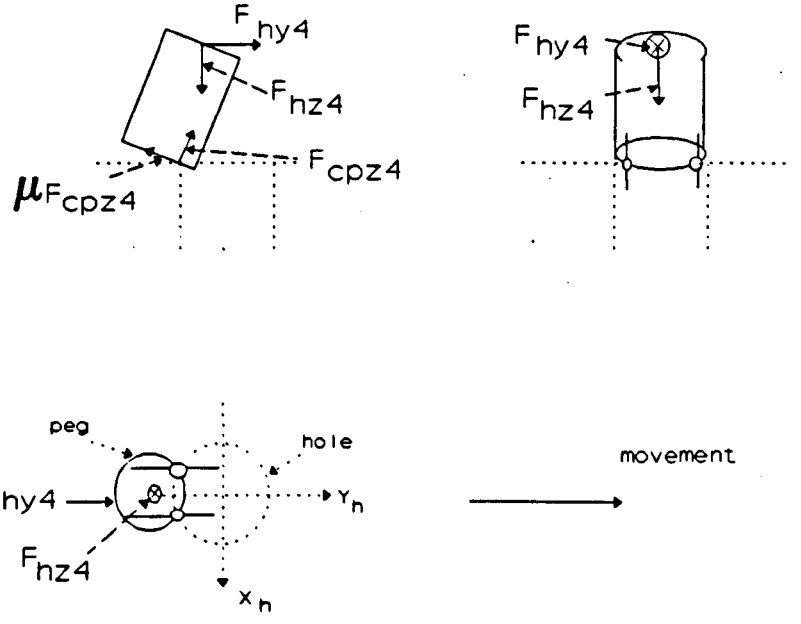

Fig. 53 Forces acting on the peg from two-point contact phase

The forces along the Y_h axis are obtained as follows:

$$|F_{hy4}| = \mu|F_{cpz4}|\cos|\theta_{hx4}| - |F_{cpz4}|\sin|\theta_{hx4}| + m|a_{hy4}| \qquad (113)$$

where

$$a_{hy4} = \frac{2\Delta Y_{h4}}{t_4^2} \qquad (114)$$

and the forces along the Z_h axis are obtained as follows:

$$|F_{cpz4}|\cos|\theta_{hx3}| + \mu|F_{cpz4}|\sin|\theta_{hx3}| = F_{hz4} \tag{115}$$

After the side surface of peg touches the hole, F_{cy4} would prevent further movement (see Fig. 54).

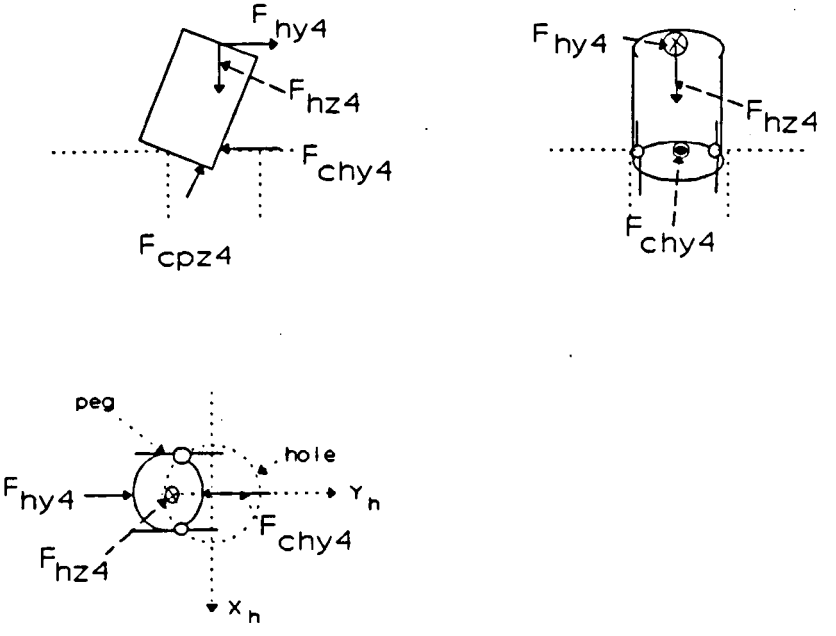

Fig. 54 Forces acting on the peg when it touches the hole with side surface

Because the assembly operation is quasi-static movement, the designed force along Y_h axis, F_{hy4} and time, t_4, can be obtained as follows:

$$|F_{hy4}| \geq \frac{\mu}{\cos\theta_{hx3} + \mu\sin\theta_{hx3}}|F_{hz4}|$$

$$t_4 \geq \sqrt{\frac{2mR_h}{|F_{hy4}| - \frac{\mu}{\cos\theta_{hx3} + \mu\sin\theta_{hx3}}|F_{hz4}|}} \tag{116}$$

This is based on the fact:

$$|(O_hO_p)_{hy3}| \leq R_h \tag{117}$$

Through analysis, it is found that the small $(O_hO_p)_{hx4}$ and θ_{hx4} are eliminated during

this step. At this instant (see *Appendix 3*),

$$\begin{aligned} \theta_{hx4} &= \theta_{hx3} \\ \theta_{hy4} &\approx 0 \\ (O_pO_h)_{hx4} &= 0 \\ (O_pO_h)_{hy4} &= -R_h + R_p\cos\theta_{hx5} \end{aligned} \tag{118}$$

5.5 Insertion operation without force sensor

So far, peg-hole insertion problem has been reduced to a geometry problem in the $Y_hO_hZ_h$ plane, which is defined by the axis of the hole and the base of the robot. The geometry of the peg-hole configuration can be found in *Appendix 3*.

As a conclusion, if the forces and moments applied to the peg are kept as constants before and after insertion, they must satisfy [see *Appendix 4*]:

$$\begin{aligned} F_{hy5} &< 0 \\ F_{hz5} &< 0 \\ M_{hx5} &> 0 \\ |F_{hz5}|\mu < |F_{hy5}| &< \frac{|F_{hz5}|}{\mu} \\ |M_{hx5}| \geq \frac{1}{1+\mu^2}&[|F_{hy5}|(L_g + 2\mu R_p + \mu^2 L_g) + |F_{hz5}|(R_p - \mu^2 R_p)] \end{aligned} \tag{119}$$

After the peg is inside the hole, the way to realize the insertion is to push the peg down and the at the same time rotate the peg around the X_h and Y_h axes in two directions alternately. In the period when the robot rotates the peg, in the direction increasing the value of the angle between the axes of the peg and the hole, the peg would be fixed by the hole. In the period when the robot rotates the peg, in the direction to decrease the angle between the axes of the peg and the hole, the peg would be pushed down.

The process for the tracking of O_p and θ_{hx} for all the process can be concluded as in Fig. 55 and Fig. 56:

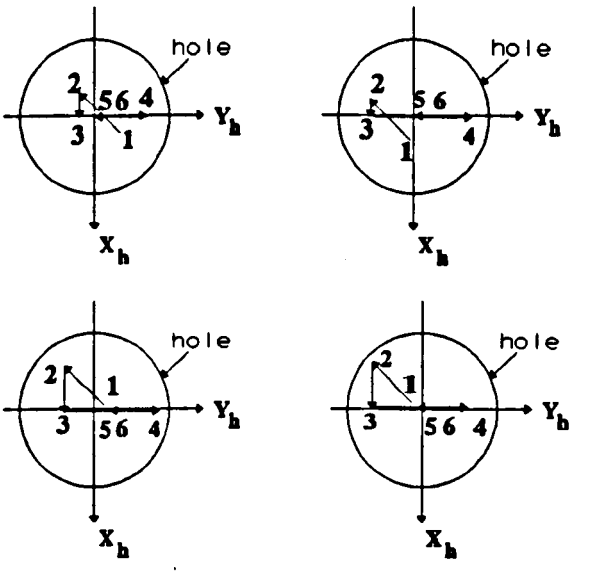

Fig. 55 Tracking of the centre of the end surface of the peg

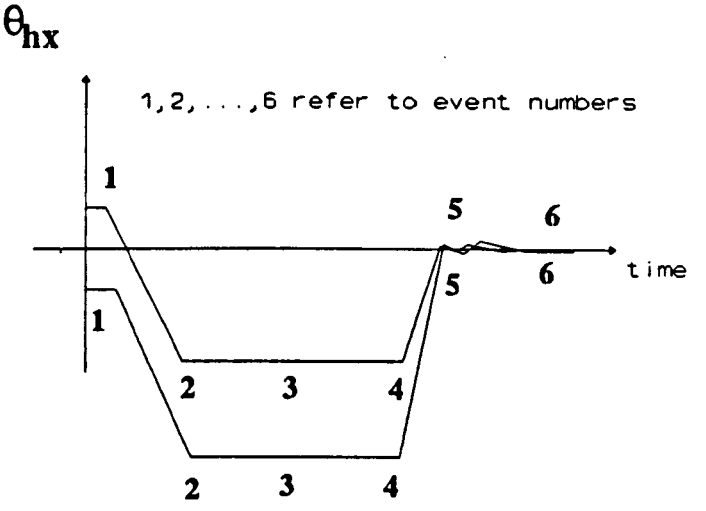

Fig. 56 θ_{hx} in the process

where numbers "*1*", "2", ..., "*6*", refer to the event numbers defined in Fig. 45.

The flow chart of the process can be presented as in Fig. 57.

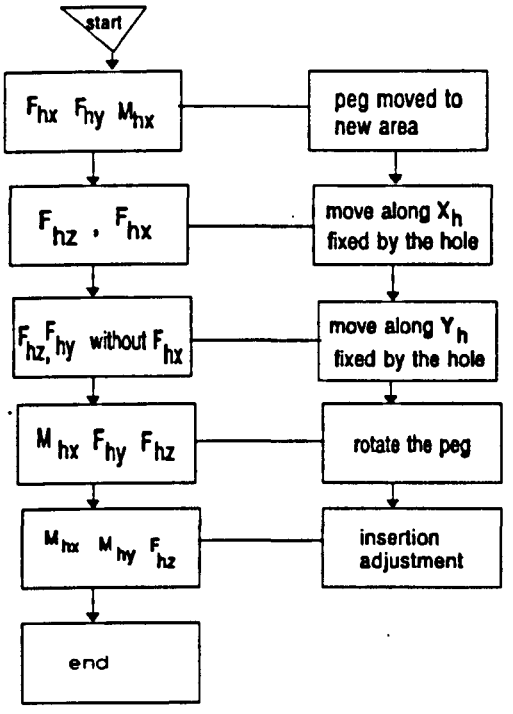

Fig. 57 The flow chart of the process

In this chapter, a novel strategy for the robotic peg-hole insertion was proposed:-

(a) With this strategy, the peg-hole insertion with limited initial state conditions can be easily achieved without a force sensor or RCC.

(b) The basic conditions for the initial state and successful adjustment are described.

(c) The principle of the strategy is related to RCC technique because of the side-surface contact, but without the need for additional compliance or a chamfer.

(d) The strategy also shares features of force sensor techniques but without force sensor feedback.

(e) The nature of the strategy enables application to other assembly operations.

CHAPTER 6 MOTION PLANNING THEORY FOR PRECISE PEG HOLE INSERTION

6.0 Introduction

The strategies to perform precise assembly operation with force sensor and without force sensor have been developed in Chapter 4 and Chapter 5, respectively. The remainder problems are: How are these strategies developed? Are there general methods to develop the strategies? Are there any other strategies which can be used in the robotic peg-hole insertion operation? In this chapter, these problems will be studied in detail. If there is a range from which any point can achieve a goal through the movement with sensors, this range is called a pre-image of the goal (68). If there is a range from which any point can achieve a goal through the movement without sensors, this range is called as a back-projection of the goal. Considering this pre-image or back-projection as a new subgoal, the new pre-image or back-projection can be found for this subgoal. If one of the pre-images or back-projections totally includes the initial range of the system, a strategy to drive the system from the initial state to the goal is found. If each subgoal is a back-projection of the last subgoal, a strategy to guide the system without sensors is found. How to find a strategy is a complex problem because the pre-images or the back-projections of one subgoal can be different according to the directions of the movements. In this chapter, the strategies in the robotic peg-hole insertion operations are investigated through the concepts of the pre-image and back-projection which are provided by other people (68, 69). For example, the pre-images which were selected as the subgoals in the robotic peg-hole insertion operations can be:-

(1) the range where the translational error is zero,

(2) the range where the angular error is zero,

The pre-image of the first subgoal can be:

(1a) the range where the projection $(O_hO_p)_{hx}$ of the displacement between O_h and O_p along the X_h is zero,

(1b) the range where the projection $(O_hO_p)_{hy}$ of the displacement between O_h and O_p along the Y_h axis is zero,

The pre-image of (1a) can be:

(1aa) the range where the sign of the projection $(O_hO_p)_{hx}$ can be identified and the state when the system enters (1a) can be identified.

The back-projection of (1a) can be:

(1ab) the range where the sign of the projection $(O_hO_p)_{hx}$ is known and when the system is moved into (1a), it would be fixed in (1a).

Comments on the strategy investigation are presented in Section 6.1, the analysis of the pre-image of the insertion operation investigation is presented in Section 6.2 and the analysis of the pre-images of the assembly operations is presented in Section 6.3.

6.1 Comments on strategy investigation

The strategy for the insertion is a loop including movement, identification and classification. The block diagram for the strategy with the force sensors can be presented as follows:

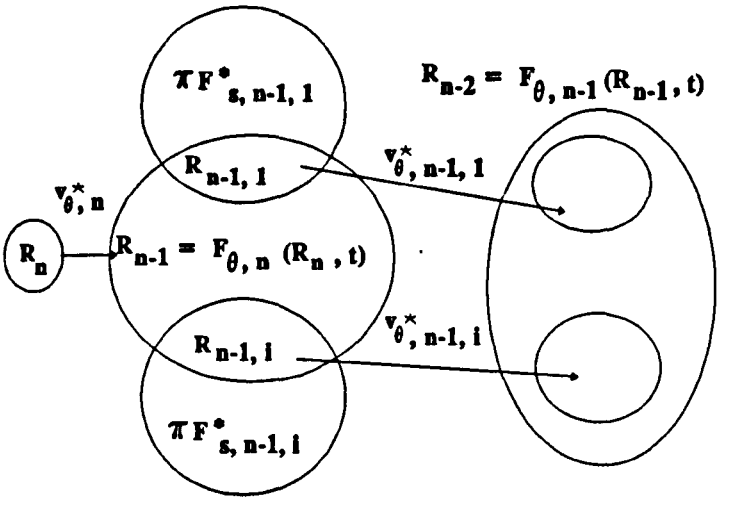

Fig. 58 The basic concept of identification and planing

where

n is the integer that a sequence of n motions can be found such that each motion terminates by the utilization of the environment or the force signals, and the final motion terminates in the goal,

$F^*_{s\ n-1,\ i}$ is the ith set of the force signals during the second step,

$R_{n-1,\ i}$ is the intersection between $\pi\ F^*_{s\ n-1,\ i}$ and R_{n-1} and,

$v^*_{\theta\ n-1,\ i}$ is the commanded velocity applied to any point in the range $R_{n-1,\ i}$.

The initial state of the peg is in the range R_n. The commanded velocity for the peg with any state in the set R_n is $v_{\theta n}$. The identification of the state is according to the forward projection $F_{\theta n}(R_n)$ and force sensor signal $F^*_{s,n-1}$. Some contact character can be identified according to these signals. Then the contact configuration can be classified into $R_{n-1,\ i}$. Each class shares some common points about the contact characters. A unitary movement is applied to one class. There are several points to

note at this stage of strategy development:

(a) One class (for example $R_{n\text{-}p_i}$) must include several sets of identifications. As analysed before, one identification can indicate several contact configurations (some movements would maintain the static position of the contact point on the peg and some movements would maintain the static position of the contact point on the hole). The relationships among one class, one identification and several contact configurations can be presented as follows:

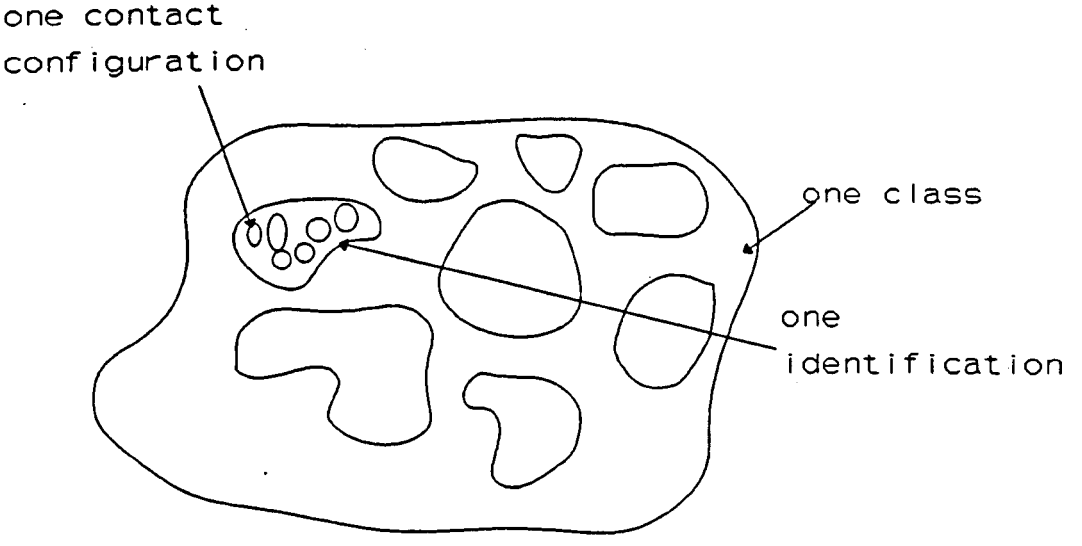

Fig. 59 Classification, identification and contact configuration

The sets of the force sensor signals in one class should share some common points on the contact characters.

(b) One class (for example $R_{n\text{-}p_i}$) must lead to one kind of motion ($v_{\theta n\text{-}p_i}$, for

example). The smallest class can be one identification. As analysed before, all the contact configurations among the motion where the positions of the contact points on the peg would share the same set of signals from wrist force sensors. All the contact configurations among the motion where the position of the contact points are static on the hole would share the same set of signals from table force sensors. With the same set of force signals, there are plenty of contact configurations. So it is difficult to classify the system only according to the signals from the force sensor.

(c) The back-projection and pre-image concepts can be used to choose some of the subgoals.

(d) The forward projection would be used to check that if these subgoals are easily recognized and can be considered as the start state for the next stage. The construction of the strategies can be concluded as follows:

If the force sensor signal is used to detect the completion of the subgoals and further recognize which of the subgoal is achieved to decide the direction of the motion, then:

$$\begin{aligned} &F_{\theta,n}(R_n) \cap \pi F_s^* = R_{n-1} \\ &F_{\theta,n-1}(R_{n-1}) \cap \pi F_s^* = R_{n-2} \\ &\quad\vdots \\ &\textit{until} \\ &F_{\theta,1}(R_1) \cap \pi F_s^* \subseteq G \end{aligned} \qquad (120)$$

If the time and environment are used to achieve the subgoal, then:

$$
\begin{aligned}
&F_{\theta,n}(R_n,\ t) \cap \pi E = R_{n-1} \\
&F_{\theta,n-1}(R_{n-1},\ t) \cap \pi E = R_{n-2} \\
&\quad\vdots \\
&\textit{until} \\
&F_{\theta,1}(R_1,\ t) \cap \pi E \subseteq G
\end{aligned}
\tag{121}
$$

6.2 The pre-image for insertion

The goal of assembly operation can be presented as follows:

$$
\begin{aligned}
\{G\} &= \{\textit{any position and orientation of the peg} | \\
&\quad \textit{the peg is inserted into the hole}\} \\
&= \{O_p, \theta |\ |O_h O_p'|_{X_h O_h Y_h} \le (R_h - R_p) \cap |O_h O_p|_{X_h O_h Y_h} \le (R_h - R_p)\}
\end{aligned}
\tag{122}
$$

The state of the goal for the assembly operation can be presented as follows:

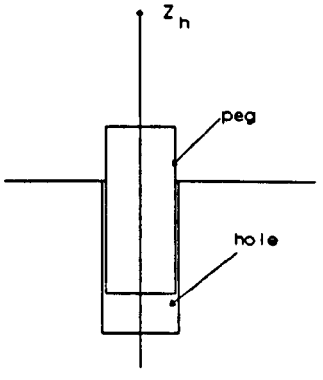

Fig. 60 The normal situation of the goal for peg-hole insertion

The pre-image for the insertion can be presented as:

$$\{G_1\} = P_{R_1,\theta_1}(\{G\}) = \{\text{any position and orientation of the peg} \mid \text{end surface of the peg is inside the hole} \cap S_1(p, R_1, \{G\}) \neq 0\}$$
$$= \{O_p, \theta \mid ((O_p)_{hx}^2 + (O_p)_{hy}^2 = \varepsilon^2) \leq (R_h - R_p \sin|\theta|)^2 \cap (O_p)_{zh} \leq 0 \cap S_1(p, R_1, \{G\}) \neq 0\} \quad (123)$$

This suggests that it is possible to decrease the difficulties in the insertion operation by tilting the peg. In the range $[0, \pi/2]$, if $|\theta|$ is increased, $(R_h\text{-}R_p \sin|\theta|)$ would increase. So the permitted initial range for O_p increases. The set including all the commanded velocities can be presented as follows:

$$S_1(p, R_1, \{G\}) = \{v_{\theta,1}^* | v_{\theta,1}^* \text{ can make the peg achieve the insertion from any point of } G_1\} \quad (124)$$

If force sensor is used, it is easy to identify when $S_1(p, R_1, \{G\})$ is not zero. If there is no force sensor, the insertion can be achieved by avoiding jamming and wedging (11, 47).

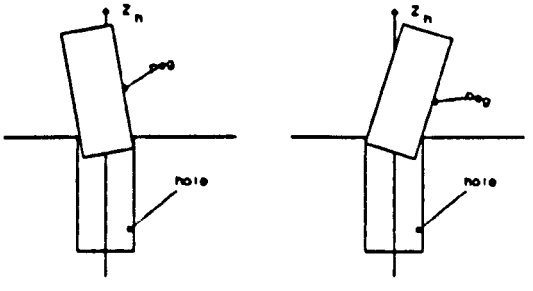

Fig. 61 The pre-image $P\{G\}$ for the peg-hole insertion

6.3 The pre-image for the assembly operation

There are eight strategies proposed here. The strategies and their subgoals are presented as follows:

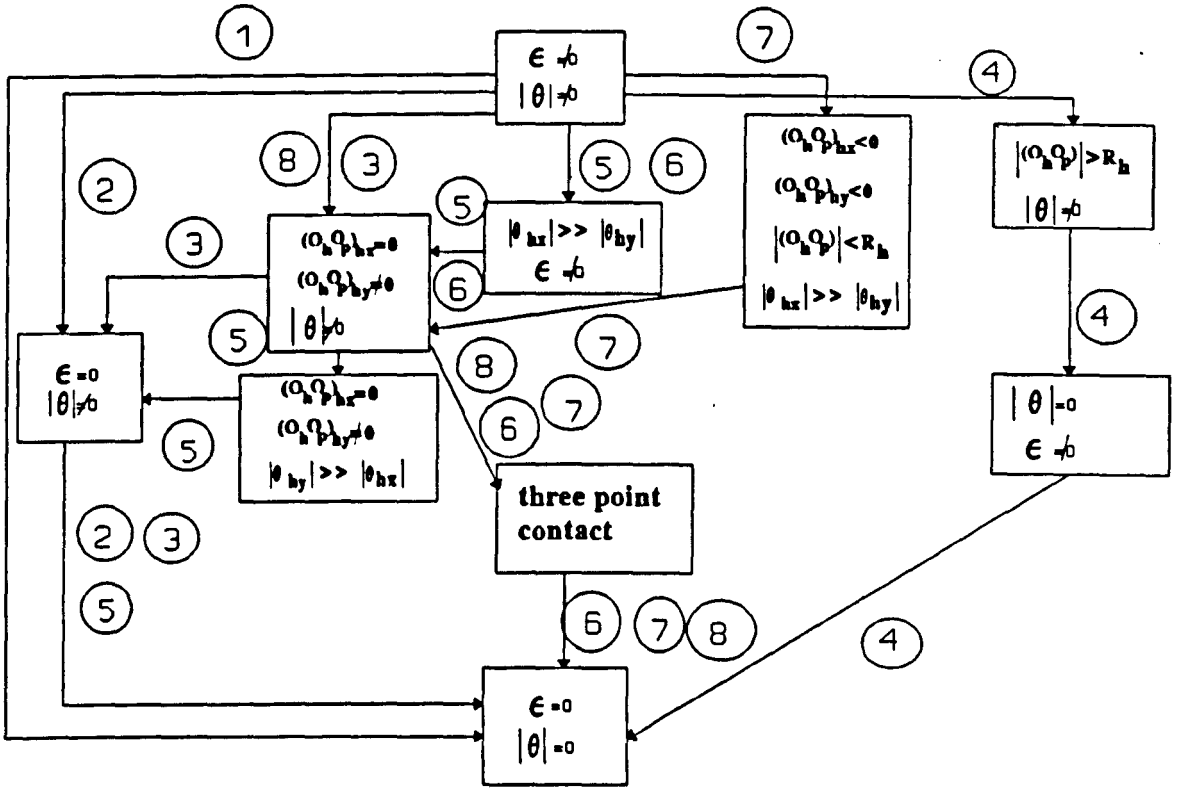

Fig. 62 The strategies of robotic peg-hole insertion operation

6.3.1 Method 1

Method 1 is to adjust the peg to eliminate the translational and rotational error simultaneous, and the subgoal of this method can be presented as follows:

$$\{G_2\} = P_{R_2,\theta_2}(\{G_1\}) = \{O_p,\theta \mid \textit{peg is in the initial area},\ S_2(p,\ R_2,\ \{G_1\},\ F_s^*) \neq 0\} \tag{125}$$

where S_2 includes all the commanded velocities to move the peg from the initial area to the insertion state. The achievement of S_1 includes:

(a) the calculation of applied force, and

(b) the design of termination predicate.

The block diagram of the first method can be presented as follows:

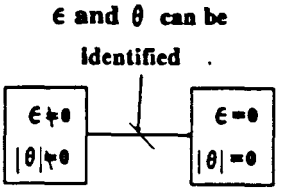

Fig. 63 The block diagram
of the first method

6.3.2 Method 2

Method 2 can be divided into two discrete steps:

(a) reduce the translational error, and

(b) reduce the rotational error.

The subgoals of this method can be presented as follows:

$$\{G_2\} = P_{R_2,\theta_2}(\{G_1\}) = \{O_p,\theta |\ |O_hO_p| = 0,\ |\theta| \neq 0,\ S_2(p, R_2, \{G_1\}, F_s^*) \neq 0\} \tag{126}$$

S_2 is the set including all the commanded velocities to move the peg from $|O_hO_p|=0$ to the state G_1 in which the peg is inside the hole.

$$\{G_3\} = P_{R_3,\theta_3}(\{G_2\}) = \{O_p,\theta |\textit{peg is in the initial area},\ S_3(p, R_3, \{G_2\}, F_s^*) \neq 0\} \tag{127}$$

S_3 is the set including all commanded velocities to move the peg from the initial area to the area where $|O_hO_p|=0$.

The block diagram of the second method can be presented as follows:

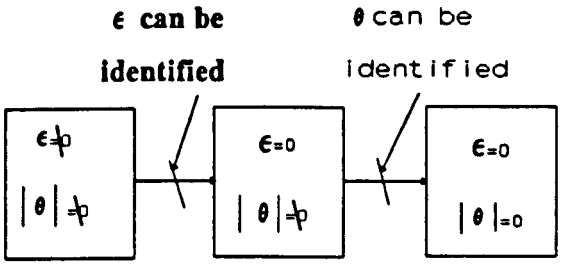

Fig. 64 The block diagram of the second method

The main difficulties of these two methods are:

(a) The directions and magnitudes of the translational and rotational errors must be measured precisely. As analysed previously, the measurement of the translational error is influenced by the rotational error θ,

(b) The accuracy of the assembly operation is restricted by the sensory uncertainty and control uncertainty.

6.3.3 Method 3

To release the demands for the measurements of the translational error directions $|O_hO_p|$, the event to eliminate $|O_hO_p|$ can be subdivided to eliminate its projections in the cartesian coordinate systems $(O_hO_p)_{hx}$ and $(O_hO_p)_{hy}$, separately. If both of the directions of the projections of the translational errors, and the state where one of the projection is eliminated can be easily identified, method 3 can simplify the insertion procedure greatly. The subgoals of this method can be presented as follows:

$$\{G_2\} = P_{R_2,\theta_2}(\{G_1\}) = \{O_p,\theta \mid |O_hO_p| = 0,\ |\theta| \neq 0,\ S_2(p, R_2, \{G_1\}, F_s^*) \neq 0\} \tag{128}$$

$$\{G_3\} = P_{R_3,\theta_3}(\{G_2\}) = \{O_p,\theta \mid (O_hO_p)_{hx} = 0,\ (O_hO_p)_{hy} \neq 0,\ |\theta| \neq 0,\ S_3(p, R_3, \{G_2\}, F_s^*) \neq 0\} \tag{129}$$

$$\{G_4\} = P_{R_4,\theta_4}(\{G_3\}) = \{O_p,\theta \mid |O_hO_p| \neq 0,\ |\theta| \neq 0,\ S_4(p, R_4, \{G_3\}, F_s^*) \neq 0\} \tag{130}$$

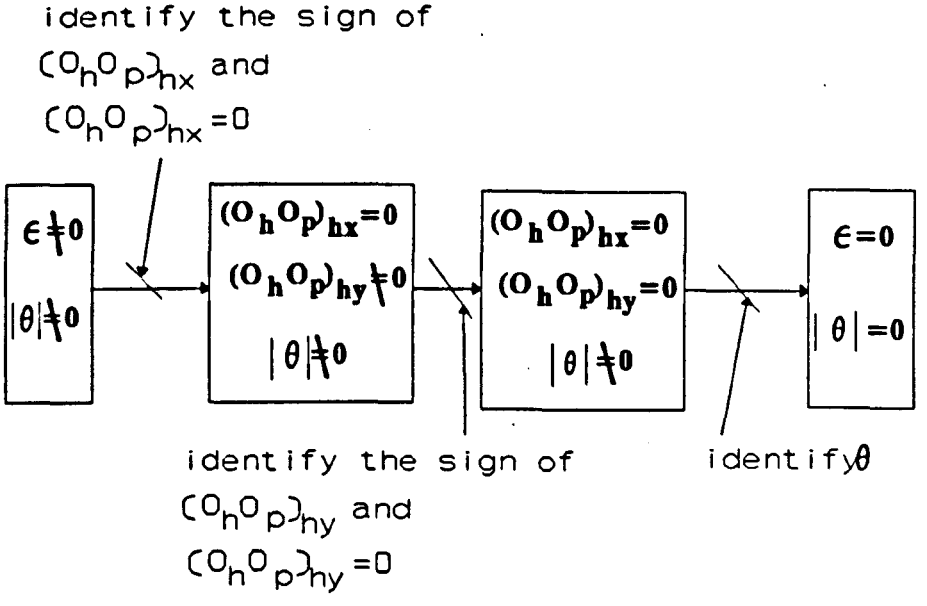

Fig. 65 The block diagram of the third method

The remaining problem is that the initial angle, even with very small magnitude, would influence the identification of:

(a) the signs of $(O_hO_p)_{hx}$ and $(O_hO_p)_{hy}$ with the nonzero angle between the axes of the peg and the hole and the defects on the contact surfaces, and

(b) the situation when

$$(O_hO_p)_{hx}=0 \tag{131}$$

or

$$(O_hO_p)_{hy}=0 \tag{132}$$

6.3.4 Method 4

To reduce the influence of the angle between the axes of the peg and the hole, method 4 is used to eliminate the angular error at the beginning of the procedure. The peg is moved away from the mouth of the hole, and is rotated along the X_h and Y_h axes until M_{hx} and M_{hy} become zero respectively. The subgoals of this method can be presented as follows:

$$\{G_2\} = P_{R_2,\theta_2}(\{G_1\}) = \{O_p,\ \theta|\ |\theta| = 0,\ (O_hO_p)_{hx} = 0,\ (O_h,O_p)_{hy} \neq 0,\ S_2(p,\ R_2,\ \{G_1\},\ F^*) \neq 0\} \tag{133}$$

$$\{G_3\} = P_{R_3,\theta_3}(\{G_2\}) = \{O_p,\ \theta|,\ \epsilon + R_h > |O_hO_p| > R_h,\ |\theta| = 0,\ S_3(p,\ R_3,\ \{G_2\},\ F^*) \neq 0\} \tag{134}$$

$$\{G_4\} = P_{R_4,\theta_4}(\{G_3\}) = \{O_p,\ \theta|,\ \epsilon + R_h > |O_hO_p| > R_h,\ |\theta| \neq 0,\ S_4(p,\ R_4,\ \{G_3\},\ F_s^*) \neq 0\} \tag{135}$$

$$\{G_5\} = P_{R_5,\theta_5}(\{G_4\}) = \{O_p,\theta|\ |O_hO_p| = \epsilon \neq 0,\ S_5(p,\ R_5,\ \{G_4\},\ F_s^*) \neq 0\} \tag{136}$$

The block diagram of the fourth method can be presented as follows:

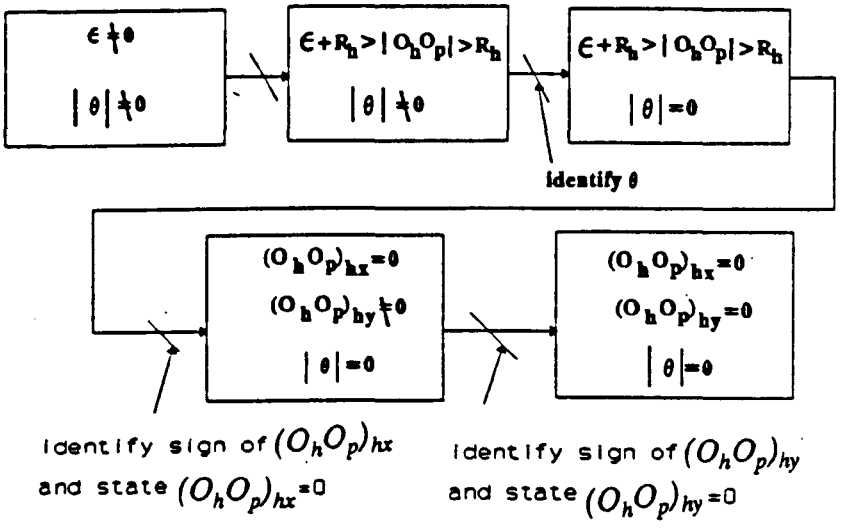

Fig. 66 The block diagram of the fourth method

The problems with this method are:

(a) The initial angle is difficult to eliminate completely,

(b) The influence of the defects of the contact surfaces on the identification of the contact states according to the force sensors are difficult to eliminated.

6.3.5 Method 5

The idea in method 5 is to increase one projection of the angular error to reduce the influence from:-

(a) the projection of another angular error, and

(b) the defects of the contact surfaces.

This method obtains the benefit from the fact that the magnitudes of projections θ_{hx} and θ_{hy} have a minimal effect on the adjustment of $(O_hO_p)_{hx}$ and $(O_hO_p)_{hy}$ respectively.

As analysed above, the projection of O_p on the $X_hO_hY_h$ plane is on the circle with same one contact point (which is related one set of force signals) and nonzero θ. So the projection of the force sensor signals and the O_p initial positional area can be presented as follows:

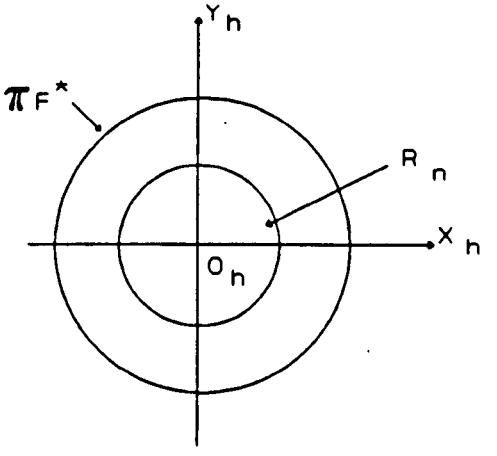

Fig. 67 Mapping of the force sensor signal and the initial area

So:

$$\pi F_s^* \cap R_n = R_n \tag{137}$$

This means that the static force sensor signals would not provide positional information when the peg is in the initial state. So it is only possible to use the force signal in some of the forward projection of the initial state. The subgoals of this method can be presented as follows:

$$\{G_2\} = P_{\theta_2,R_2}(\{G_1\}) = \{O_p,\theta \mid (O_hO_p) = 0,\ \theta_{hy} \approx 0,\ \theta_{hx} \neq 0,\ v_{\theta,2}^* = w_{hx}\ until\ F_{sz}^* = 0\} \tag{138}$$

$$\{G_3\} = P_{R_3,\theta_3}(\{G_2\}) = \{O_p,\theta \mid (O_hO_p)_{hx} = 0,\ (O_hO_p)_{hy}<0,\ \pi/2 > |\theta_{hy}| > |\theta_{hx}|,\ v_{\theta,3}^* = v_{hy}\ until\ M_{sx}^* = 0\} \tag{139}$$

It can be proven that in this case, when $M_{sx}^{*} = 0$, $(O_hO_p)_{hy} = 0$

$$\{G_4\} = P_{R_4,\theta_4}(\{G_3\}) = \{O_p,\theta \mid (O_hO_p)_{hx} < 0,\ (O_hO_p)_{hy} < 0,\ \pi/2 > |\theta_{hx}| > |\theta_{hy}|,\ v_{\theta,4}^{*} = v_{hx} \text{ until } M_{sy}^{*} = 0\} \tag{140}$$

It can be proven that in this case, when $M_{sy}^{*} = 0$, $(O_hO_p)_{hx} = 0$ (Appendix 5), i.e.

$$F_{\theta_4}(\{G_4\}) \cap \pi(M_{sy}^{*} = 0) = \{O_p,\theta \mid (O_hO_p)_{hx} = 0\} \tag{141}$$

$$\{G_5\} = P_{R_5,\theta_5}(\{G_4\}) = \{\textit{peg is in the initial area which can be moved to the new area where } (O_hO_p)_{hx} < 0,\ (O_hO_p)_{hy} < 0,\ \frac{\pi}{2} > |\theta_{hx}| > |\theta_{hx}|\} \subseteq R_n \tag{142}$$

The block diagram of the fifth method can be presented as follows:

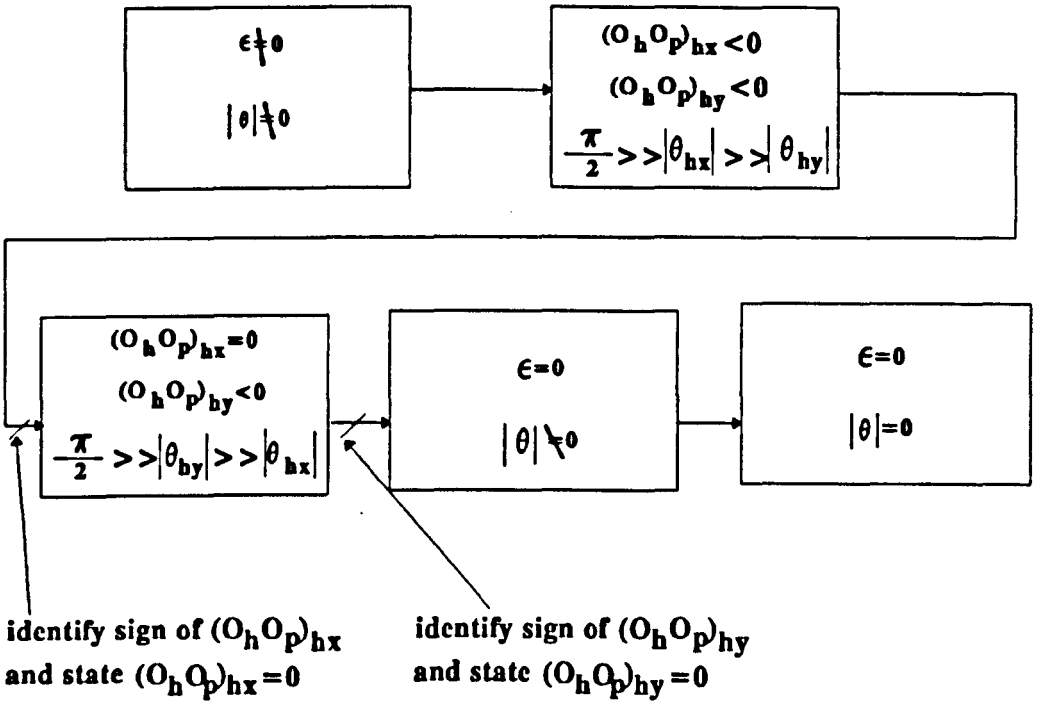

Fig. 68 The block diagram of the fifth method

6.3.6 Method 6

To simplify the procedure, it is also possible to move the peg along the Y_h axis after O_p touches the Y_h axis (G_3 in the method 5). The side-surface contact between the peg and hole can be easily achieved recognizably. The rotation and translation can be performed according to the wrist force sensor to achieve the insertion through three point contact. Because this is a combined motion the sensor signal is used either to detect phase termination or to guide the adjustment motion. The subgoals of this method can be presented as follows:

$$\{G_2\} = P_{R_2,\theta_2}(\{G_1\}) = \{O_p,\theta \mid \textit{peg has three contact points with } Z_h O_h Y_h \textit{ plane } \& \textit{ symmetric plane, } v_{\theta,2}^{*} \textit{ keeps three point contact until } F_s^{*}=0\ \} \quad (143)$$

$$\{G_3\} = P_{R_3,\theta_3}(\{G_2\}) = \{O_p,\theta \mid (O_hO_p)_{hx} = 0,\ (O_hO_p)_{hy} < 0,\ \frac{\pi}{2} > |\theta_{hx}| > |\theta_{hy}|,\ v_{\theta,3}{}^* = v_{hy},\ until\ M^*_{sx} = 0\} \tag{144}$$

It can be proven that the intersection of the forward projection of G_3 with the direction along Y_h axis and the projection of $M_{sx}=0$ on the positional space is that the peg has three contact points with the hole, i.e.,

$$F_{\theta,3}(G_3) \cap \pi(M^*_{sx} = 0) = \{O_p,\theta \mid \textit{peg and hole have three contact points}\ \} \tag{145}$$

G_4 and G_5 are same as that in method 5.

The block diagram of the sixth method can be presented as follows:

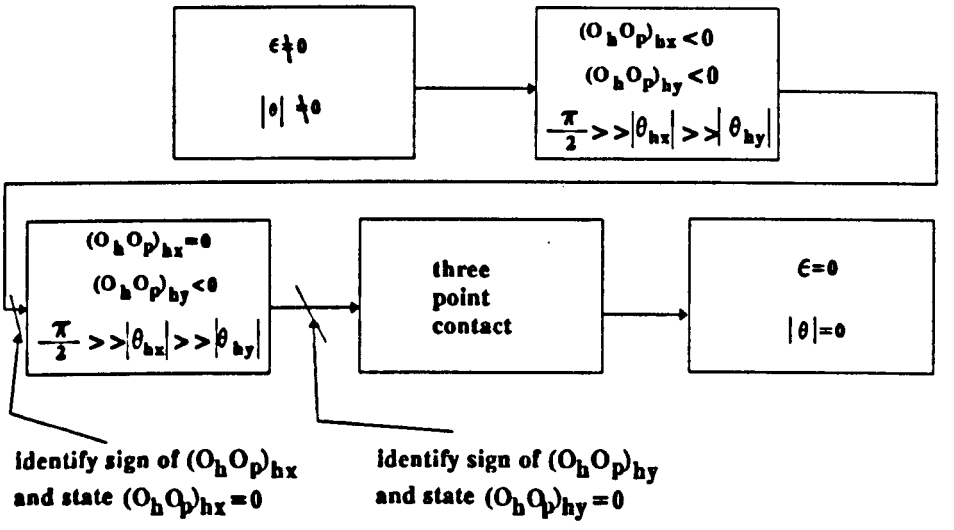

Fig. 69 The block diagram of the sixth method

6.3.7 Method 7

It is possible to use the constraints of the environment and the compliance produced by the structure to avoid the use of the force sensors. The nominal applied force from the robot can be calculated. The problem caused by the model error, control error can be compensated by the compliance during the procedure.

The difference is that every subgoal termination is achieved by utilizing the process time and the constraints of the environment. The subgoals of this method can be presented as follows:

$$\begin{aligned} \{G_1\} &= P_{R_1,\theta_1}(\{G\}) = \{O_p,\theta \mid \textit{when the end-surface of the peg is inside the hole, } S_1(\{G\}, R_1, t) \neq 0\} \\ &= \{O_p,\theta \mid |O_hO_p| < R_h - R_p\sin|\theta| \cap (O_p)_{hz} \leq 0, \\ &\quad S_1(p, R_1, \{G\}, t) \neq 0 \textit{ until } t=t_n\} \end{aligned} \tag{146}$$

where $n = 5$ for this method. The applied forces to achieve the insertion without force sensor and RCC have been studied (**11, 39** and **53**).

$$\{G_2\} = P_{R_2,\theta_2}(\{G_1\}) = \{O_p,\theta \mid \textit{peg and hole have three contact points, rotating and pushing the peg until } t = t_{n-1}\} \tag{147}$$

$$\{G_3\} = P_{R_3,\theta_3}(\{G_2\}) = \{O_p,\theta \mid (O_hO_p)_{hx} = 0,\ (O_hO_p)_{hy} < 0,\ \frac{\pi}{2} > |\theta_{hx}| > |\theta_{hy}|,\ v_{\theta,3}^{\ *} = v_{hy},\ \textit{until } t = t_{n-2}\} \tag{148}$$

$$\{G_4\} = P_{R_4,\theta_4}(\{G_3\}) = \{O_p,\theta \mid (O_hO_p)_{hx} < 0,\ (O_hO_p)_{hy} < 0,\ |O_hO_p| < R_h|\ \frac{\pi}{2} > |\theta_{hx}| > |\theta_{hx}|,\ v_{\theta,4}^{\ *} = v_{hx}\ \textit{until } t = t_{n-3}\} \tag{149}$$

$$\{G_5\} = P_{R_5,\theta_5}(\{G_4\}) = \{O_p,\theta \mid \textit{peg is i n the initial area},\ v_{\theta,5}^{\ *} = v_{hx} + v_{hy} + w_{hx},\ \textit{until } t = t_{n-4}\} \tag{150}$$

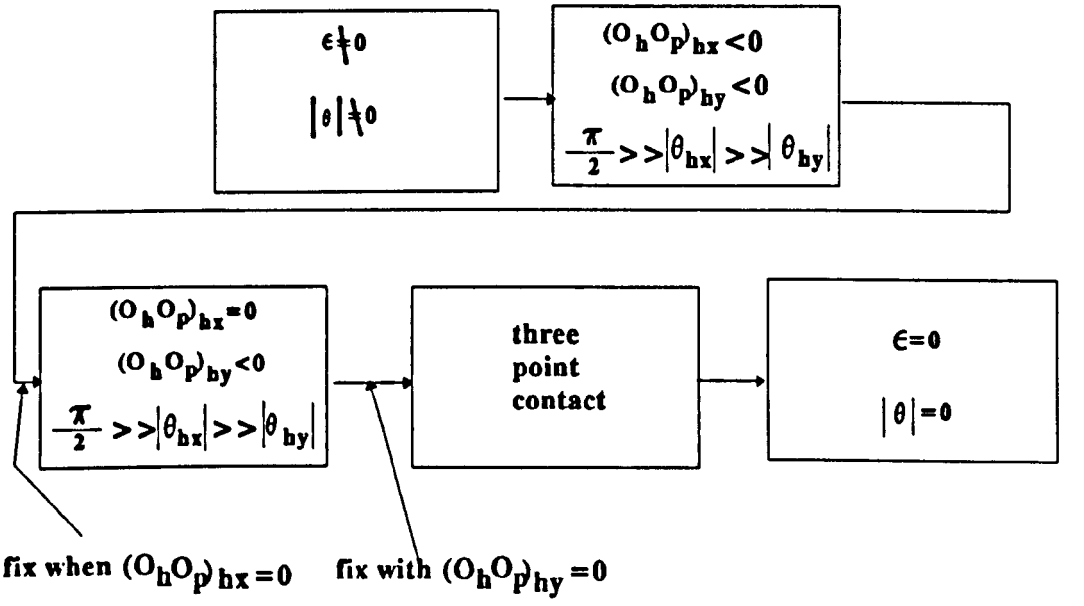

Fig. 70 The block diagram of the seventh method

6.3.8 Method 8

After O_p touches the hole, the peg is moved along Y_h axis. If the peg is pushed down, the peg would be on the point where $(O_hO_p)_{hy} = 0$. The peg can be rotated to be inserted into the hole. The subgoals of this method can be presented as follows:

$$\{G_2\} = P_{R_2,\theta_2}(\{G_1\}) = \{O_p,\theta|(O_hO_p) \approx 0,\ v_{\theta,2}{}^* = v_{hz} + w_{hx} \text{ until } t = t_{n-1}\} \quad (151)$$

$$\{G_3\} = P_{R_3,\theta_3}(\{G_2\}) = \{O_p,\theta|(O_hO_p)_{hx} \approx 0,\ (O_hO_p)_{hy} < 0,\ \pi/2 > |\theta_{hx}| > |\theta_{hy}|, \quad (152)$$
$$v_{\theta,3}{}^* = v_{hy} \text{ with constant } F_{hz}, \text{ until } t = t_{n-2}\}$$

$$\{G_4\} = P_{R_4,\theta_4}(\{G_3\}) = \{O_p,\theta||O_hO_p| < \varepsilon,\ |\theta| < \Theta,$$
$$v_{\theta,4}{}^* = w_{hx} \text{ to make } \frac{\pi}{2} > |\theta_{hx}| > |\theta_{hy}|\} \quad (153)$$

where Θ is a definition for the range of the initial angle between the axes of the peg and the hole.

In this chapter, various strategies for the robotic peg-hole insertion operation were analysed. The strategy provided in Chapter 4 with a force sensor and the strategy provided in Chapter 5 without a force sensor are regarded as the most reliable methods. The movement of the peg insertion operation with the strategy presented in Chapter 5 will be simulated in the next Chapter. It will show how the peg is inserted into the hole with constant applied forces from the robot. The experiments of the assembly operation will be presented in Chapter 8.

CHAPTER 7 SIMULATION OF ROBOTIC PEG-HOLE INSERTION OPERATION

7.5 Rotate the peg into the hole

7.5.1 Nominal movement of the peg

7.5.2 The applied forces in the fourth step

7.5.3 The movement of the peg and the contact forces between the peg and hole in the fourth step

7.6 Insert the peg into the hole deeply

7.7 Simulation of peg-hole assembly operation

7.0 Introduction

In previous chapters, the strategy investigation has been studied. The strategies provided in Chapter 5 and Chapter 6 are considered to be the most reliable methods, especially the method presented in Chapter 6 which can perform precise assembly operation without force sensors or RCC. Avoiding the use of a force sensor brings many advantages:-

(a) operational time is reduced,

(b) operational cost is reduced,

(c) problems caused by damage to the force sensors are avoided and,

(d) the assembly system is simplified.

The remainder problems can be presented as follows:-

(a) whether strategy works in practice or how the peg moves with the input forces and contact forces,

(b) whether the contact forces are small enough to avoid damage to the system and,

(c) how should the input forces be designed?

(d) what is the initial area for the system?

It is easy to think that there is no need for the simulations if the experiments can be done. However the simulation can provide the location of contact point in the insertion operation and the contact force. The values of the contact forces can be used to judge the performance of the strategy. Particular useful is that the simulation program can be used to analyse the general insertion operation without the specific requirements to the types of the robots.

7.1 The simulation method used in this thesis

The block diagram of the simulation of the movement of the peg can be presented as follows:

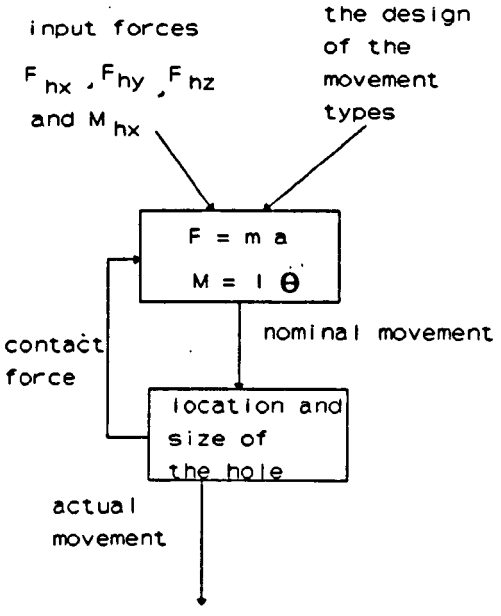

Fig. 71 The block diagram of the simulation of the movement of the peg

The diagram means that the nominal movement of the peg can be calculated through the input forces, the design of the movement types, the mass of the peg and the inertial mass of the peg. Through that the nominal state of the peg is determined. While this nominal state must be constrained by the location of the hole. Then the actual state of the peg is decided by the nominal state of the peg and the location of the hole. The contact forces can be calculated, too.

7.2 Rotate and move the peg from the initial area to a new area

7.2.1 Nominal movement

During [0 s, 0.5 s], the peg is rotated around the X_h axis with the angle $\Delta\theta_{hx1}^*$ and moved along the X_h and Y_h axes with the displacements ΔX_1^* and ΔY_1^*:

$$\begin{aligned} \Delta Y_{h,1}^* &= -\frac{R_h}{1+\sqrt{2}} \\ \Delta X_{h,1}^* &= -\frac{R_h}{1+\sqrt{2}} \\ \Delta\theta_{hx,1}^* &= -10\theta_{h1} \end{aligned} \tag{154}$$

where θ_{h1} is the maximum value of the variables $\theta_{hx,1}$ and $\theta_{hy,1}$:

$$\begin{aligned} -\theta_{h1} < \theta_{hx,1} < \theta_{h1} \\ -\theta_{h1} < \theta_{hy,1} < \theta_{h1} \end{aligned} \tag{155}$$

The nominal movement of the peg O_p can be presented as follows:

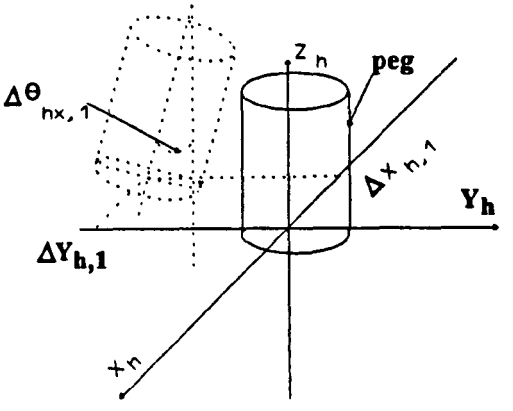

Fig. 72 The peg nominal movement in the first step

The types of the movements in the first step can be described as follows:

	$\Delta X_{h,1}$	$\Delta Y_{h,1}$	$\Delta Z_{h,1}$	$\Delta\theta_{hx,1}$	$\Delta\theta_{hy,1}$	$\Delta\theta_{hz,1}$
types	guided motion	guided motion	guided motion	guided motion	fixed	fixed

Table 10 The types of the movement in the first step

The simulation of the input to the peg and the movement of the peg in the first step can be presented in Fig. 103-106.

7.3 Push the peg to the hole with F_{hz} and move the peg along the X_{hp} with F_{hx}

7.3.1 Nominal movement

During [0.5 s, 1.0 s], the peg is pushed to touch the hole and is moved along the X_h axis after half the time has elapsed. The nominal movement of the peg in the second step can be presented as follows:

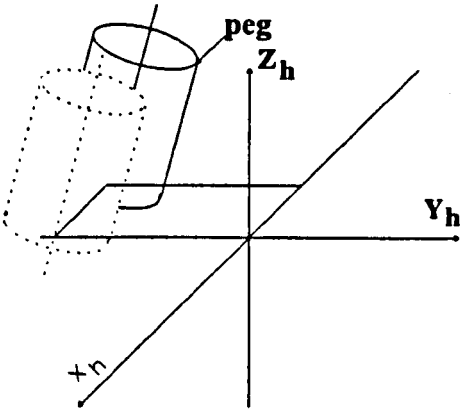

Fig. 73 The peg nominal movement in the second step

The movement types can be presented in the following table:

time	$\Delta x_{h,2}$	$\Delta y_{h,2}$	$\Delta z_{h,2}$	$\Delta \theta_{hx,2}$	$\Delta \theta_{hy,2}$	$\Delta \theta_{hz,2}$
the first half of the second step	free or compliant	free or compliant	guided or compliant	fixed	free or compliant	fixed
the second half of the second step	guided and compliant	compliant	guide and compliant	fixed	compliant	fixed

Table 11 The types of the peg movement in the second step

7.3.2 Applied forces in the second step

The design of the applied forces should satisfy the following conditions:

(1) $F_{hz,2}$ is big enough to push the peg to touch the hole in half of the duration of the operation time in this step,

(2) $F_{hx,2}$ is big enough to move the peg from any point in the possible initial range for the second step to achieve the two point contact state and,

(3) A better design is to make $F_{hz,2}$ and $F_{hx,2}$ as small as possible to reduce the contact forces between peg and hole.

During the first half of the second step, only constant force $F_{hz,2}$ acts on the peg. During the second half, both $F_{hz,2}$ and $F_{hx,2}$ act on the peg. The applied forces in the simulation can be presented in Fig. 103-106.

7.3.3 The location of the contact points

To analyse the movement of the peg, it is necessary to analyse the contact state and contact forces between the peg and hole. The contact force analysis is also useful for the strategy performance study.

7.3.3.1 One point contact state

In general, when the peg is pushed by F_{hz} to touch the hole, there is one contact point between the peg and hole. The projections of the end-surface of the peg and the upper-surface of the hole on $X_hO_hY_h$ plane can be presented as follows:

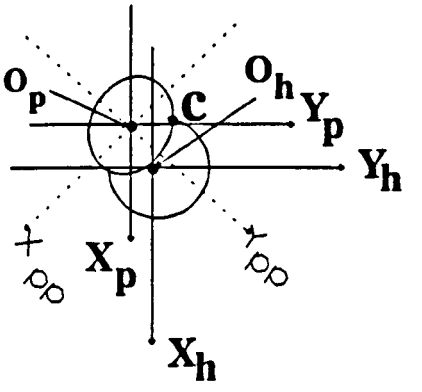

Fig. 74 Projections of end-surface of peg and upper-surface of hole with one contact point

To discuss the coordinates of the contact point, it is better to analyse the system in the $X_{hp}O_{hp}Y_{hp}$ coordinate frame. The projection of the contact point:

(a) is one of two common points between the projections of the circle of the end-surface of the peg and of the circle of the upper-surface of the hole,

(b) is a greater distance from X_{pp} compared with the other common point,

(c) is on the same side of Y_{hp} axis as the centre of the end-surface of the peg. Or, the distance between the contact point and Y_{pp} is smaller than that between the contact point and Y_{hp}:

$$|(c)_{ppy}| < |(c)_{hpy}| \tag{156}$$

The location of the contact point can be calculated according to:

$$(c)_{hpx}^2+(c)_{hpy}^2=R_h^2$$
$$(c)_{ppx}^2+(c)_{ppy}^2=R_p^2 \qquad (157)$$

$$(c)_{ppx}=(c)_{hpx}-(O_p)_{hpx}$$
$$\cos|\theta|(c)_{ppy}=(c)_{hpy}-(O_p)_{hpy} \qquad (158)$$

According to these equations, the coordinate of contact point can be calculated in simulation program. After that the coordinates can be transferred to that in the basic peg-hole system frames $O_hX_hY_hZ_h$ and $O_pX_pY_pZ_p$.

7.3.3.2 Two point contact state

The state with two point contact can be represented as follows:

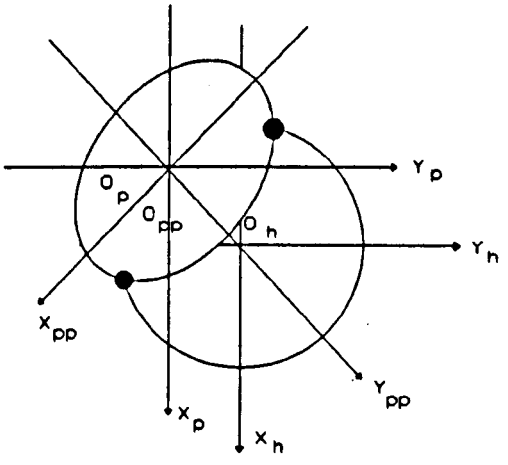

Fig. 75 Projections of end-surface of peg and upper-surface of hole with two contact points

The contact force through the new contact point prohibits the movement along X_h axis. The direction of the contact force is similar to that in the one point contact state. If the value of F_{hpz} is big enough to keep the peg from jumping out of the hole,

$$|F_{hpz,2}| \geq |F_{cppx,2}\tan(\alpha_{zhpx,2})| \geq |F_{hpx,2}\tan(\alpha_{zhpx,2})| \qquad (159)$$

the peg is fixed in the two point contact state. At this moment, the short axis of the

elliptical projection of the circle of the end-surface of the peg is through O_h because the two contact points are symmetrical along the short axis. $(O_p)_{hpx}$ can be calculated as follows:

$$(O_p)_{hpx}=(O_p)_{hpy}\frac{\theta_{hpy}}{\theta_{hpx}} \tag{160}$$

The purpose of this step is to reduce the value of $|(O_p)_{hx}|$ which is calculated through $(O_p)_{hpx}$.

The simulation of the coordinates of the contact point can be presented in Fig. 115-118, where $(c_i)_{ppx} = 0$ or $(c_i)_{ppy} = 0$ means that c_i does not exist, $i = 1, 2$.

From the simulation results, it is clear that:

(a) When $0.5\ s < t < 0.9\ s$, the peg is moved along the X_h axis:

$$(c_2)_{ppx} = 0 \tag{161}$$

$$(c_2)_{ppy} = 0 \tag{162}$$

(i) there is one contact point between the peg and hole and,

(ii) It is clear that when the peg is moved along the X_h axis, the value of $|(O_pc)_{hpx}|$ is increased and the value of $|(O_pc)_{hpy}|$ is reduced.

(b) When $0.9\ s < t < 1\ s$, the peg is fixed with two contact points. The peg-hole system is in the two-point contact state:

$$(c_2)_{ppy,2} = (c_1)_{ppy,2} \tag{163}$$

$$(c_2)_{ppx,2} = -(c_1)_{ppx,2} \tag{164}$$

7.3.4 The direction of the contact force

The direction of the contact force can be analysed as follows. The direction of the contact force should be perpendicular to the contact lines which are tangential lines of the circle of the end-surface of the peg and of the circle of the upper-surface of the hole at the contact point. Since $X_{hp}O_{hp}Y_{hp}$ is a plane including the tangential line of the circle of the upper-surface of the hole, the projection of the contact force and the tangential line of the circle of the upper-surface of the peg are perpendicular to each other in $X_{hp}O_{hp}Y_{hp}$ plane:

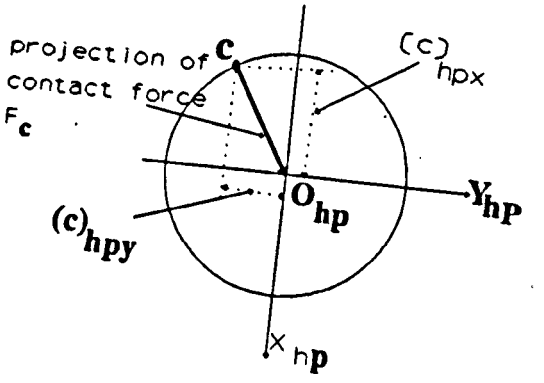

Fig. 76 Projection of contact force in $X_{hp}O_{hp}Y_{hp}$ plane

The projection of the contact force in $X_{pp}O_{pp}Y_{pp}$ plane is perpendicular to the tangential line of the circle of the end-surface of the peg:

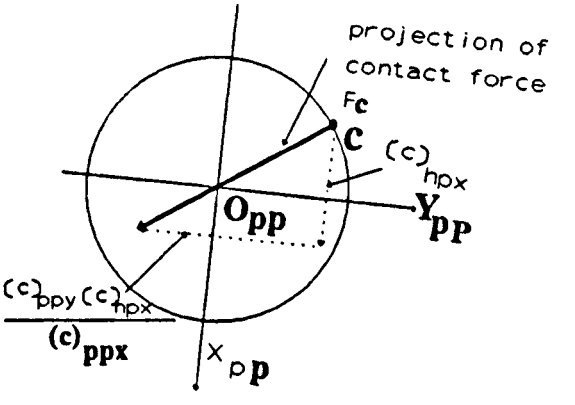

Fig. 77 Projection of contact force in $X_{pp}O_{pp}Y_{pp}$ plane

The projection of the contact force in $X_{pp}O_{pp}Y_{pp}$ plane is through O_{pp}.

If the length of the projection of the contact force in $X_hO_hY_h$ plane is R_h, the length of the contact force along X_{hp} and X_{pp} is:

$$|F_{chpx,2}| = |F_{cppx,2}| = |(c)_{hpx,2}| \tag{165}$$

The length of the projection of the contact force along Y_{hp} axis is:

$$|F_{chpy,2}| = |(c)_{hpy,2}| \tag{166}$$

The length of the projection of the contact force along Y_{pp} axis is:

$$|F_{cppy,2}| = |c_{hpx,2}\frac{c_{ppy,2}}{c_{ppx,2}}| \tag{167}$$

The projections of the contact force on $Z_{hp}O_{hp}Y_{hp}$ plane and on $Z_{hp}O_{hp}X_{hp}$ plane can be presented as follows:

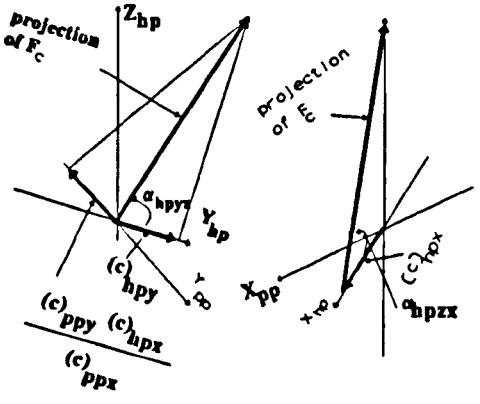

Fig. 78 Projections of the contact force on $Z_{hp}O_{hp}Y_{hp}$ and $Z_{hp}O_{hp}X_{hp}$ planes

$$\frac{\cos(\alpha_{ppyz})}{\cos(\alpha_{hpyz})} = \frac{(c)_{ppy}\times(c)_{hpx}}{(c)_{ppx}\times(c)_{hpy}} \tag{168}$$

$$\alpha_{ppyz} + \alpha_{hpyz} + |\theta| = \pi \tag{169}$$

So the angles α_{hpyz}, α_{ppyz}, α_{hpzx} and α_{ppzx} can be calculated as follows:

$$\alpha_{hpyz}=\arctan\left(\frac{\left|\frac{c_{ppy}\times c_{hpx}}{(c)_{ppx}\times(c)_{hpy}}\right|+\cos|\theta|}{\sin|\theta|}\right) \tag{170}$$

$$\alpha_{ppyz}=\pi-\theta-\alpha_{hpyz} \tag{171}$$

$$\alpha_{hpzx}=\arctan\left(\frac{\left|\frac{c_{ppy}\times c_{hpy}}{(c)_{ppx}\times(c)_{hpy}}\right|+\cos|\theta|}{\sin|\theta|}\right) \tag{172}$$

$$\alpha_{ppzx}=\arctan\left(\tan(\alpha_{ppyz})\times\frac{(c)_{ppx}}{(c)_{ppy}}\right) \tag{173}$$

During the movement of the peg along X_h axis, $|(c)_{ppx}|$ and $|(c)_{hpy}|$ increase and $|(c)_{ppy}|$ and $|(c)_{hpy}|$ decrease. That means during that period, α_{hpyz} decreases. The minimum value of α_{hpyz} occurs when the peg-hole system is in the two-point contact state. If

$$(O_p)_{ppy}=0 \tag{174}$$

or

$$(c)_{hpx}=0 \tag{175}$$

then

$$\alpha_{hpyz}=\frac{\pi}{2}-\theta \tag{176}$$

The angles $\alpha_{hpyz,2}$ and $\alpha_{hpzx,2}$ can be simulated as follows:

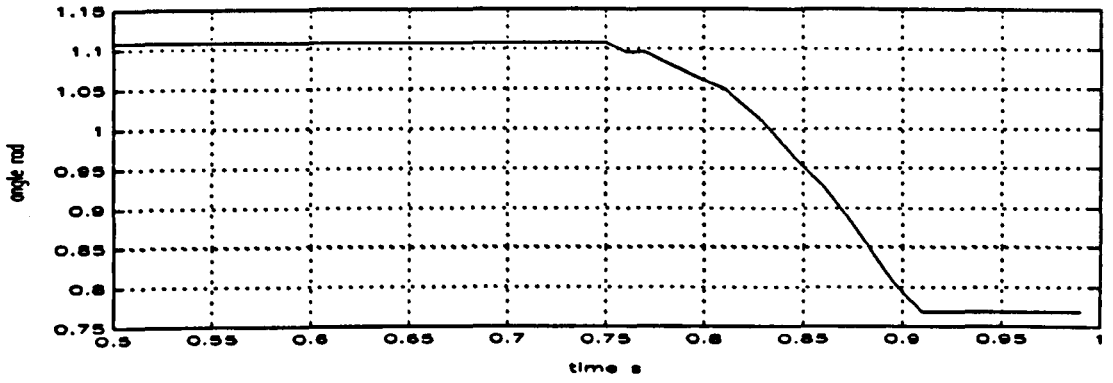

Fig. 79 The angle $\alpha_{hpzx,2}$ versus time

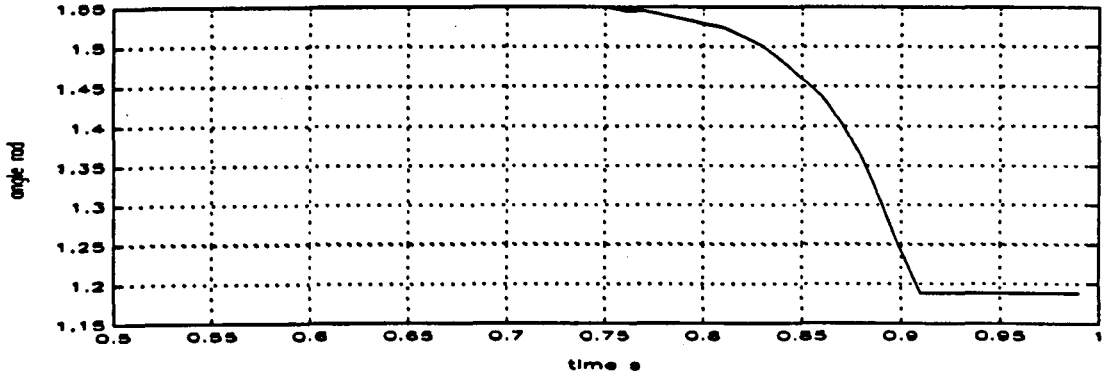

Fig. 80 The angle $\alpha_{hpzy,2}$ versus time

From the simulation, it is clear that:

(1) during the movement of the peg along the X_h axis, both of the angles α_{hpyz} and α_{ppyz} decrease until the peg-hole system is in two point contact state, which occurs at $t = 0.9\ s$ in the simulation,

(2) α_{hpyz} and α_{ppyz} have their minimum values when the peg-hole system is in the two point contact state.

The contact forces along the X_{hp} axis can be presented as follows:

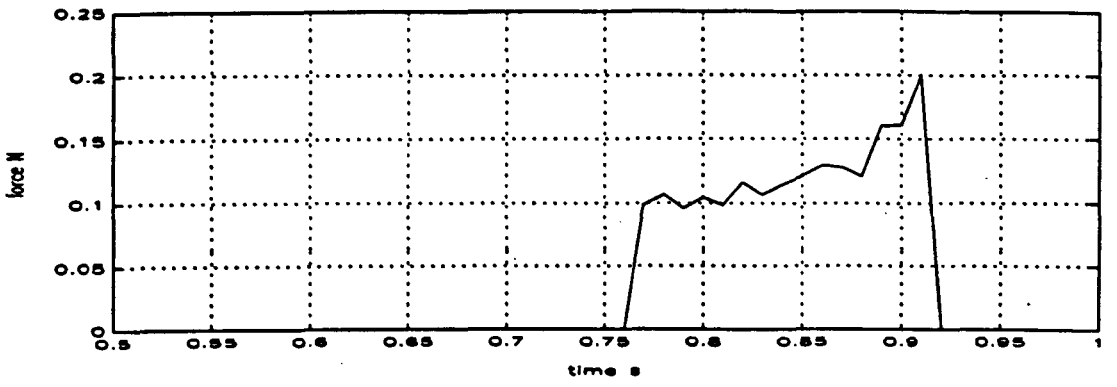

Fig. 81 The projection $(F_{c1})_{hpx,2}$ of the contact force on the first contact pointin the second step

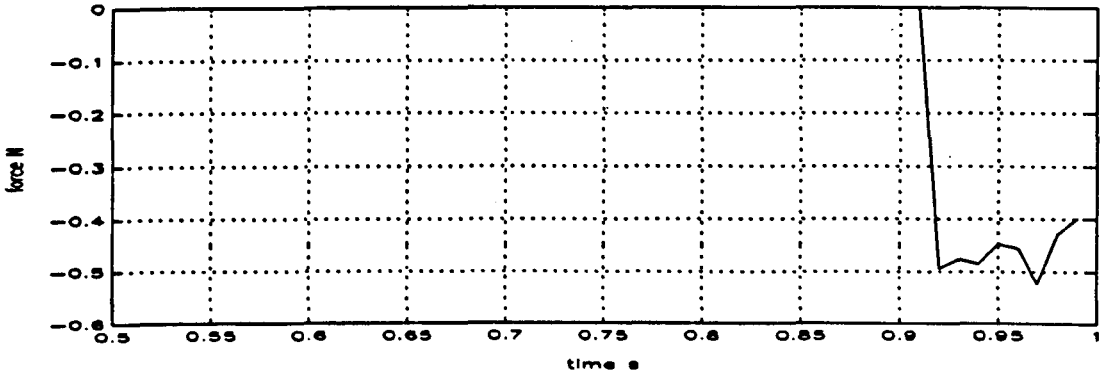

Fig. 82 The projection $(Fc_2)_{hpx,2}$ of the contact force on the second contact point in the second step

From the simulations of the contact forces during the movement of the peg along the X_h axis, it is clear that:

(1) If $0.5\ s < t < 0.9\ s$, there is one contact point,

$$(F_{c2})_{hpx,2} = 0 \tag{177}$$

$F_{chpx,1}$ increases.

(2) if $0.9\ s < t < 1\ s$, there are two contact points,

$$\begin{aligned} (F_{c1})_{hpx,2} &= 0 \\ (F_{c2})_{hpx,2} &\approx -F_{hx,2} \end{aligned} \tag{178}$$

so the peg is fixed at this point.

The values of the contact forces are similar to those in the strategy using force

sensors. So the contact forces are small enough to avoid damage to the peg-hole system.

7.3.5 Frictional force

The major problem in the study of the frictional force is about their directions. The frictional force is:

(1) in the plane which includes the tangential line of the circle of the end-surface of the peg and the tangential line of the circle of the upper-surface of the hole. This plane is called as tangential plane.

(2) opposite to the projection of the velocity of the contact point of the peg on the tangential plane.

The tangential plane can be presented as follows:

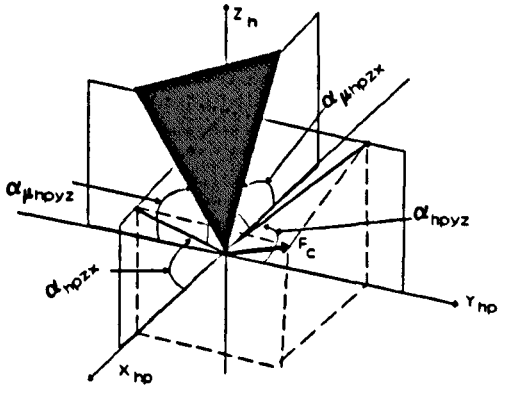

Fig. 83 Tangential plane in $O_{hp}X_{hp}Y_{hp}Z_{hp}$

where:

$\alpha_{\mu hpzx}$: is the angle between the common line of the tangential plane and $X_{hp}O_{hp}Z_{hp}$ and $-X_{hp}$ axis and,

$\alpha_{\mu hpyz}$: is the angle between the common line of the tangential plane and $Y_{hp}O_{hp}Z_{hp}$ and $-Y_{hp}$ axis:

The frictional force along the X_{hp} axis can be presented as follows:

$$\alpha_{\mu hpzx} = \frac{\pi}{2} - \alpha_{hpzx} \tag{179}$$

$$\alpha_{\mu hpyz} = \frac{\pi}{2} - \alpha_{hpyz} \tag{180}$$

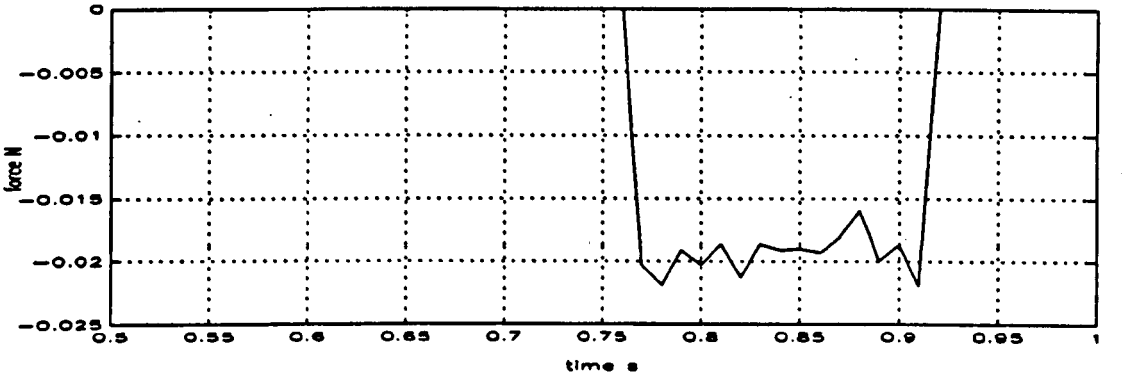

Fig. 84 The projection $f_{chpx,2}$ of the frictional force in the second step

It is clear that:

(1) the frictional force exists when there is one contact point between the peg and the hole, and

(2) the value of the frictional force is much smaller than that of the contact force along X_{hp} axis.

7.3.6 The movement of the peg in the second step

The simulation of the movement of the peg along X_h axis can be presented in Fig. 106-111.

From the simulation of the movement of the peg in the second step, it is clear that:

(1) during the movement of the peg along the X_{hp} axis, both of $|(O_hO_p)_{hz}|$ and $|(O_hO_p)_{hx}|$ decrease and,

(2) when the peg is fixed with two contact points, it is at its lowest point in this step. $|(O_hO_p)_{hx}|$ is small.

7.4 Movement of the peg along the Y_h axis

7.4.1 Nominal movement

During [1.0 s, 1.5 s], the peg is moved along the Y_h axis. The nominal movement of the peg can be presented as follows:

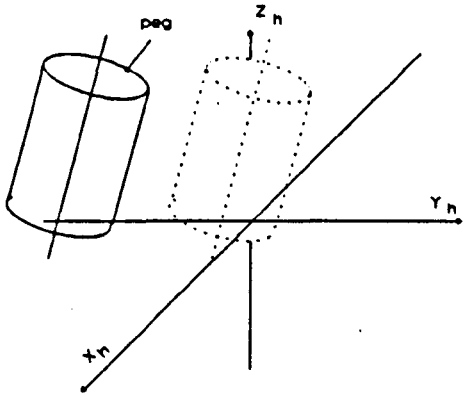

Fig. 85 The peg nominal movement in the third step

The peg would be fixed when there are three contact points between the peg and the hole. The movement types can be presented as follows:

	ΔX_3	ΔY_3	ΔZ_3	$\Delta\theta_{hx3}$	$\Delta\theta_{hy3}$	$\Delta\theta_{hz3}$
types	compliant	guided and compliant	guided and compliant	compliant	compliant	fixed

Table 12 The types of the peg movement in the third step

7.4.2 Input forces

The design of the applied forces should satisfy the following conditions:

(1) $F_{hz,3}$ is big enough to push the peg to touch the hole in half the time of the total operation time in this step,

(2) $F_{hy,3}$ is big enough to move the peg from any point in the possible initial range of the second step to achieve two point contact state and,

(3) A better design is to make $F_{hz,3}$ and $F_{hy,3}$ as small as possible to reduce the

contact forces between the peg and the hole.

The applied forces $F_{hpy,3}$ and $F_{hpz,3}$ in simulation can be presented in Fig. 103-106.

7.4.3 The contact state during the movement of the peg along the Y_{hp} axis

7.4.3.1 The movement of the peg along the Y_h axis

At the beginning of this step, the contact state is in two-point contact. When the peg is moved along the Y_h axis, the short axis is not through O_h. Then there is one contact point between the peg and the hole. The contact force through this point helps the adjustment of the peg along the X_h axis and the rotational movement around the X_h axis until there are two contact points between the peg and the hole. The direction of this adjustment changes after the two point contact state. So the peg-hole system changes between one-point contact state and two point contact state:

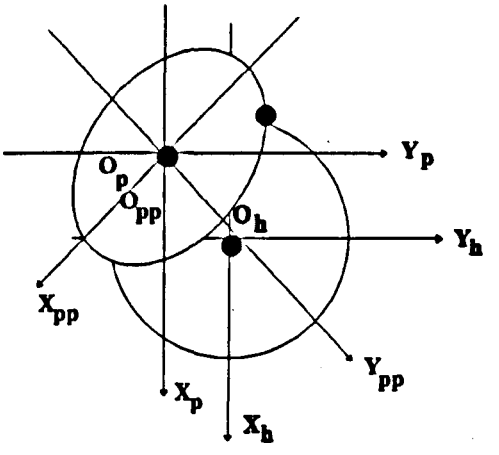

Fig. 86 One point contact state whilst the peg is moved along Y_h axis

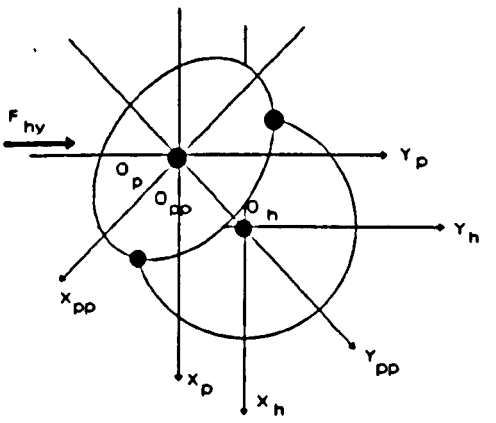

Fig. 87 Two point contact state when the peg is moved along Y_h axis

7.4.3.2 The fixation of the peg with the bottom and side-surface contact

This step achieves a three point contact state. In this state, because the applied force is along the Y_h axis, $(O_p)_{hx}$ and θ_{hx} decrease.

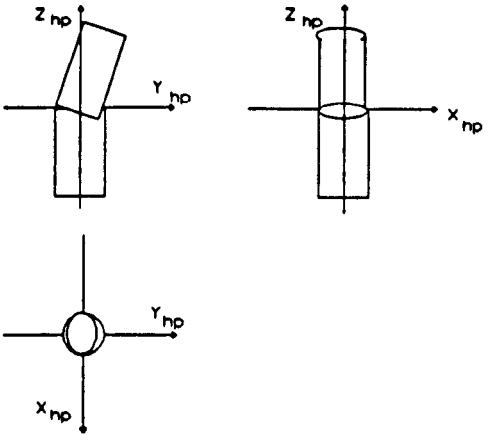

Fig. 88 Three point contact state of peg-hole system

The position of the peg in the three point contact state can be calculated using θ_{hpx}.

$$
\begin{aligned}
(c_1)_{hpy} = (c_2)_{hpy} &= \frac{R_h(1 + \cos^2\theta_{hpx}) - 2R_p\cos\theta_{hpx}}{1 - \cos^2\theta_{hpx}} \\
(c_1)_{ppy} = (c_2)_{ppy} &= \frac{2R_h\cos\theta_{hpx} - R_p(1 + \cos\theta_{hpx})}{\cos^2\theta_{hpx} - 1} \\
(O_p)_{hpy} &= (c_1)_{hpy} - (c_1)_{ppy}\cos\theta_{hxp} \\
(O_p)_{hpx} &= 0 \\
(O_p)_{hpz} &= (c_1)_{ppy}\tan\theta_{hpx}
\end{aligned}
\qquad (181)
$$

The locations of the contact points can be presented in Fig. 115-118.

From the simulation, it is clear that:

(a) during the movement of the peg along the Y_h axis which occurs in the situation when $t < 1.33\ s$, there is one contact point between the peg and the hole. $(c_1)_{ppy}$ decreases,

$$(c_2)_{ppx} = 0 \tag{183}$$

$$(c_2)_{ppy} = 0 \tag{184}$$

(b) when the peg fixed with the hole which occurs when $t > 1.33\ s$ in the simulation, there are three contact points between the peg and the hole.

$$(c_2)_{ppx} = -(c_1)_{ppx} \tag{185}$$

$$(c_2)_{ppy} = (c_1)_{ppy} \tag{186}$$

7.4.4 The contact force during the peg is moved along the Y_h axis

The contact forces can be presented in Fig. 111-114.

7.4.5 The movement of the peg along the Y_h axis

The simulation of the movement of the peg can be presented in Fig. 107-110.

From the simulation, it is clear that:

(1) During the movement of the peg along the Y_h axis, $(O_hO_p)_{hz}$, $(O_hO_p)_{hx}$ and θ_{hy} are reduced,

(2) When the peg contacts the peg with its bottom and side-surfaces during [*1.34 s, 1.51 s*], $(O_hO_p)_{hx}$ is almost zero. The peg is fixed at its lowest point during the movement of the peg along the Y_h axis.

7.5 Rotate peg into the hole

7.5.1 Nominal movement of the peg

During [1.5 s, 2.0 s], the peg is rotated into the hole. The nominal movement of the peg can be presented as follows:

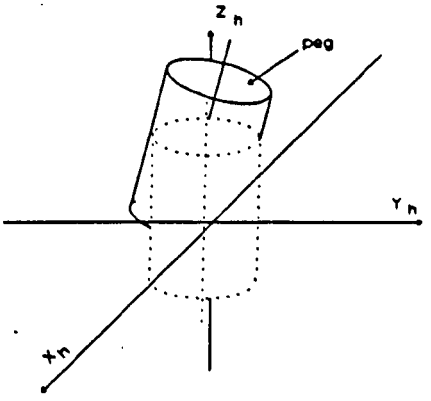

Fig. 89 The peg nominal movement in the fourth step

The types of the movement can be presented as follows:

parameter	ΔX_4	ΔY_4	ΔZ_4	$\Delta\theta_{hx,4}$	$\Delta\theta_{hy,4}$	$\Delta\theta_{hz,4}$
types	compliant	compliant	guided and compliant	compliant	guided and compliant	fixed

Table 13 The types of the peg movement in the fourth step

7.5.2 The applied forces in the fourth step

The peg is inserted into the hole using the three point contact. If the applied forces and moments remain the same before and after the insertion:

$$|F_{hz,4}|\mu < |F_{hy,4}| < \frac{|F_{hz,4}|}{\mu} \tag{187}$$

$$|M_{hx,4}| \geq \frac{1}{1+\mu^2}[|F_{hy,4}|(L_g + 2\mu R_p + \mu^2 L_g) + |F_{hz,4}|(R_p^2 - \mu^2 R_p^2)] \tag{188}$$

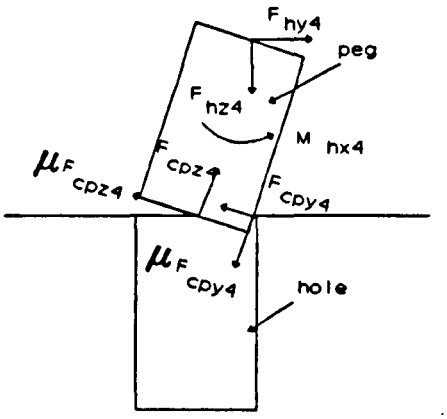

Fig. 90 The contact configuration for the adjustment phase

the peg can then be inserted into the hole. The applied forces in the simulation can be described in Fig. 103-106.

7.5.3 The movement of the peg and the contact forces between the peg and hole in the fourth step

(1) Before the peg is inserted into the hole,

$$|\theta_{hx,4}| \geq \arccos\frac{r_p}{r_h} \tag{189}$$

the contact forces $F_{chpz,4}$, $F_{chpy,4}$ and acceleration $\theta_{hx,4}$ can be calculated. If the peg contacts the hole with the side-surface and the bottom-surface of the peg, the relationship between $(O_p)_{hpz,4}$ and $\theta_{hpx,4}$ can be described as follows:

$$\tan\theta_{hpx,4} = \frac{2R_h - R_p\cos\theta_{hpx,4}}{(O_p)_{hpz,4} + R_p\sin\theta_{hpx,4}} \tag{190}$$

The contact configurations can be divided into three:

(a) the peg contacts the hole with the bottom-surface and the side-surface of the peg. Both of $F_{chpz,4}$ and $F_{chpy,4}$ exist,

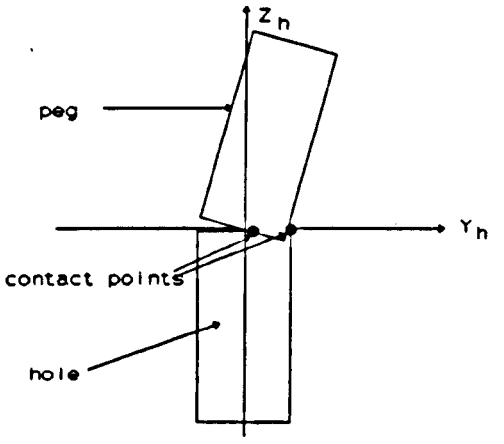

Fig. 91 The contact configuration when the contact points are on the bottom and side-surfaces of the peg before the insertion operation

(b) the peg contacts the hole with the bottom-surface of the peg. Only $F_{chpz,4}$ exists in this case,

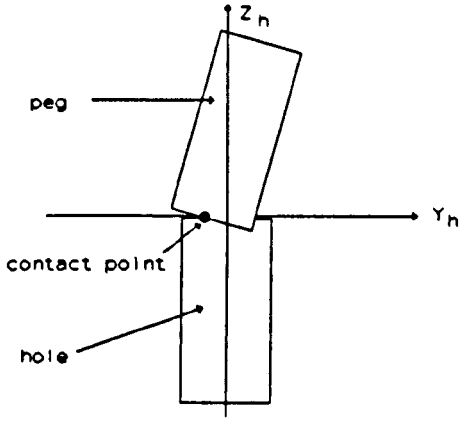

Fig. 92 The contact configuration when the contact points are on the bottom surface of the peg before the insertion operation

(c) the peg contacts the hole with the side-surface of the peg, only $F_{chpy,4}$ exists in this case,

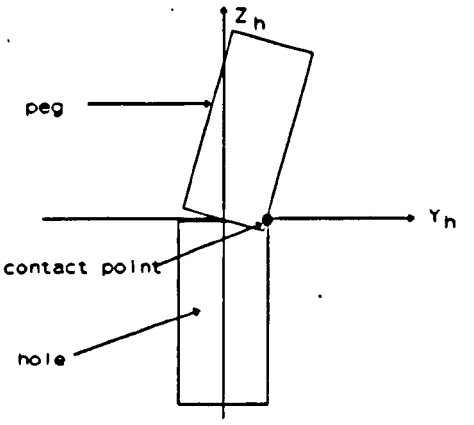

Fig. 93 The contact configuration when the contact point is on the side-surface of the peg before the insertion operations

(2) the peg is inserted into the hole, and $\theta_{hx,4} < 0$

The contact forces and the movement of the peg can be simulated. The contact configurations of the peg-hole system can be divided into four:

(a) there is one contact point between the peg and the hole, and $(c)_{hy,4} < 0$:

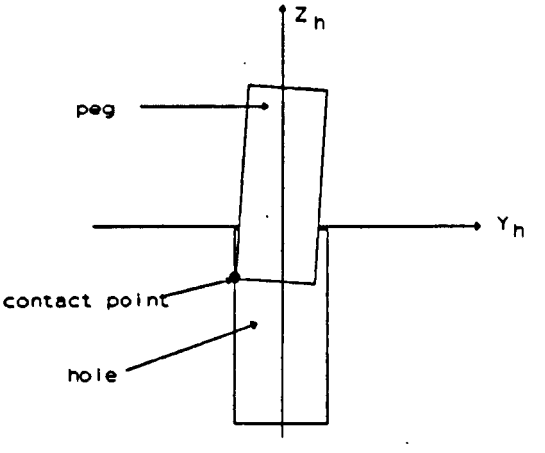

Fig. 94 The contact configuration when $(c_{hy,4}) < 0$ after the peg is inserted into the hole and $\theta_{hx,4} < 0$

(b) there is one contact point between the peg and the hole, and $(c)_{hy,4} > 0$:

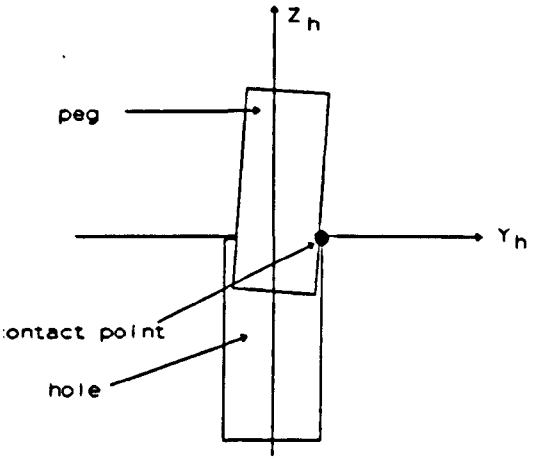

Fig. 95 The contact configuration when $(c_{hy,4}) > 0$ after the peg is inserted into the hole and $\theta_{hx,4} < 0$

(c) there are two contact points between the peg and the hole, and $(c_1)_{hy,4} > 0$, $(c_2)_{hy,4} < 0$

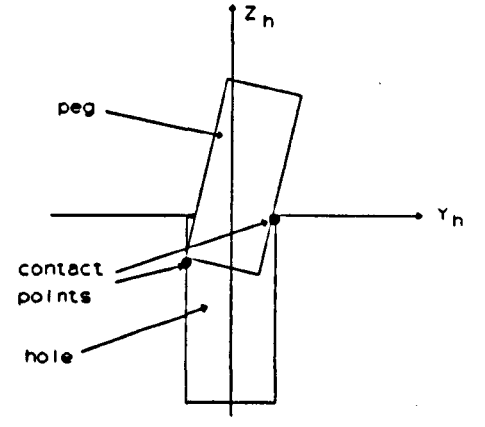

Fig. 96 The contact configuration when $(c_1)_{hy,4} < 0$ and $(c_2)_{hy,4} > 0$ after the peg is inserted into the hole and $\theta_{hx,4} < 0$

(d) there is no contact point between the peg and the hole

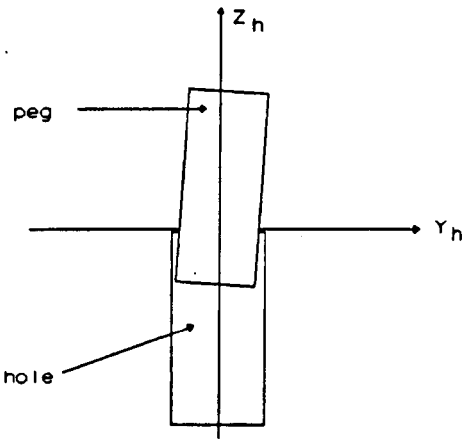

Fig. 97 The contact configuration without contact points after the peg is inserted into the hole and $\theta_{hx,4} < 0$

(3) the peg is inserted into the hole, and $\theta_{hx,4} > 0$

The contact forces and movement of the peg can be simulated. The contact configurations can be divided into three:

(a) there is one contact point between the peg and the hole, and $(c)_{hpy,4} < 0$,

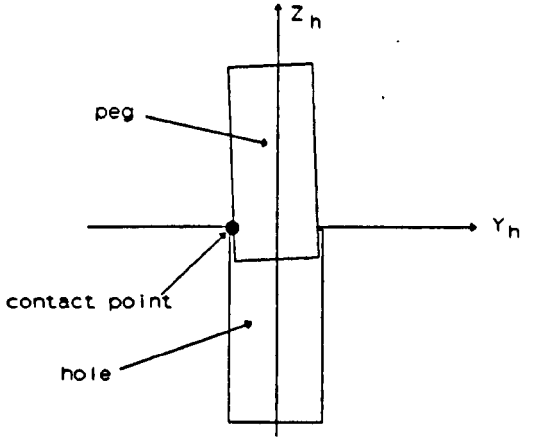

Fig. 98 The contact configuration when $(c)_{hy,4} < 0$ and $\theta_{hx,4} > 0$ after the peg is inserted into the hole

(b) there is one contact point between the peg and hole, and $(c)_{hpy,4} > 0$,

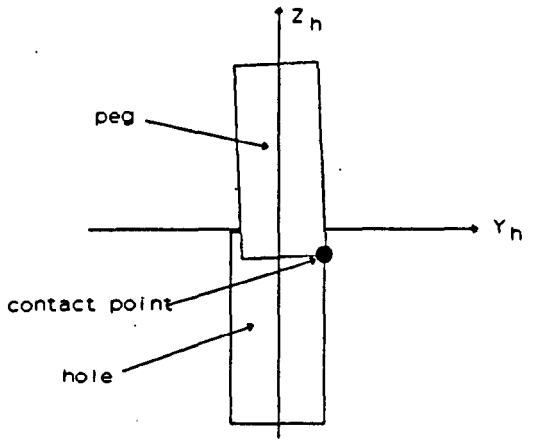

Fig. 99 The contact configuration when $(c)_{hy,4} > 0$ and $\theta_{hx,4} > 0$ after the peg is inserted into the hole

(c) there are two contact points between the peg and the hole, and $(c_1)_{hpy,4} > 0$ and $(c_2)_{hpy,4} < 0$:

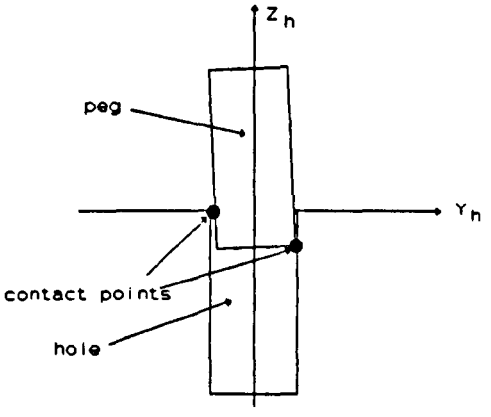

Fig. 100 The contact configuration when there are two contact points between the peg and the hole when $\theta_{hx,4} > 4$ after the peg is inserted into the hole

(d) there is no contact point between the peg and the hole

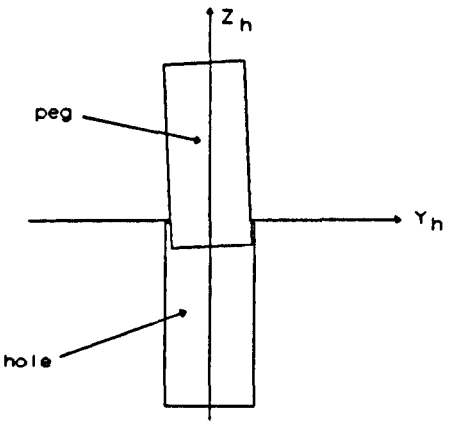

Fig. 101 The contact configuration when there is no contact point when $\theta_{hx,4} > 0$ and the peg is inserted into the hole

The simulation of the movement of the peg can be presented in Fig. 107-109.

7.6 Insert the peg into the hole deeply

In this step, the peg is inserted into the hole. The applied force $F_{hz,5}$ as designed is to insert the peg deeply into the hole.

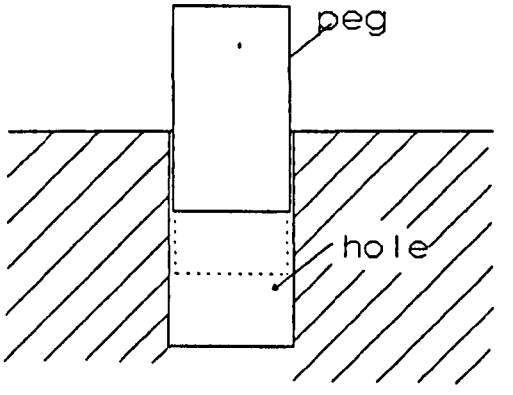

Fig. 102 Insertion operation

The applied forces in the simulation can be presented in Fig. 103-106.

The types of the movement of the peg in this step can be shown as follows:

names	ΔX_5	ΔY_5	ΔZ_5	$\Delta\theta_{hx,5}$	$\Delta\theta_{hy,5}$	$\Delta\theta_{hz,5}$
types	compliant	compliant	guided and compliant	compliant	compliant	fixed

Table 14 The types of the peg movement in the fifth step

The contact forces and the movement of the peg can be simulated in the method similar to step 4.

7.7 Simulation of peg-hole assembly operation

$R_h^* = 16\ mm$,

$R_p^* = 15.99\ mm$,

$m_p^* = 1\ kg$,

$i_p = 0.65\ kgm^2$,

$R_h = 12\ mm$,

$R_p = 11.99\ mm$,

$m_p = 1.1$ kg,

maximum(noise/applied force) = 0.1,

time for each step is 0.5 *second*.

The applied forces to the peg during the assembly operations in the simulation can be presented as follows:

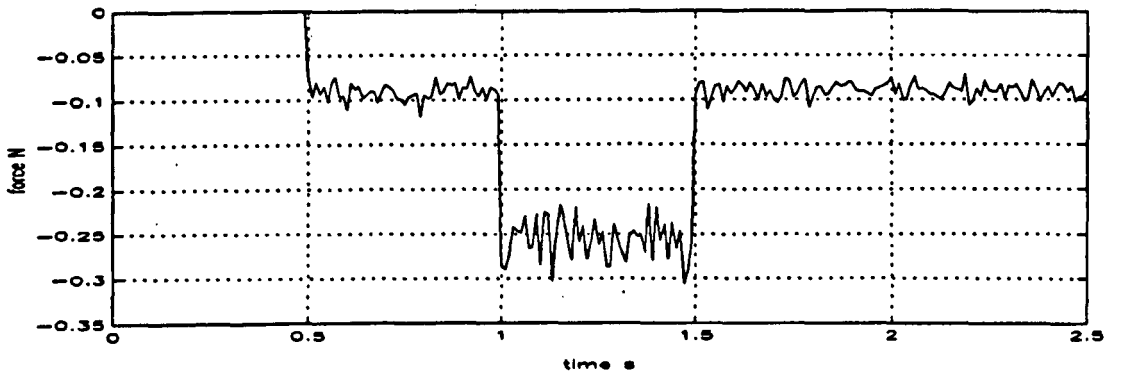

Fig. 103 The input force F_{hz} along Z_h axis

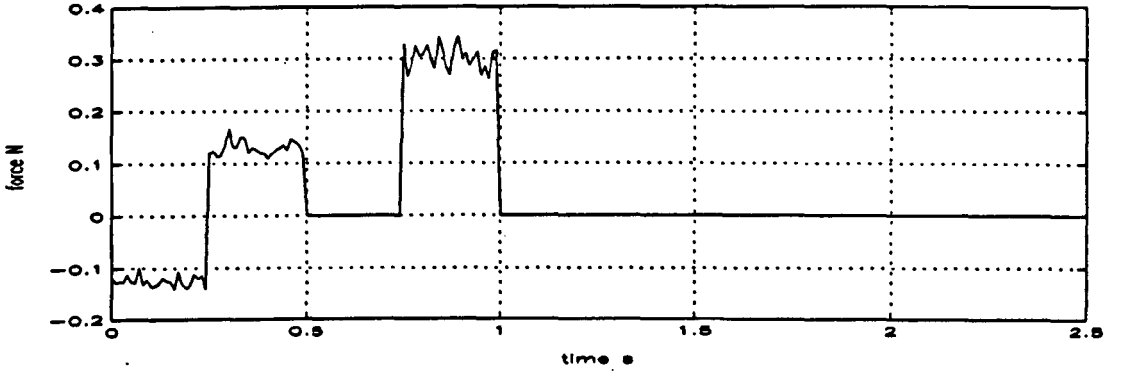

Fig. 104 The input force F_{hx} along X_h axis

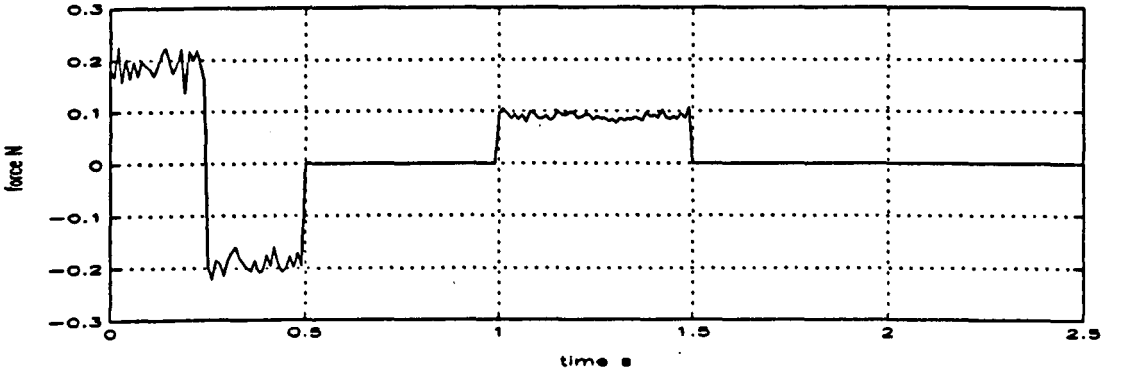

Fig. 105 The input force F_{hy} along Y_h axis

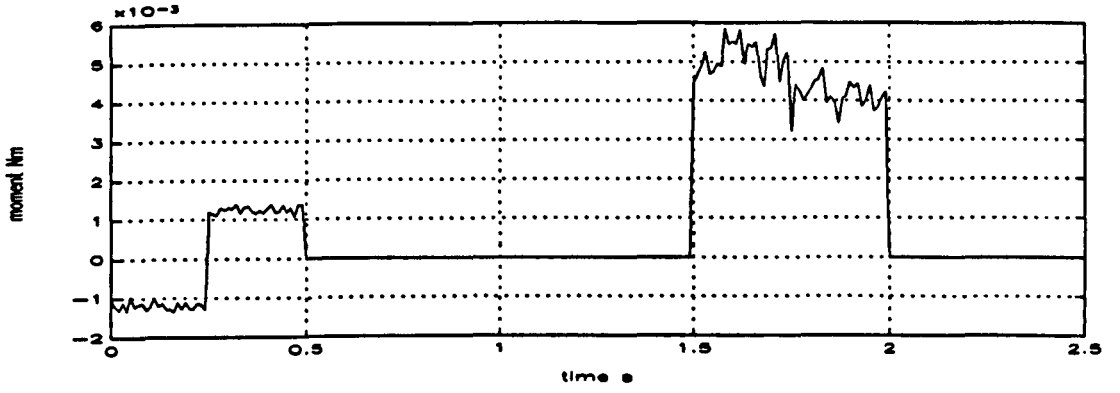

Fig. 106 The input moment M_{hx} around the X_h axis

The movement of the peg in the assembly operation in the simulation can be presented as follows:

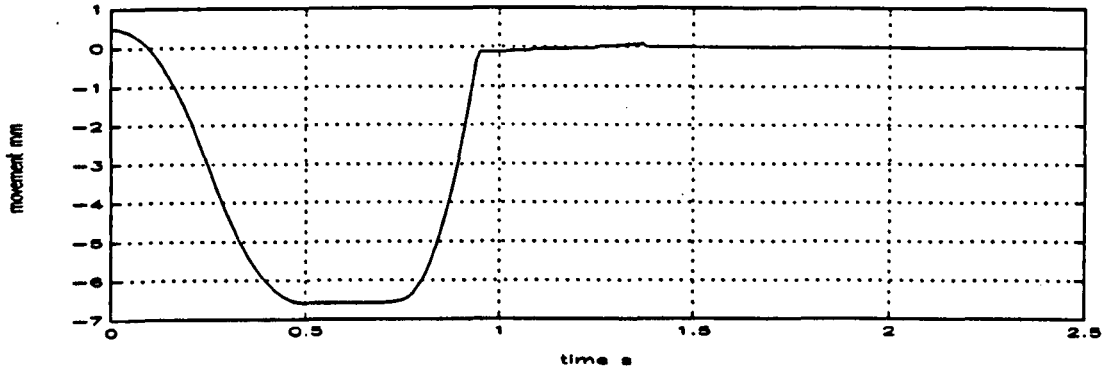

Fig. 107 The projection $(O_hO_p)_{hx}$

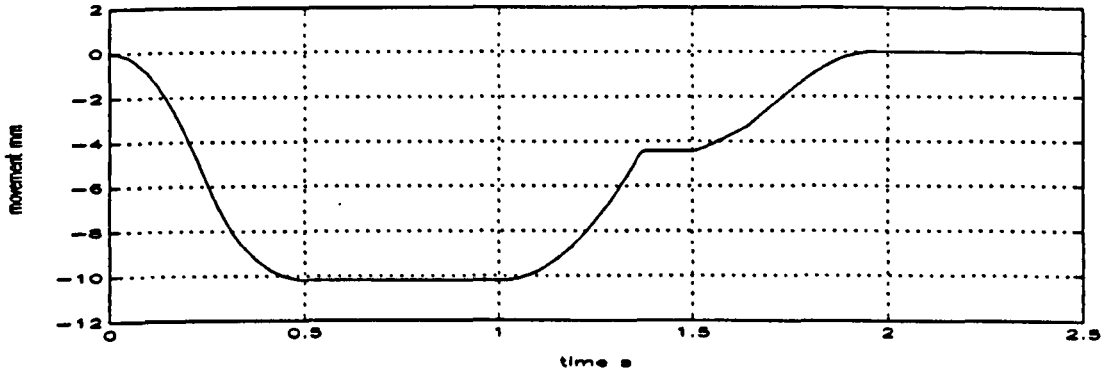

Fig. 108 The projection $(O_hO_p)_{hy}$

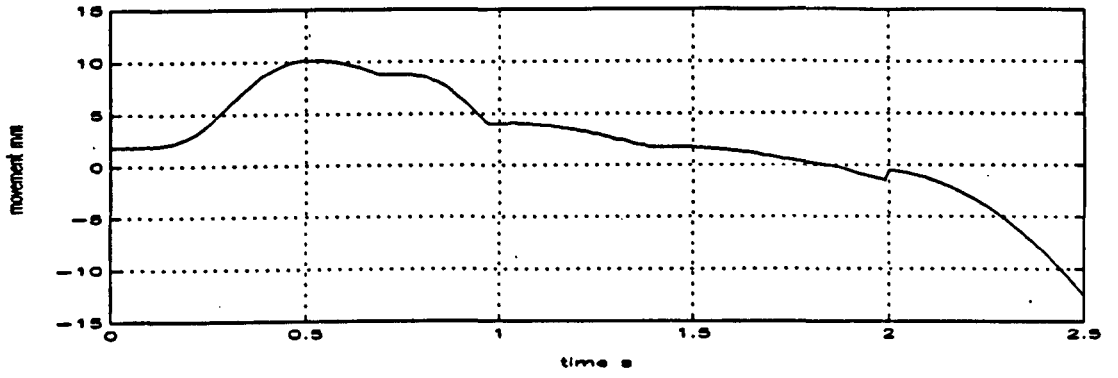

Fig. 109 The projection $(O_hO_p)_{hz}$

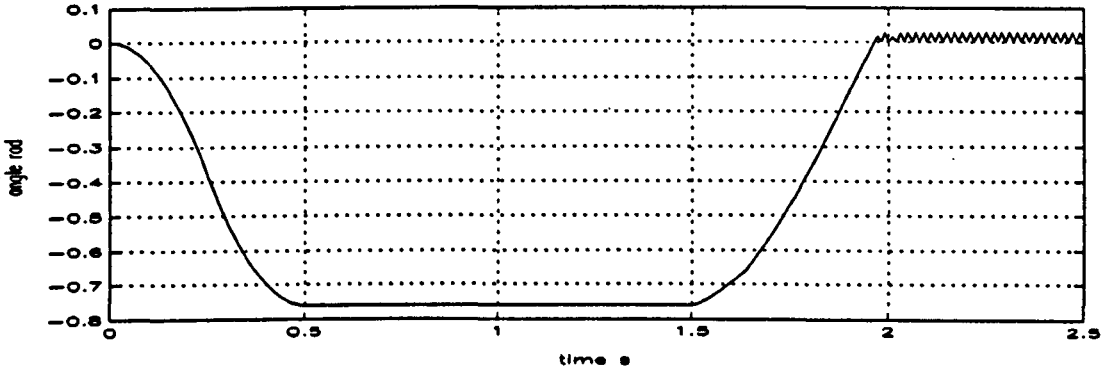

Fig.110 The projection θ_{hx}

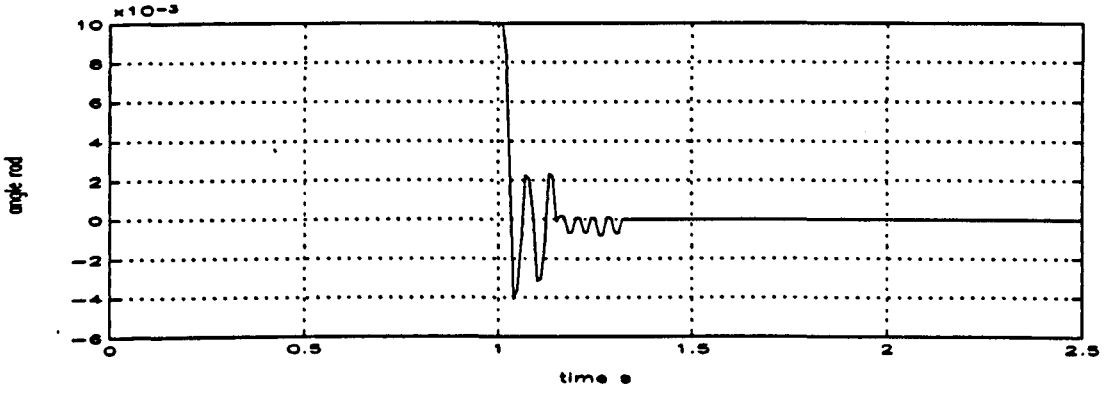

Fig.111 The projection θ_{hy}

The contact forces between the peg and the hole in the assembly operation in the simulation can be presented as follows:

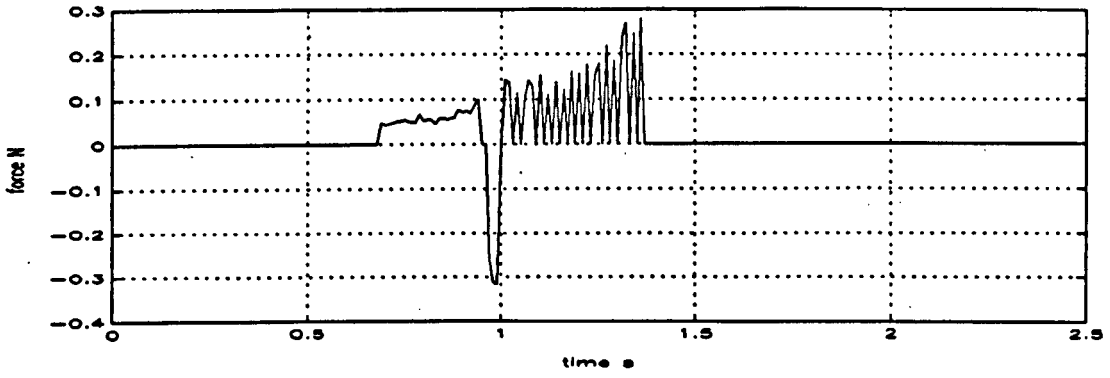

Fig. 112 The projection F_{chpx} of the contact force along X_h axis

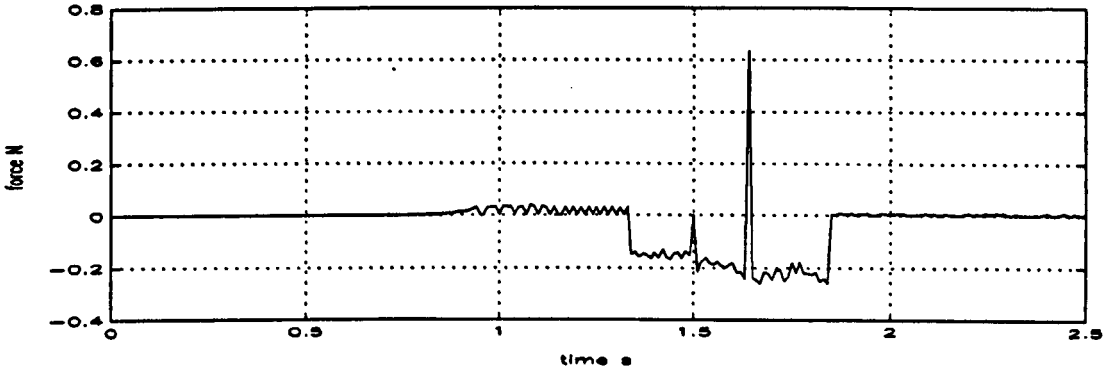

Fig. 113 The projection F_{chpy} of the contact force along Y_h axis

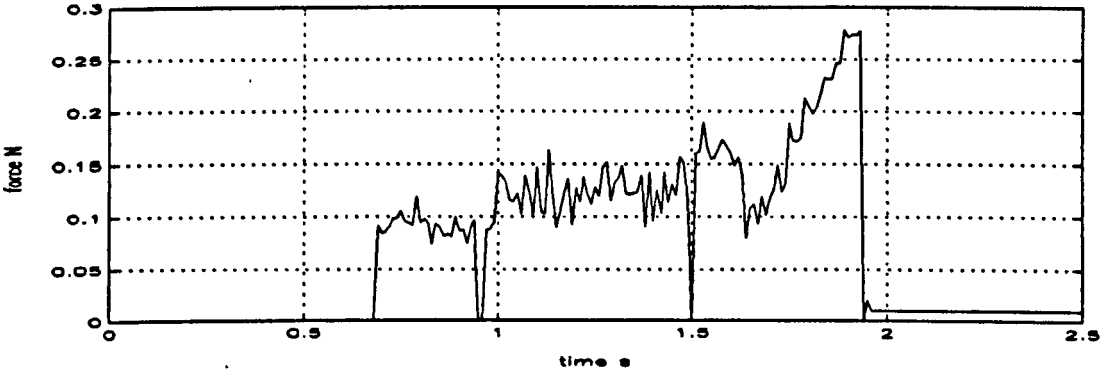

Fig. 114 The projection F_{chz} of the contact force along the Z_h axis

The location of the contact points on the bottom of the peg can be presented as follows:

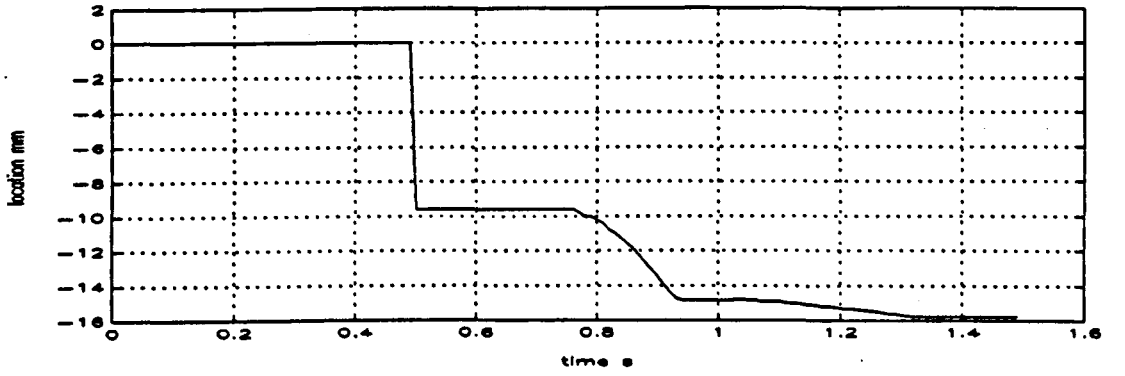

Fig. 115 The projection $(C_1)ppx$ of the first contact point along X_{pp} axis

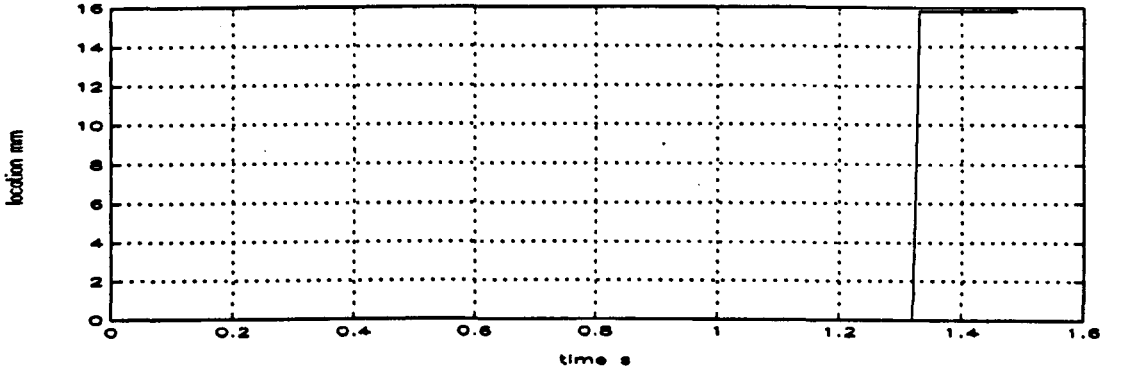

Fig. 116 The projection $(C_2)_{ppx}$ of the second contact point along X_{pp} axis

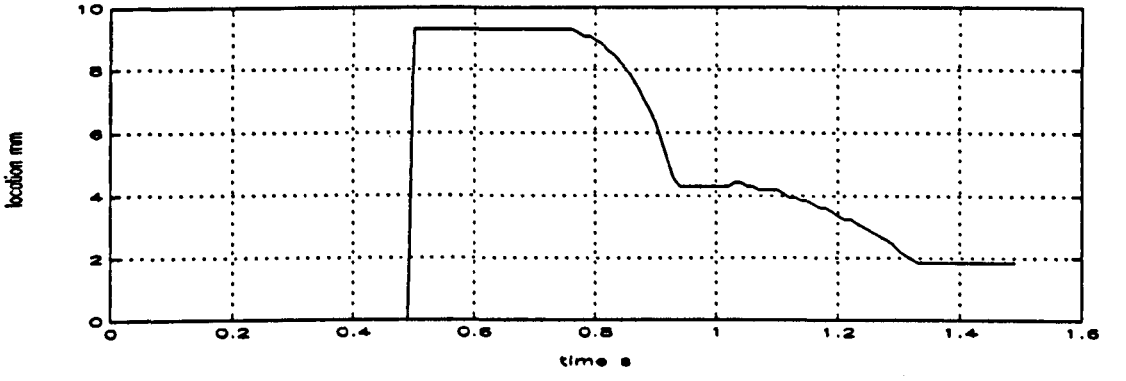

Fig. 117 The projection $(C_1)_{ppy}$ of the first contact point along Y_{pp} axis

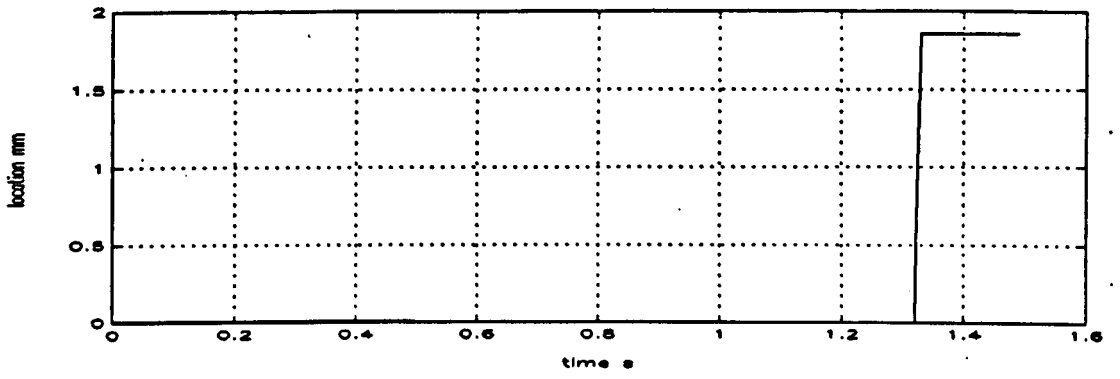

Fig. 118 The projection $(c_2)_{ppy}$ of the second contact point along Y_{pp} axis

In this chapter, the method not requiring force sensors or RCC has been simulated. The simulation includes the applied forces, the movements of the peg, the locations of the contact points, contact forces and frictional forces. The purposes of the simulations are:

(1) to prove the validity of the insertion methods,

(2) to improve the analysis of trends of the locations of the contact points, the contact forces and frictional forces,

(3) to study the movement of the peg,

(4) to study the allowable initial range of the position of the peg for the strategy and,

(5) to study the input designs.

In the next chapter, the experiments using UMI-RTX robot without force sensors will be described.

CHAPTER 8 EXPERIMENTS

8.0 Introduction

The strategy investigation has now been completed. The insertion operation using the strategy where the use of the force sensors or RCC was avoided were simulated in the last chapter. In the simulation programs,

(1) the input forces from the robots are assumed to include the nominal designed input forces and noises,

(2) the types of the robots in the system were not defined. The links of the robots were assumed to be rigid and,

(3) the peg and hole were assumed to be cylindrical.

In practice, the actual input forces are exactly the same as those in the simulation program. The links of the robot are not rigid and would be deformed by the forces between the robot and the peg. The peg and the hole are not strictly geometrically cylindrical. All of these slight differences would make the movement of the peg in practice differ from that in the simulation although they would not influence the feasibility of the strategy in practice.

In this chapter, the experiments using UMI-RTX robot will be presented.

8.1 UMI-RTX robot

8.1.1 The Geometry of the UMI-RTX robot:

In UMI-RTX robot, there is a column, shoulder, upper arm, lower arm, wrist and gripper. The height of the robot is 1251 mm, the total movement radius is 1010.4 mm. The diagram below shows the RTX-robot:

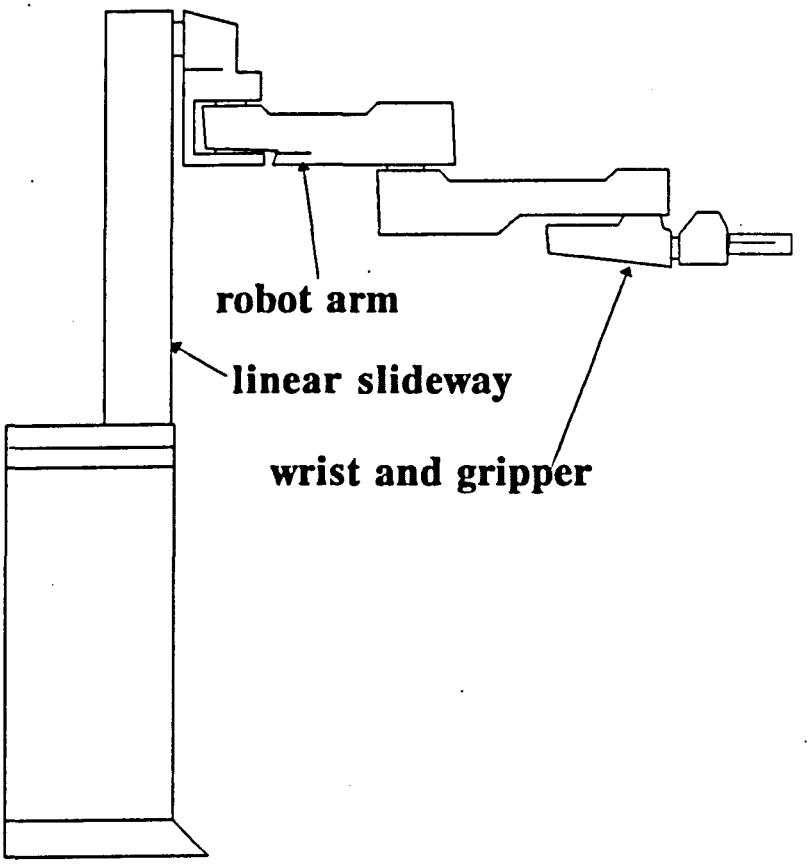

Fig. 119 The diagram of UMI-RTX robot

8.1.2 Drivers in the UMI-RTX robot

There are seven precision 24 V DC motors in RTX robot. One with 20 W output power, is used to control the vertical motion. Six others with 30 W output power are used to control other axes.

The shoulder motor and elbow motor drive the upper-arm and lower-arm, respectively. Both of them drives the arms through a gearbox and a two-stage belt reduction. The final pulley is fixed to the arms. The intermediate combined pulley is on an eccentric spindle that allows the secondary belt tension to be adjusted. The shoulder motor is fixed on a slotted plate which is used to allow the primary belt tension to be adjusted.

The wrist unit is fixed to the lower arm through a plate. This wrist mounting plate is driven by the wrist yaw motor located in the upper-arm through a gearbox and a

series of pulleys.

The wrist unit is fixed by four screws to the lower arm's wrist plate. This means that the wrist unit can be taken off, and some other piece of equipment, such as the peg attached. There are two gear motors, called wrist 1 and wrist 2 in the unit. Each drives a spiroid bevel gear, which in turn drives an output bevel gear.

The gripper consists of two identical moulded jaws, each linked to a tip.

In each motor, a two-phase optical incremental encoder is fitted. The software can monitor the movement and the direction of the motors.

8.1.3 Encoders

In each encoder, there is a small printed circuit board, attached to the motor, and a moulded plastic disc pressed on the extended motor spindle.

The disc has vanes which pass between the two slotted opt-switches mounted on the pcb. A square wave arranged to be 90^0 degrees out of phase to the other is generated by each of the switches.

8.1.4 Torques to the arm joint

The motors are driven using pulse width modulation. The width of the pulse of current, which is supplied to the motor every 16 ms, regulars the torques to the arm joints. The amount of current drawn by the motor is dependent on:-

(1) the speed of the motor,

(2) the current-limiting circuitry the motor drive circuits.

The current that can be drawn by the motor decreases in a linear way with an increase in motor speed. Motor torque is proportional to motor current.

8.1.5 Repeatability

The repeatability of the RTX's movement is +/-0.5 mm at the wrist pivot.

8.1.6 RTX's electronics

Behind the column, the control unit electronics are mounted. The main controller card is fixed by nuts in the T-slots on the column. The main controller in an IP (intelligent peripheral) board which consists of IP 0, IP 1 and the motor-driving circuitry. There is also an external motor driver (EMD board), mounted on the side of the column, which powers the zed motor, and a power supply behind the column main support bracket. Each IP is an Intel 8031 micro controller and includes an Intel 8156 256-byte RAM with input/output, a 27128 EPROM, and a 8243 input/output expander. In each IP, proportional, integral and differential (PID) control algorithm is fitted.

The motor drivers are Sygnetics L293E chips, each supplying a nominal third of an amp to each motor.

8.1.7 How the IPs control the motors

When one of the RTX's motors is programmed to move to a new position, the processor in the IP controlling that motor computes a velocity-versus-time curve for the motion. This processor, called velocity profiling, is performed by software. The servo control of the motors is proportional, integral and differential terms which can be fixed by the controlling computer. Offset is needed to overcome the friction of the motor and the deadband is needed to give a range within which RTX will assume it has achieved its destination.

The output of the servo loop to the motor is a pulse of current,of fixed amplitude and with a width from 0 to 64 units.

The current supplied to the motor depends on the five control parameters, and also on the error returned from the previous cycles.

8.1.8 The RTX library

As mentioned previously, RTX is driven by seven motors which are controlled jointly

by two processing units called intelligent peripherals. The intelligent peripherals are refereed to as IP0 and IP1, and each one has responsibility for specific motors. The intelligent peripherals are controlled by a communications protocol called IPC--Intelligent peripheral communications.

The basic commands in the library can be presented as follows:

(a) preparing the arm at the start of an operation, keyword including INIT COMMS, VERSION, RESTART, DEFINE ORIGIN,

(b) defining how the arm will move, keyword including READ, WRITE, SET MODE,

(c) initiating movement of the arm, including GO, INTERPOLATE,

(d) getting reports on the arm's current status, including MOTOR STATUS, GENERAL STATUS,

(e) stopping the arm, keyword including STOP,

(f) using IPC directly, keyword including RAW COMMAND, RAW RESPONSE.

There are two sets of parameters used to define the arm movement:-

(a) the control parameters, which use the keyword READ and WRITE,

(b) the motor modes, which use the keyword SET MODE.

There are three pairs of options in the motor mode:-

(a) force and position mode,

(b) absolute or relative motion (in position mode only),

(c) user input and output.

In force mode, the motor uses a constant force to the part of RTX that is being driven. If RTX robot meets an obstacle, the motor does not try to drive the RTX to push any harder. If that amount of force can move the obstacle, then it moves; otherwise, the arm of the robot will stop.

In position mode, the force increases when the arm meets an obstacle: RTX keeps pushing with more and more force up to the maximum force defined.

8.2 The peg-hole system

The picture of the peg is presented as follows:

Fig. 120 The picture of the peg used in the experiments

The material of the peg is 45# steel. The diameter of the peg is 31.99 mm. The length of the peg is 60 mm.

The picture of the hole is presented as follows:

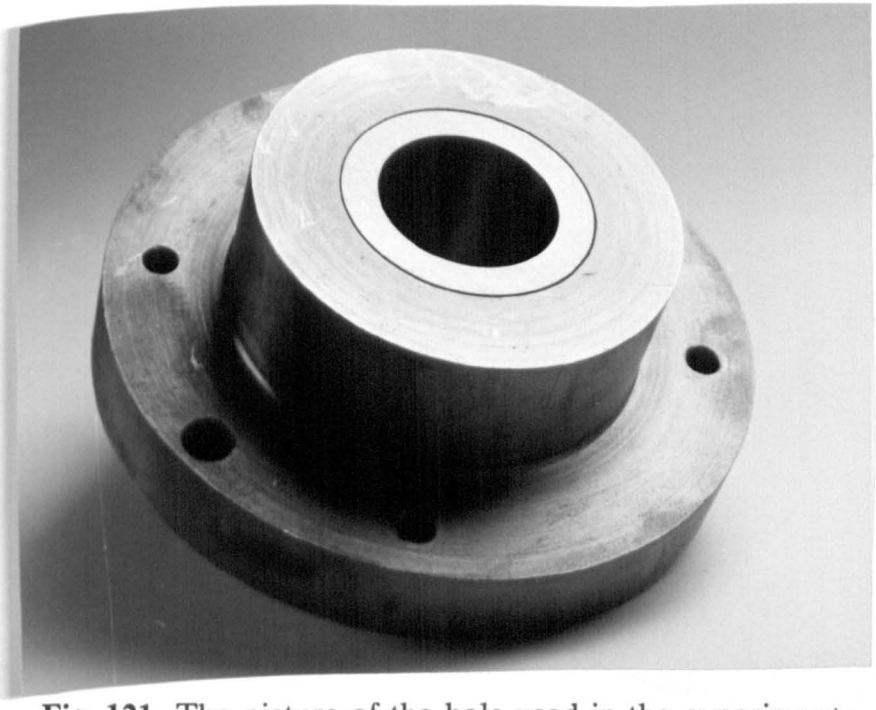

Fig. 121 The picture of the hole used in the experiments

The material of the hole is 45# steel. The diameter of the hole is 32.01 mm. The depth of the hole is 31 mm.

8.3 The Experiments environment

The experiment are simply set up, which can be described as follows:

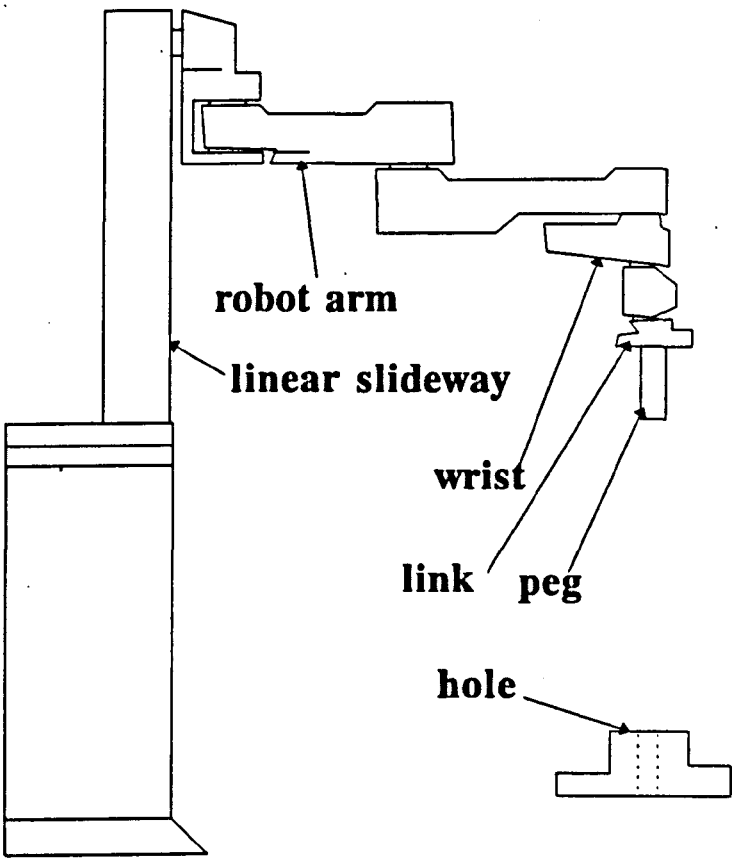

Fig. 122 The robotic peg-hole system

Both of the robot and the hole are fixed. The peg is connected with the wrist of the robot.

8.4 The robotic peg-hole insertion operations without force sensors

The robotic peg-hole insertion operation has been achieved reliably in the experiments. The assembly operation has been recorded in the video. The following series of pictures illustrates the intermediate steps.

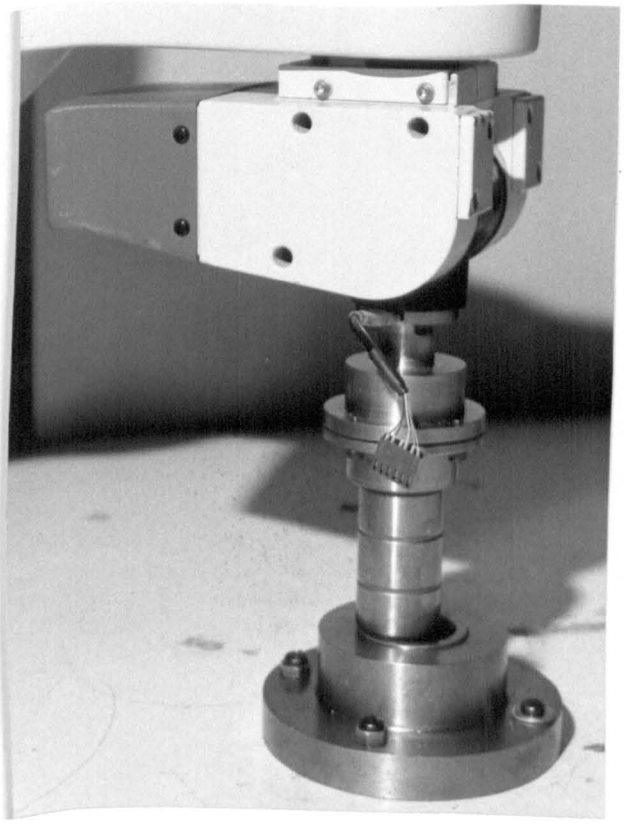

Step 1: Initial inherited state

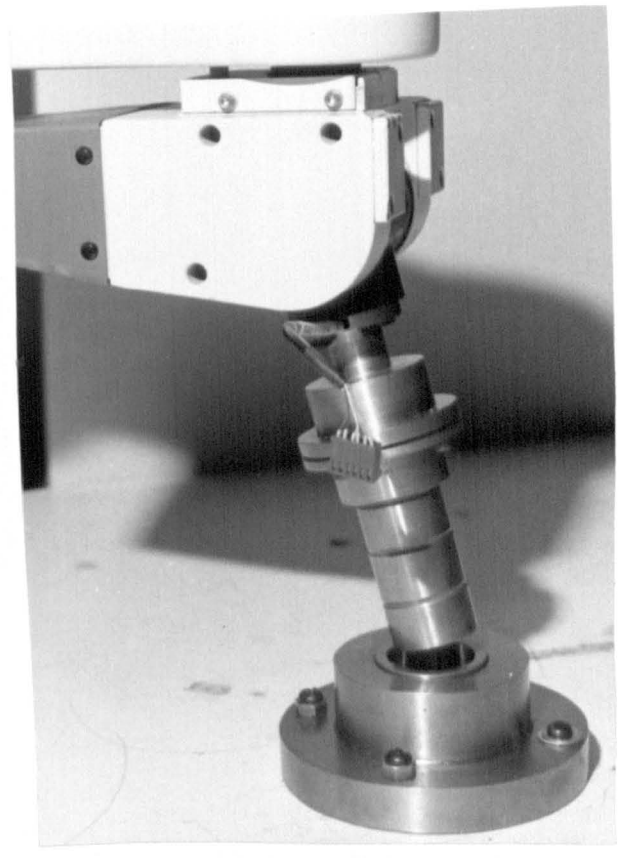

Step 2: Moving to new area

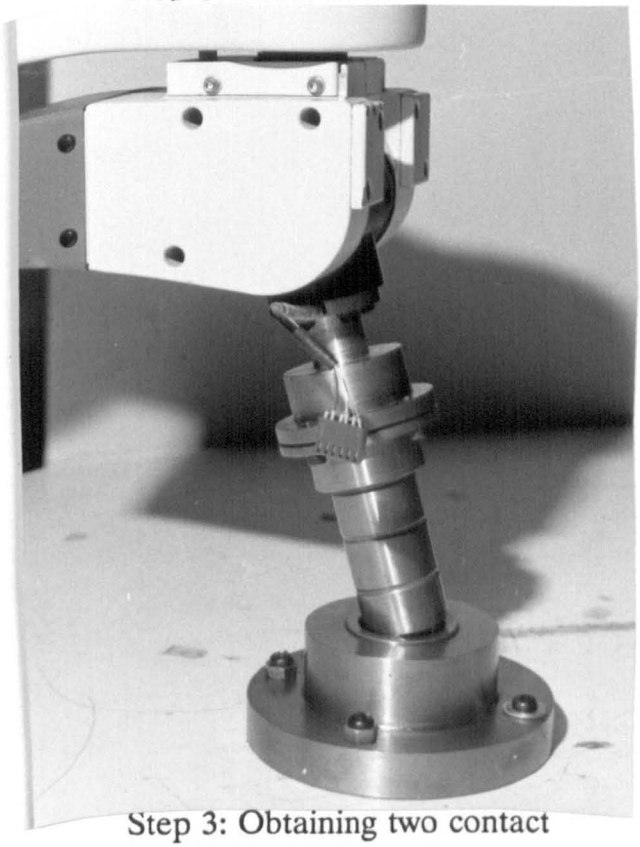

Step 3: Obtaining two contact points

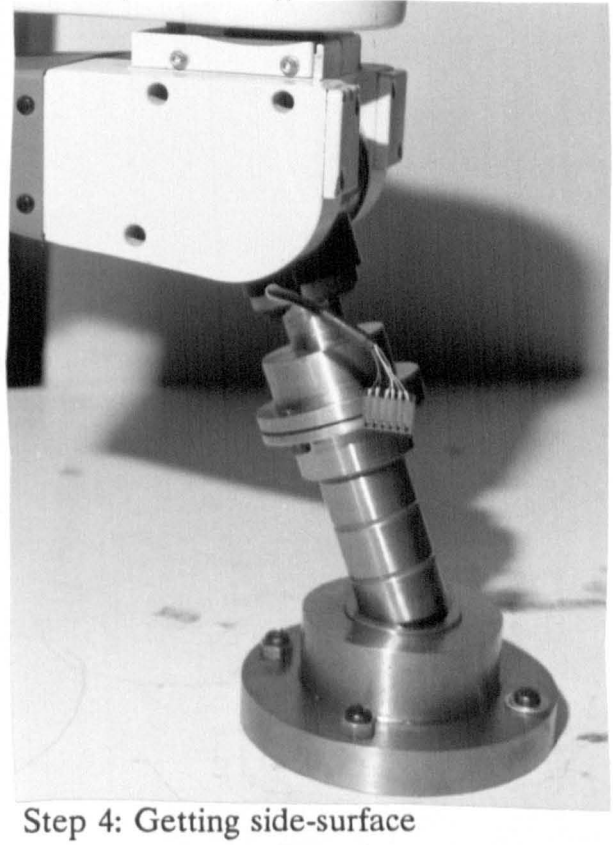

Step 4: Getting side-surface point

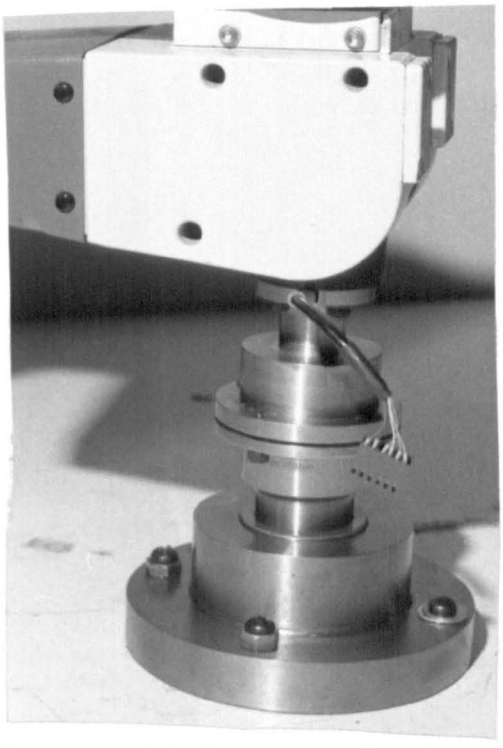

Step 5 and 6: Insertion adjustment and start

Fig. 123 Intermediate steps in experiments

The operation time was 2.5 s. The maximum contact force was 0.5 N. With the use of enhanced SCARA UMI-RTX robots, there are some comments worth to be noted as follows:

(a) The rotation of the peg around *hx* is achieved by the combination of the movements of the motors for the wrist.

(b) In step (c), the movement of the peg along the Y_h axis is achieved by the rotation of the shoulder. The values of $|(O_hO_p)_{hx}|$ and $|\theta_{hy}|$ are further reduced through the free controller of the elbow and the wrists. For the robots which cannot provide free movement about two axes , the strategy would still be valid. In that case, $|(O_hO_p)_{hx}|$ is reduced when the peg is moved to approach three point contact state and $|\theta_{hy}|$ is reduced in the insertion process.

(c) There were 10 trials of assembly operations for a selected range of pegs and holes giving a perfect success rate.

(d) The operational time for each step is a selectable parameter. Here the

operational time for each step was 0.5 seconds. Then the input forces from the robot were designed to guarantee to move the peg from any point in the last sub-goal to achieve the new sub-goal. If the operational time is re-designed, the input forces must be re-designed. The less the operational time is, the greater the input forces and contact forces must be provided.

(e) If the axis of the hole is slightly off-vertical, the free-control of the wrist and the internal compliance of the robot would help the insertion process. However, if the angle between the nominal and actual axes of the hole is great, there is difficulty to use this strategy.

(f) In the first phase of step (d) $[t_3 - t_4]$, the peg is rotated back to reduce the value of $|\theta_{hx}|$ and pushed into the hole. The rotational angle $\Delta\theta_{hx}$ is bigger than all the possible angle $|\theta_{hx}|$ in the side-surface contact state. During the rotation, the peg is pushed down to the hole to keep three-point contact state. Therefore when $\theta_{hx} = 0$, the end-surface of the peg is already in the hole. The further rotation is prohibited by the hole. In the second phase of step (d) $[t_4 - t_5]$, the peg is pushed into the hole.

(g) There is no additional compliance in the experimental assembly operations using UMI-RTX robot. In the insertion process, the free control of some links and the internal compliance in the UMI-RTX robot help the insertion process.

In this Chapter, the successful experiments of peg-hole insertion operation were described. The clearance of the assembly is 0.02 mm. The length of the peg is 60 mm. The operational time is about 2.5 seconds. These experiments prove the feasibility of the strategy without force sensors using the UMI-RTX robot.

CHAPTER 9 DISCUSSION

9.0 Introduction

9.1 Six-component force sensor design analysis

9.2 The force sensor signals and the location relationship between the peg and the hole

9.3 The requirement of the identification of the peg-hole system

9.4 A strategy provided to achieve the robotic peg-hole insertion with force sensor feedback

9.5 A strategy provided to achieve the robotic peg-hole insertion without the use of force sensor

9.6 Experiments and simulation work

9.0 Introduction

The objective of this thesis is to achieve the robotic peg-hole insertion operation with high-precision, high-speed and low-cost.

9.1 Six-component force sensor design analysis

At the beginning the six-component force sensors, which were popularly used in the robotic peg-hole insertion operation, were selected as the feedback devices. Many force sensors, used in previous assembly research, have been heavily studied and the general rules in the six-component force sensor design were concluded.

9.2 The force sensor signals and the location relationship between the peg and the hole

The main problem was if the signals from the force sensors were used to identify the location relationship between the peg and the hole, which could guide the elimination of the translational and rotational errors between the peg and the hole. This problem was often over-looked. In this thesis, it was found that the validity of the location relationship identification between the peg and the hole using force sensors depended on:

(a) if the force sensory signals could be used to obtain the magnitudes and the directions of the contact forces and the moments between the peg and the hole and,

(b) if the magnitudes and the directions of the contact forces and the moments could be used to identify the location relationship between the peg and the hole.

The first item could be easily achieved and the algorithm describing the relation

between the force sensory signals and the contact forces and the moments between the peg and the hole was decided by the structure of the force sensors.

The second item if the location relationship between the peg and the hole could be identified according to the magnitudes and the directions of the contact forces and the moments between the peg and the hole remained a serious problem, which was often over-simplified. To illustrate this problem clearly, two concepts--the centre of the overlap of the projections of the contact surfaces and the centre of the contact area were provided. The former one was always related to the location relationship between the peg and the hole. The later one was certainly related to the values of the contact forces and the moments. Therefore if the centre of the overlap of the projections of the contact surfaces and the centre of the contact area coincide with each other, the location relationship between the peg and the hole could be obtained from the values of the contact forces between the peg and the hole and the second item could be easily achieved. In this thesis, however, it was found that these two measures would coincide if and only if that:

(a) the angle between the axes of the peg and the hole was zero and,

(b) the contact surfaces were absolutely smooth.

In practice, the non-zero angle between the axes of the peg and the hole and the defects of the contact surfaces always exist, so the centre of the overlap of the contact surfaces and the centre of the contact area do not coincide with each other. In a conclusion, the location relationship between the peg and the hole cannot be obtained directly from the signals from the force sensors. The problem then was how the translational and rotational errors between the peg and the hole could be eliminated and the peg could be eventually inserted into the hole if the location relation between the peg and the hole could not be identified according to the force

sensor signals?

9.3 The requirement of the identification of the peg-hole system

In this thesis, it was further pointed out that the major point of the insertion operation is whether the required information about the peg and the hole can be obtained from the signals from the force sensor and other knowledge of the system, rather than whether the whole location relationship between the peg and the hole can be identified from the signals of the force sensors.

9.4 A strategy provided to achieve precise robotic peg-hole insertion with force sensor feedback

The key points of the strategy could be presented as follows: At the beginning, one set of the force sensory signals corresponded to a range for the system to lie within. Combined with the prior knowledge of the system, the range for the system to lie within can be further reduced. The first command was designed which could perform the system to achieve the first sub-goal from any point in this range. This sub-goal could be considered as the new initial range and the new command could be found to perform the system to achieve the new sub-goal recognizably reccursively. Eventually, a sub-goal was found to be included in the goal where the peg was inserted into the hole.

9.5 A strategy provided to achieve robotic peg-hole insertion without the use of force sensor

Furthermore, it was found that the function of the force sensor signals could be replaced through the use of the environment. In other words, the peg from any

point in the initial area could be moved by first unitary command and fixed by the hole in the first sub-goal. This sub-goal could be considered as a new initial range and the new command to perform the system to achieve the new sub-goal reccursively and eventually a sub-goal was found to include the final goal.

9.6 Experiments and simulation work

These two strategies have been carried out with experiments and further verified through the simulation. The movement of the peg, the location of the contact points, the direction and magnitude of contact forces during the assembly operation can be obtained in the simulation. Because there was no definition of the robot type in the simulation, the potential of the use of these strategies with various types of the robots was recognized.

CHAPTER 10 CONCLUSIONS

In this thesis, the robotic peg-hole insertion operation was investigated. The assembly operation, as an important production link, plays an important role in the modern industry. The most widely used assembly operation model, the peg-hole insertion operation, has been heavily studied.

At the beginning of this thesis, it was pointed out that the robotic peg-hole insertion operation with force sensor signals as feedback does not always work. This is due to the fact that:-

(a) the force sensory signals can only be used to calculate the location of the centre of the contact area,

(b) the translational error between the peg and the hole can only be calculated from the location of the centre of the overlap area,

(c) in most cases, the centre of the contact area and the centre of the overlap area do not coincide.

It is difficult, then to calculate the positional relationship between the peg and the hole according to the force sensory signals. It brings the difficulty in the robotic peg-hole insertion operation.

A strategy to perform the robotic peg-hole insertion operation, by overcoming the difficulty analysed previously, has been proposed. The peg is moved to a new area where the direction of the projection of the centre of the end-surface of the peg with respect to the centre of the hole along the line normal to that which is through the centre of the hole and the base of the robot can be obtained from the the sign of the force sensor signals. Then the movement of the adjustment to reduce the amount of the absolute value of the projection of the centre of the end-surface of the peg with respect to the centre of the hole along the line normal to that which is through the centre of the hole and the base of the robot can be obtained. The state where

the projection of the centre of the end-surface of the peg on the top-surface of the hole is on the line which is through the centre of the hole and the base of the robot can be identified when the moment around the line connecting the centre of the hole and the base of the robot suddenly changes to zero. Afterwards the peg is moved along the line which is through the centre of the hole and the base of the robot and stops when the moment around the line normal to the line which is through the centre of the hole and the base of the robot suddenly changed to zero. The peg is rotated and inserted into the hole with the feedback from the force sensor.

The input forces design and the allowed initial range for the axis of the peg were analysed. Next, the attention focused on the possibility to reduce the demands on the force sensors. A strategy to achieve the precise assembly operation without the force sensors or RCC was proposed.

The peg is moved to a new area where the direction of the projection of the end-surface of the peg with respect to the centre of the hole along the line normal to that which is through the centre of the hole and the base of the robot is known and from which any point can be moved to a state where the projection of the centre of the end-surface of the peg on the top surface of the hole is along the line which is through the centre of the hole and the base of the robot and fixed there. Afterwards the peg is moved to reduce the absolute value of the distance between the projection of the centre of the end-surface of the peg and the centre of the hole along the line which is through the centre of the hole and the base of the robot and stopped where this value is at its minimum value under the angle between the axes of the peg and the hole. Then the peg is rotated and inserted into the hole. The input force design and the allowed initial area for the axis of the peg were analysed. After the strategies were provided, the principles of strategy investigation were analysed

through the use of the concepts of pre-images and back-projections. The strategies provided in Chapter 4 with the use of the force sensor and in Chapter 5 without the use of the force sensor were considered as the most reliable methods.

The strategy provided in Chapter 5 was the best method since there is no need for the use of the force sensors. To analyse its feasibility, the assembly operation insertion was simulated. The location of the contact points and the directions of the contact forces can be obtained from the positional relationship between the peg and the hole. The movement of the peg can be determined by the input forces from the robot and the locational relationship between the peg and the hole. The value of the contact forces can be obtained according to the movement of the peg, the location of the contact point, the direction of the contact forces and the input forces. The feasibility of the strategy was also proven. In the simulation program, no particular type of robot was assumed. So the strategy provided in Chapter 5 was not limited to any particular type of robots. The input force design, and the allowed initial area for the axis of the peg were analysed.

The experiments of the robotic peg-hole insertion operation with the clearance of 0.02 mm using UMI-RTX robot were carried out.

In this thesis, the basis for robotic peg-hole insertion operation has been investigated. The assembly operation using the strategy provided in this thesis is precise, reliable, fast, cheap and requires force sensors or no force sensors. To our knowledge, it is the first time these precise assembly operations with clearance of 0.02 mm have been achieved with cheap robot and without precise feedback. This strategy can also be used for assembly operations with other shaped objects which may be required in industry. When the strategy is widely used in industry, assembly operation with cheap robots may be available and more human-free factories may be established at

Furthermore, the strategy investigation method used in this thesis can also be useful in other research.

CHAPTER 11 RECOMMENDATIONS FOR THE FUTURE WORK

11.0 Introducation

The robotic peg-hole insertion has been simply achieved with high-precision, high-speed, low-cost and without the requirements of the use of the force sensors. The experiments have been carried out with SCARR UMI-RTX robot. The validity of the strategies has also been verified through the simulation where the robot types have not been specially defined.

11.1 The application of the new strategies with other types of the robots

The simulation results provide the potential of the use of these strategies with various types of robots. However, to use these methods with other kinds of the robots still needs a lot of experimental and research work such as the analysis of:

(a) the influences of the flexibility of the robotic links,

(b) the maximum forces which can be provided by the robots,

(c) the maximum errors between the nominal force and the actual force from the robot and between the nominal and actual coordinate frames.

11.2 The application of the new strategies in other shaped objects assembly operation

It has already been noticed that these new strategies can be used in other shaped objects assembly operation with slight improvements. The simulation work about this research is in process. If these methods can be successfully used in various shaped objects assembly operation, many practical assembly problems can be solved with high precision, high speed and low-cost.

11.3 The theoretical approach in the general strategy investigation

Furthermore, much research work in the strategy investigation for the robotic peg-hole insertion, such as the sub-goal selection and the use of the compliant motion to achieve the defined sub-goal, can be useful in the general strategy investigation. It is necessary to conclude these works using a more theoretical approach.

11.4 Application of the strategies in industry

A lot of time and effort is also needed to transfer these strategies from the laboratories to the industry.

REFERENCES

1 **Cho, H. S., Warnecke, H. J.** and **Gweon, D. G.** Robotic assembly: a synthesizing overview. *Robotica*, 1987, **5**(2), 153-165.

2 **Nevins, J. L.** and **Whitney, D. E.** Research on advanced automation. *Computer,* 1977, **10**(12), 24-39.

3 **Nevins, J. L.** and **Whitney, D. E.** Assembly research. *Automatic*, 1979, **16**, 595-613.

4 **Whitney, D. E.** Discrete parts assembly control-an overview. *ASME J. Dynamic Systems, Measurement and Control*, 1979, **101**(1), 8-15.

5 **Darke, S. H., Waston, P. C.** and **Simunovic, S. N.** High speed robot assembly of precision parts using compliance instead of sensory feedback. *Proc. 7th Int. Symp. on Industrial Robot, Tokyo, Japan, Manufacturer Association*, 1977, 87-98.

6 **De Fazio, T. L., Seltezer, D. S.** and **Whiteny, D. E.** The instrumented remote centre compliance. *The Industrial Robot*, 1984, **11**(4), 238-242.

7 **Lane, J. D.** Evaluation of a Remote Centre Compliance Device. *Assembly Automation*, 1980, **1**(1), 36-46.

8 **McCallion, H., Johnson, G. R.** and **Pham, D.T.** A Compliance device for inserting a peg into a hole, *The Industrial Robot,* 1979, **6**(2), 81-87.

9 **Watson, P. C.** The Remote Centre Compliance system and its application to high speed robot assemblies", *SME, Robotic International,* 1977, n. AD77-718.

10 **Waston, P. C.** Remote Centre Compliance. *US Patent*, 1978, 4098001.

11 **Whitney, D. E.** Quasi-static assembly of compliantly supported rigid parts. *Trans.*

ASME J. Dyn. Sys. Meas. and Con., 1982, **104**(1), 65-77.

12 **Whitney, D. E.** and **Nevins, J. L.** What is the RCC and what can it do? *Proc. 9th Int. Symp. on Industrial Robots, Washington, D.C.U.S.A.*, 1979, 135-192.

13 **Arai, T.** and **Kinoshita, N.** The part mating forces that arise when using a worktable with compliance. *Assembly Automation*, 1981, **1**(4), 204-210.

14 **Xu, Y. S.** and **Paul, R.P.**, A robot compliant wrist system for automatic assembly, *IEEE Int. Conf. Rob. Autom.*, 1990, 1750-1755

15 **Badano, F., Betemps, M., Redarce, T.** and **Jutard, A.** Robotic assembly by slight random movements. *Robotica*, 1991, **9**(1), 23-29.

16 **Jeomg, K. W.** and **Cho, H. S.** Development of a pneumatic vibratory wrist for robotic assembly, *Robotica*, 1989, **7**(1), 9-16.

17 **Hoffman, B. D., Pollack, H.** and **Weissman, B.** Vibratory insertion process: A new approach to non-standard component insertion. *Tech Pap, Soc Manufacture Engineers*, 1984, MS 84-371. 11p.

18 **Mohri, N., Saito, N.** and **Takeguchi, M.**, A New Method of Inserting Operation Applied by Ultrasonic Vibration in Assembly Process, *Proc. USA-JAPAN Symposium of Flexible Automation Crossing Bridges: Advances in Flexible Automation and Robotics*, 743-748

19 **Strip, D.P.**, A passive mechanism for insertion of convex peg, *IEEE Int. Conf. Rob. Autom.*, 1989, 242-248

20 **Caillot, F.** and **Kerlidon, M.** Air Steam Compliance. *5th Int. Conf. on Assembly Automation*, 1984, 225-233.

21 **Hesse, S.** Position in der handhabetechink. *Sozialische Rationalisierung*, 1980, **9**, 204-207.

22 **Mashinostroeniya, V.** Assembling joints by magnetic methods of orientation. *Russian Engineering J.*, 1976, **56**(4), 68-71.

23 **Mashinostroeniya, V.** Using a rotating magnetic field for the grippers of industrial robots. *Russian Engineering J.*, 1977, **57**(6), 43-45.

24 **Artique, F.** and **Francois, C.** Automatic assembly by reference searching and position adjustment before insertion. *Proc. of Ro Mansy (Morecki et al, eds.)*, 1985, 431-438.

25 **Galloway, G.**, and **Goumas, P.** Force/torque sensing in automated PCB assembly: a case study, *Robotic Engineering*, 1986, **8**(9), 6-11.

26 **Goto, T.,Inoyama, T.** and **Takeyasu, K.** (1). Precise insertion operation by tactile controlled robot HI-T-HAND Expert 2. *Proc. 4th International Symposium on Industrial Robots Tokyo, Japan, Soc. of Manufacturing Engineers Illinois Inst. of Technology,* 1974, 154-160.

27 **Goto, T, Inoyama, T.** and **Takeyasu, K.** (2). Precise insert operation by tactile controlled robot. *The Industrial Robot*, 1980, 210-213.

28 **Goto, T., Takeyasu, K.** and **Inoyama, T.** Control algorithm for precise insert operation robots", *IEEE Trans. on Sys. Man. and Cyder,* 1980, **10**(1), 19-25.

29 **Hirzinger, G.** and **Brunet, U.**, Fast and Self-improving Compliance Using Digital Force-Torque-Control, *4th International Conference on Assembly Automation*, 1983, 268-281

30 **Hopkins, S. H., Bland, C. J.** and **Wu, M. H.** Force sensing as aid to assembly. *Int. J. Prod. Res.*, 1991, **29**(2), 293-301.

31 **Inoue, H.** Force feedback in precise assembly tasks, *Artificial Intelligence Laboratory, Massachusetts Institute of Technology,* 1974, AI Memo-308 (Reprinted

in Winston, P. H., and Brown, R. H., eds., Artificial Intelligence: An MIT Perspective, MIT Press. 1979).

32 **Kim, H.G.**, A New Interpretation of Force/Servo Control of Robot Arms, *IEEE/RSJ International Workshop on Intelligent Robots and Systems IROS'91*, 1991, 1623-1627

33 **Lee, C. S. G** and **Smith, R. H.** Force feedback control in insertion process using pattern analysis technique. *Amer. Control Conference, San Diego, U.S.A., American Automatic Control Council,* 1984, 39-44.

34 **Ohishi, M., Kakinuma, T** and **Yokoyama, S.** One procedure concerning the peg-hole insertion of the assembly operation. *Proc. 15th. Int. Symp. on Industrial Robot, Tokyo, Japan,* 1985, 811-817.

35 **Piller, G.** A compact six degree of freedom force sensor for assembly robot. *Proceedings of the Twelfth International Symposium on Industrial Robots (IFS Publications, UK),* 1982, 121-129.

36 **Romiti, A., Belforte, G., D'Alfio, Quagliott, N. F.** and **diTorino, P.** A Self_adaptive guided assembler (SAGA). *SME Tech. Pap. Ser MS, 82-225,* 1982, 8p.

37 **Qiao, H., Dalay, B. S.** and **Parkin, R. M.** A Robotic peg-hole insertion operation using a six component force sensor. *Proc. Instn. Mech. Engrs*, 1993, **207**, 289-306.

38 **Qiao, H, B. S. Dalay** and **R. M. Parkin**, 1995, A Novel and Practical Strategy for the Precise Robotic Peg-Hole Insertion Operation, *International Journal of Robotica, vol. 13 29-35*

39 **Sanderson, A. C.** and **Perry, G.** Sensory-based robotic assembly system: Research and application in electronic manufacturing. *Proc. IEEE*, 1983, **71**(7), 856-871.

40 **Splanding, G. H.** A three-axis force sensing system for industrial robots. *Proceedings of the third International Conference on Assembly Automation (IFS Publications, UK), Institute Of Production Automation, Boeblngen, Germany,* 1982, 565-576.

41 **Stokic, D. and Vukobratovic, M.** Simulation and control synthesis of manipulator in assembly technical parts. *Trans. A.S.M.E.* 1979, **101**, 332-338.

42 **Takeyasu, K., Goto, T and Inoyama, T.** Precision insertion control robot and its application. *ASME J. Engineering for Industry,* 1976, 98(4), 1313-1318.

43 **Van Brussel, H., Bellien, H and Thielemana, H.,** Force sensing for advanced robot control. *Proceedings of Robot Vision and Sensory Controls,* 1985, 59-68.

44 **Van Brussel, H. and Simons, J.** (1). The adaptable or compliance concept and its use for automatic assembly by active force feedback accommodation. *Proc. 9th Int. Symp. on Industrial Robots Washington, D.C. Society of Manufacturing Engineerings, Robot Institute of AM,* 1979, 167-181.

45 **Van Brussel, H., and Simons, J.** (2). Automatic assembly by active force feedback accommodation. *Proc. the 8th Int. Symp. on Industrial Robots Stuttgart, West Germany, Italian Society for Industrial Robots, Italian Machine Tool Manufacturers Association,* 1978, 181-193.

46 **Wu, C. H.** Compliance control of a robot manipulator based on joint torque servo. *International Journal of Robotics Research,* 1985, 4(3), 55-71.

47 **Kasai, M. and Takeyasu, K.** Trainable assembly system with an active sensory table processing 6 axes. *Proc. 11th Int. Symp. on Industrial Robots Tokyo, Japan, Soc. of Manufacturing Engineerings of Technology Res. Inst.-Robot Inst. of AM,* 1981, 210-212.

48 **Ahn, D. S., Cho, H. S., Ide, K., Miyazaki, F.** and **Arimoto, S.** Learning task strategies in robotic assembly systems, *Robotica*, 1992, **10**, 409-418.

49 **Asada, H.** Teaching and learning of compliance using neural nets. *Proc. IEEE Int. Conf. Robotics*, 1990, **7**, 9-16.

50 **Cho, D. S, Cho, H.S., Ide, K., Miyazaki, F.** and **Arimoto, S.** Learning task strategies in robotic assembly system. *Robotica*, 1991, **10**, 409-418.

51 **Hirzinger, G.** Robot learning and teach-in based on sensory feedback. *Proceeding of the IEEE Conference on Robots and Automation (IFS Publication, UK),* 1986, 155-163.

52 **Simons, J., Van Brussel, H., De Schutter, J.** and **Verhaert, J.** A self-learning automation with variable resolution for high precise assembly by industrial robots. *IEEE Trans. Automatic Control*, 1982, **27**(5), 1109-1113.

53 **Simunovic, S.** Force information in assembly processes. *Proc. 5th Int. Symp. on Ind. Robots, Soc. of Manufacturing Engineers Illinois Inst. of Technology Res. Inst.-Robot List of AM,* 1975, 415-431.

54 **Simunovic, S. N.** An information approach to parts mating. *Ph.D thesis, Department of mechanical engineering, Massachusettes Institute of Technology*, 1979.

55 **Whitney, D. E.** Force feedback control of manipulator fine motions. *J. Dynamic Sys., Measurement and Control,* 1977, **98**, 91-97.

56 **Railbert, M. H.** and **Craig, J, J.** Hybrid position/force control of manipulators. *J. Dynamic. Sys. Measurement, Control.* 1981, **102**, 126-133.

57 **Mills, J. K.** and **Goldenberg, A. A.**, Force and Position Control of Manipulators During Constrained Motion Tasks, *IEEE Transactions on Robotics and*

Automation, 1989, 5(1), 30-46

58 **Sailsbury, J. K.** Active stiffness control of a manipulator in cartesian coordinate. *Paper Delivered at IEEE conf. on Decision and Control*, 1980.

59 **Ohwovoriel, M. S., Rath, B.** A theory of parts mating for assembly operation. *Proc. Robot and Man Symp. 81.* 1981.

60 **Erdmann, M.**, On Representation of Friction in Configuration Space, *Int. Jour. Rob. Research*, 1994, 13(3), 240-271

61 **Erdmann, M.**, A configuration space friction cone, *IEEE/RSJ International Workshop on Robots and Systems IROS'91*, 1991, 455-460

62 **Elmaraghy, H. A.** and **Payanaleh, S.**, Contact Prediction and Reasoning for Compliant Robot Motions, *IEEE Transactions on Robotics and Automation*, 1989, 5(4), 533-538

63 **Kapur, D.** and **Mundy, J.L**, Geometric Reasoning, *The MIT Press*, 1989

64 **Luh, J.Y.S.** and **Krolak, R.J.**, A Mathematical Model for Mechanical Part Description, *Communication of the ACM*, 8(2), 125-129

65 **Qiao, H.**, Dalay, B. S., Parkin, R. M., 1995, Simulation and Experiments of Precise Robotic Peg-Hole Insertion Operations Without Force Sensors and RCC, *Submitted to 26th ISIR (International Symposium of Industry Robots)*

66 **Mason, M. T.**, Compliance and force control for computer controlled manipulators. *IEEE Transactions on System, Man, and Cybernetics*, 1981, SMC-11, 418-432.

67 **McCallion, H., Wong, P.C.** Some thoughts on the automatic assembly of a peg and a hole. *Industrial Robot*, 1975, 2(4), 141-146.

68 **Lozano-Perez, T., Mason, M. T., Taylor, R. H.** Automatic synthesis of fine

motion strategies. *1St International Symp. of Robotics Research*, 1983, 65-96.

69 **Erdmann, M.** Using backprojections for fine motion planning with uncertainty. *The International Journal of Robotics Research,* 1986, 5(1), 19-45.

70 **Donald, B. R.** Planning multi-step error detection and recovery strategies. *The International Journal of Robotics Research,* 1990, 9(1), 3-60.

71 **Erdmann, M.** and **Mason, M. T.** An exploration of sensorless manipulation. *IEEE Int. Conference on Robotics and Automation*, 1989, 1569-1574.

72 **Peshkin, M.A.** and **Sanderson, A.C.**, Planning Sensorless Robot Manipulation of Sliding Objects, *IEEE Conf. Rob. Auotm.*, 1986, 1107-1112

73 **Qiao, H., Dalay, B. S.** and **Parkin, R. M.**, 1993, Precise Robotic Chamferless Peg-Hole Insertion Operation without Force Sensors and RCC, *Journal of IMechE, Proc. Journal of Mechanical Engineering, vol 208, 89-104*

74 **Qiao, H., Dalay, B. S.** and **Parkin, R. M.**, 1994, Robotic Peg-Hole Insertion: An Analysis of A Novel Strategy, *International Conference on Mechatronics, Co-sponsored by IFAC and ASME, Tampere, Finland, February, 15-18, 1994, 457-471*

75 **Qiao, H., Dalay, B. S.** and **Parkin, R. M.**, 1994, Analysis of the Robotic Peg Hole Insertion Operation, *Proceedings of the 1994 Engineering System Design and Analysis Conference, co-sponged by ASME , vol.8, part c. 823-836*

76 **Asada, H.** and **Hirai, S.** Towards a symbolic-level force feedback: recognition of assembly process states. *5th International Symp. of Robotics Research,* 1989, *241-346.*

77 **Asada, H.** and **Hirai, S.** Towards a symbolic-level force feedback recognition of assembly process states. *Proc. 5th Int. Symp. of Robotics Research, Tokyo, Soc. of Manufacturing Engineerings Illinois Inst of Technology Res. Inst.-Robot, Inst of*

AM, 1989, 341-346.

78 **Brooks, R. A.** Symbolic error analysis and robot planning. *The International Journal of Robotics Research,* 1982, 1(4), 29-68.

79 **Brost, R.C.,** Planning Robot Grasp in the Presence of Uncertainty. *CMU-RI-TR. 85-12, Computer Science Department, the Robotics Institute, Carneigie-Mellon University,* 1985

80 **Caine, M. E., Lozano-Perez, T., Seering, W. P.** Assembly strategies for chamferless parts. *Proc. IEEE Int. Conf. Robotics and Automation,* 1989, 472-477.

81 **Desai, R. S., Volz, R. A.** Identification and verification of termination condition in presence of sensor errors and geometric uncertainties. *IEEE International Conference on Robotics and Automation,* 1989, 2, 800-807.

82 **Donald, B. R.** and **Pai, D. K.** The motion of planar, compliantly connected rigid bodies in contact, with applications to automatic fastening. *The International Journal of Robotics Research,* 1993, 12(4), 307-337.

83 **Donald, B.R.** and **Jennings, J.,** Constrctive recognizability for task-direction robot programming, *Robotics and Autonomous Systems,* 1992, 9, 41-74

84 **Erdmann, M.A.,** On Motion Planning with Uncertainty, *AI-TR-810,* 1984

85 **John C.,** On Compatibility for Fine Motion Plans, *IEEE Conf. Rob. Autom,* 1989, 177-182

86 **Juan, J.** and **Paul, R.P.,** Automatic Programming of Fine-Motion for Assembly, *IEEE Int. Conf. Rob. Autom.,* 1986, 1582-1587

87 **Laugier, C.** Planning fine motion strategies by reasoning in the contact space. *IEEE International Conference on Robotics and Automation,* 1981, 653-659.

88 **Lozano-Perez, T.** The design of a mechanical system. *Reprinted in Winston,P.H., and Brown,R.H. eds. 1979. Artificial Intelligence: An MIT Perspective. MIT Press.*

89 **Mason, M. T.** Compliant motion. *Robot Motion, Planning and Control,* 1988, 305-322.

90 **Merlet, J. P.** A new method for inserting a peg in a hole using a robot. *4th Int. Conf. On Assembly Automation, Japan Society of Precision Engineering,* 1983, 400-403.

91 **Jain, A.** and **Donath, M.** Knowledge representation system for robot-based automated assembly. *ASME, Journal of Dynamic Systems, Measurement, and Control,* 1989, **111**, 462-469.

92 **Pai, D. K.** and **Leu, M. C.** Uncertainty and compliance of robot manipulators with applications to task feasibility. *The International Journal of Robotics Research,* 1991, **10**(3), 200-214.

93 **Paul, R. P. C.** and **Shimano, B.** Compliance and control. *Proceedings of the 1976 Joint Automatic Control Conference,* 1976, 694-699.

94 **Peshkin, M.A.** and **Sanderson, A.C.,** The motion of a Pushed, Sliding Object, *CMU-RI-TR-83-18, The Robotics Institute, Carnegie-Mellon University,* 1985

95 **Qiao, H., Dalay, B. S.** and **Parkin, R. M.,** 1994, Fine Motion Strategies for the Assembly Operations, *Accepted by Journal of IMechE, Proc. Journal of Mechanical Engineering*

96 **Qiao, H., Dalay, B. S.** and **Parkin, R. M.,** 1995, Fuzzy Logical Expression of the Signals From the Force Sensor in Robotic Peg-Hole Insertion Operation, *Accepted by ISMCR'95 (International Symposium on Measurement and Control in Robotics)*

97 **Sawada, C., Ishikawa, H., Kawase, K., Takata, M.** Specification and generation of a motion path for compliant motion. *IEEE International Conference on Robotics and Automation,* 1989, 808-815.

98 **Schneider, S. A., Robert, H.** and **Cannon, J.** Experimental object-level strategic control with cooperating manipulators. *The International Journal of Robotics Research,* 1993, **12**(4), 338-350.

99 **Taylor, R. H.** The synthesis of manipulator control programs from task-level specifications. *Stanford Artificial Intelligence Laboratory,* 1976, AIM-282.

100 **Turner, J. U., Subramaniam, S.** and **Gupta, S.** Constraint representation and reduction in assembly modelling and analysis. *IEEE Transaction on Robotics and Automation,* 1992, 8(6), 741-750.

APPENDIX 1

THE RANGE OF PROJECTION OF (O_p) IN THE NEW AREA

Since the initial state range of the projection of O_p on $X_h O_h Y_h$ is a circle with radius of ε_1 (see Fig. 46),

$$(O_h O_p)^2_{hx1} + (O_h O_p)^2_{hy1} \leq \epsilon_1^2 \tag{191}$$

then the second state range is also a circle with the same radius, but different locations:

$$[(O_h O_p)_{hx2} - \Delta X_{h2}]^2 + [(O_h O_p)_{hy2} - \Delta Y_{h2} - L_g \sin\Delta\theta_{hx2}]^2 \leq \epsilon_2^2 \tag{192}$$
$$\epsilon_2 = \epsilon_1$$

The location of O_p in the second state, shown in Fig. 49, must satisfy the quadrant identified in Fig. 124:

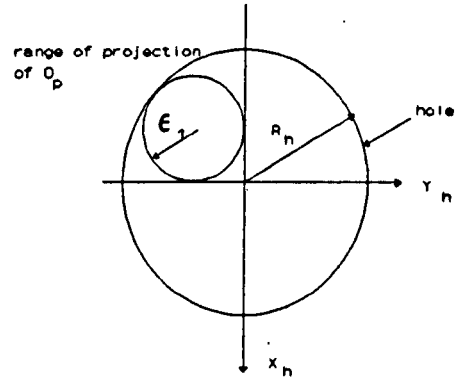

Fig. 124 Actual maximum range of O_p in the second state

So the maximum value of ε_2, is unchanged from the first state and, is related to the radius of the hole:

$$\epsilon_{2m} = \epsilon_{1m} = \frac{R_h}{\sqrt{2}+1} \tag{193}$$

APPENDIX 2

PROJECTION OF RANGE OF (O_p) WITH TWO CONTACT POINTS

The projections of the end-surface of the peg and the upper-surface surrounding the hole with an angle of θ_3 can be expressed as in Fig. 125:

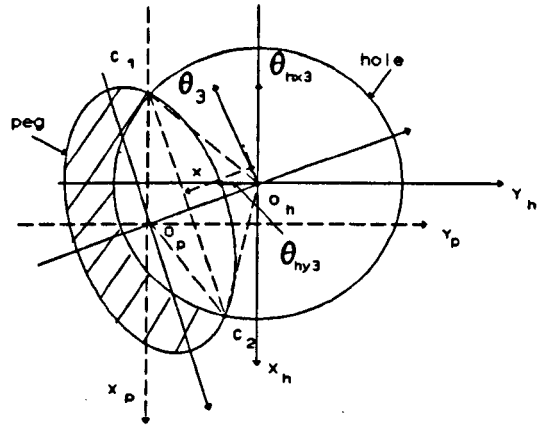

Fig. 125 Projections of contact surfaces with two point contact

where

(1) $\alpha_{\theta 3}$ is the angle between X_h axis and angle θ_3, which is considered as a vector here,

$$\alpha_{\theta 3} = \arctan\frac{\theta_{hy3}}{\theta_{hx3}} \tag{194}$$

The magnitude of the angle θ_3 is

$$|\theta_3| = \sqrt{\theta_{hx3}^2+\theta_{hy3}^2} \tag{195}$$

and x is the distance between O_h and line segment C_1C_2

(2) The projection of the end-surface of the peg is a ellipse, where the major axis is along the direction of θ with length of $2R_p$, and the length of the minor axis is $2R_p \cos|\theta_3|$.

(3) The key feature of the two-contact point state is that, the minor axis of the ellipse must pass through the upper-surface centre of the hole.

This conclusion can be explained as follows. Both of C_1 and C_2 are on $X_hO_hY_h$ plane, so (C_1C_2) is parallel to the plane $X_hO_hY_h$. (C_1C_2) is parallel to the major axis of the ellipse and C_1 and C_2 are symmetric about the minor axis of the ellipse. On the other hand, C_1 and C_2 are on the circle of the hole, so they are also symmetric about one radius of the hole. As a result, the minor axis of the ellipse coincides with a radius of the hole.

(4) If the distance between the line joining C_1, C_2 and O_h is defined as x, then:

$$\begin{aligned}(O_hO_p)_{hx3} &= [x\cos|\theta_3| + x]\sin(\arctan\frac{\theta_{hy3}}{\theta_{hx3}}) \\ (O_hO_p)_{hy3} &= [x\cos|\theta_3| + x]\cos(\arctan\frac{\theta_{hy3}}{\theta_{hx3}})\end{aligned} \tag{196}$$

Expressing these as a ratio:

$$\frac{(O_hO_p)_{hx3}}{(O_hO_p)_{hy3}} = \frac{1}{\tan(\arctan\frac{\theta_{hx3}}{\theta_{hy3}})} = \frac{\theta_{hy3}}{\theta_{hx3}} \tag{197}$$

then the range for the deviation of the centre of end-surface of the peg can be expressed as follows:

$$\begin{aligned}(O_hO_p)_{hx3} &= \tan(\frac{\theta_{hy3}}{\theta_{hx3}})(O_hO_p)_{hy3} = \tan\alpha_{\theta 3}(O_hO_p)_{hy3} \\ [(O_hO_p)_{hy3} - \Delta Y_{h2} - L_g\sin\Delta\theta_{hx2}]^2 &+ [(O_hO_p)_{hx3}]^2 \le \epsilon_1^2\end{aligned} \tag{198}$$

APPENDIX 3

GEOMETRY OF THE PEG-HOLE CONFIGURATION WITH THREE CONTACT POINTS BEFORE INSERTION AND WITH TWO CONTACT POINTS AFTER THE INSERTION OPERATION

(a) For the three contact point phase before the insertion starts, the general configuration can be presented as in Fig. 126.

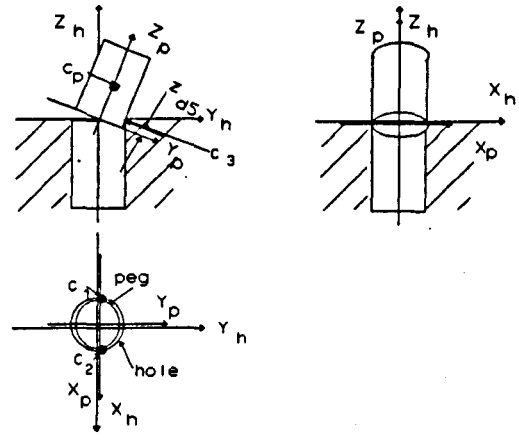

Fig. 126 Three point contact phase

where c_p is the centre of the peg, and z_{d5} is the distance between the side contact point to the end-surface of the peg. The locations of the contact points and the centre of the peg must be the functions of the angle θ_{hx5} as follows:

$$\begin{aligned} \sqrt{(R_p)^2 - (C_1)^2_{py5}} &= \sqrt{(R_h)^2 - (C_1)^2_{hy5}} \\ (-(C_1)_{hy5} + R_h)\cos\theta_{hx5} &= (-(C_1)_{py5} + R_p) \\ z_{d5} &= (-(C_1)_{hy5} + R_h)\sin|\theta_{hx5}| \end{aligned} \qquad (199)$$

From Equ. 199, these equations can be obtained:

$$\frac{R_h + (C_1)_{hy5}}{R_p + (C_1)_{py5}} = \frac{R_p - (C_1)_{py5}}{R_h - (C_1)_{hy5}} \qquad (200)$$

and

$$\frac{(C_1)_{hy5} + R_h}{(C_1)_{py5} + R_p} = \cos\theta_{hx5} \tag{201}$$

Combining Equ. 198, 199 and 200, 201, it can be shown that:

$$z_{d5} = -\frac{2R_h - 2R_p\cos\theta_{hx5}}{\sin\theta_{hx5}} \tag{202}$$

so

$$\begin{aligned}(O_hO_p)_{hy4} &= R_h + z_{d5}\sin\theta_{hx5} - R_p\cos\theta_{hx5} \\ &= -R_h + R_p\cos\theta_{hx5}\end{aligned} \tag{203}$$

(b) After $|\theta_{hx5}|$ is smaller than θ_{min} which is defined as in Fig. 127.

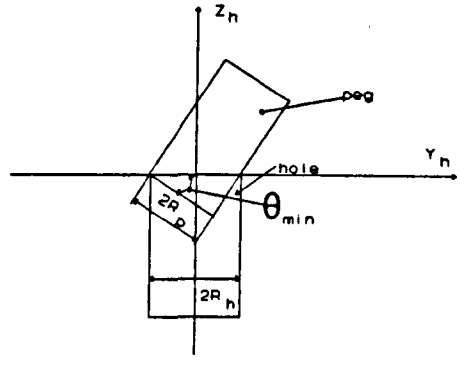

Fig. 127 θ_{min} and the start of insertion

$$\theta_{min} = \arccos(\frac{R_p}{R_h}) \tag{204}$$

the insertion operation starts. Then the basic positional relationships can be presented as follows (C_1 and C_2 coincide with each other):

$$\begin{aligned}2R_p\cos\theta_{hx5} - z_{d5}\sin\theta_{hx5} &= 2R_h \\ (c_p)_{pz5} &= -R_p\sin\theta_{hx5} + (\frac{1}{2}L_g - z_{d5})\cos\theta_{hx5} \\ (c_p)_{py5} &= R_h + R_p\cos\theta_{hx5} - (\frac{1}{2}L_g - z_{d5})\sin\theta_{hx5}\end{aligned} \tag{205}$$

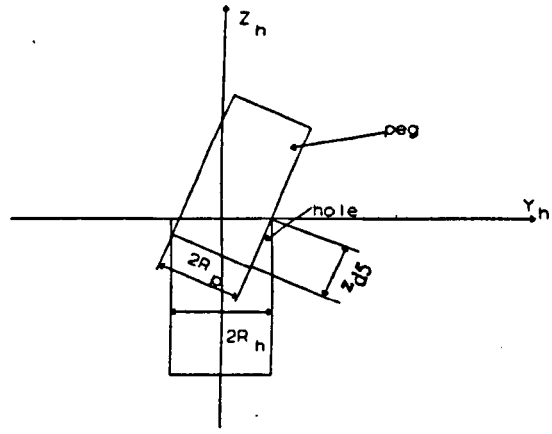

Fig. 128 Peg-hole configuration when
$|\theta_{hx5}| < |\theta_{min}|$

The relationship between the angle θ_{hx5} and z_{d5} remains the same before and after the peg enters the hole if it touches the hole with both end-surface and side-surface (see Fig. 128) which is same as Equ. 233. Similarly, the relationships between $(c_p)_{hy5}$ and θ_{hx5} and between $(c_p)_{hz5}$ and θ_{hx5} are also kept the same.

APPENDIX 4

FORCES ANALYSIS DURING THE ADJUSTMENT AND INSERTION WHEN THE PEG AND HOLE HAVE THREE CONTACT POINTS

The forces acting on the peg during three point contact can be presented as in Fig. 129.

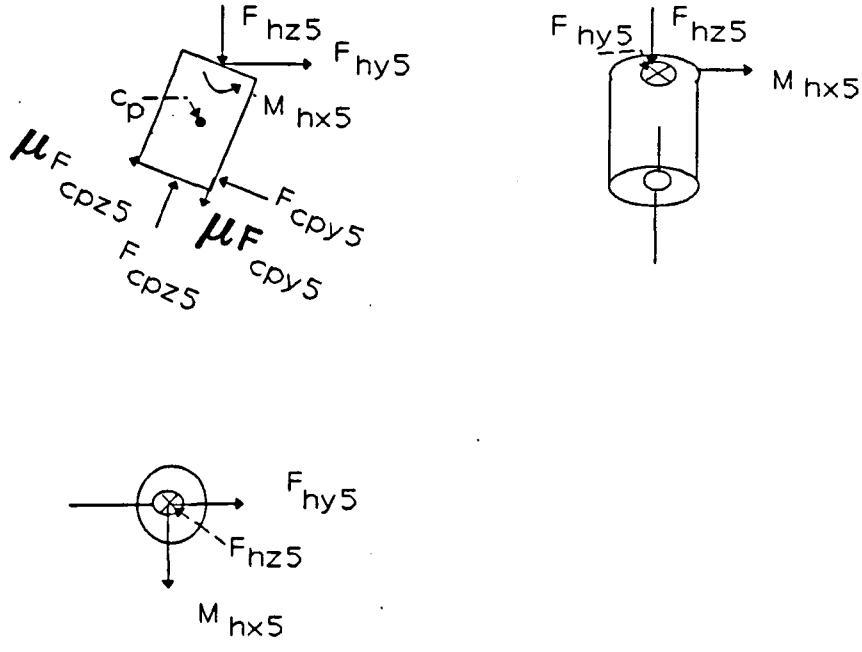

Fig. 129 Forces acting on the peg with three point contact

The equations can be presented as follows:

$$|F_{hy5}| - |F_{cpy5}|\cos\theta_{hx5} - \mu|F_{cpy5}|\sin|\theta_{hx5}| - \mu|F_{cpz5}|\cos\theta_{hx5} + |F_{cpz5}|\sin|\theta_{hx5}| = ma_{hy5}$$

$$-|F_{hz5}| + |F_{cpy5}|\sin|\theta_{hx5}| - \mu|F_{cpy5}|\cos\theta_{hx5} + |F_{cpz5}|\cos\theta_{hx5} - \mu|F_{cpz5}|\sin|\theta_{hx5}| = ma_{hz5}$$

$$M_{hx5} - |F_{cpy5}|(L_g - z_{d5}) - \mu|F_{cpy5}|R_p - |F_{cpz5}||(C_1)_{py5}| - \mu|F_{cpz5}|L_g = I\alpha_{hx5} \quad (206)$$

M_{hx5} must be big enough to rotate the peg. It should be noted that the directions of

If the peg can be controlled to touch the hole with three contact points before insertion and with two contact points after insertion when $|\theta_{hx5}|$ decreases, the assembly operation can be achieved. The way to ensure these touch is to make F_{cpy5} and F_{cpz5} positive in the specified direction with assumption that $a_{hy5} = a_{hz5} = 0$. Due to the fact that in this case,

$$\begin{aligned} \sin|\theta_{hx5}| &\approx 0 \\ \cos|\theta_{hx5}| &\approx 1 \end{aligned} \tag{207}$$

The contact forces can be approximated as follows:

$$\begin{aligned} |F_{cpz5}| &= \frac{|F_{hz5}| + |F_{hy5}|\mu}{1 + \mu^2} \\ |F_{cpy5}| &= \frac{|F_{hy5}| - |F_{hz5}|\mu}{1 + \mu^2} \end{aligned} \tag{208}$$

To make both of the contact forces positive, the forces F_{hy5} and F_{hz5} must satisfy:

$$|F_{hy5}| > |F_{hz5}|\mu \tag{209}$$

Here F_{hz5} is a designable value. The M_{hx5} must satisfy the following condition to rotate the peg during the three point contact state:

$$M_{hx5} \geq \frac{1}{1+\mu^2}[|F_{hy5}|(L_g + 2\mu R_p + \mu^2 L_g) + |F_{hz5}|(R_p - \mu^2 R_p)] \tag{210}$$

These conclusions can be reached as in Fig. 130:

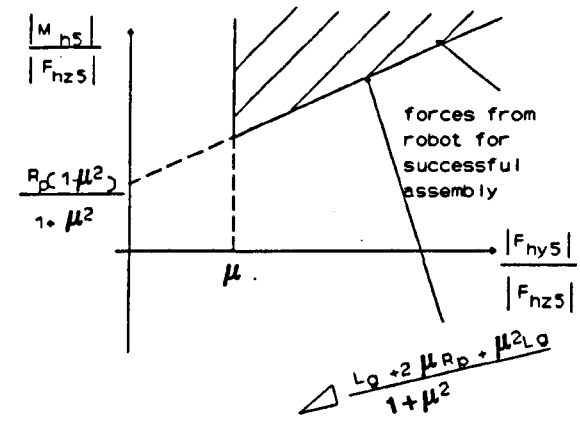

Fig. 130 Forces applied to the peg from the robot during three point contact phase

After the peg inserts the hole, the dynamical situation can be presented as in Fig. 131.

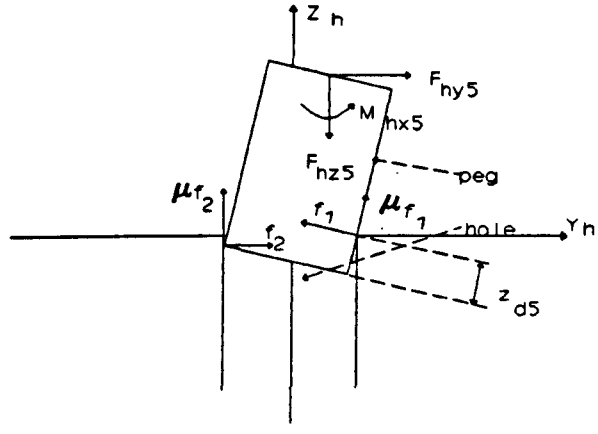

Fig. 131 Forces acting on the peg after the peg inserts the hole

where μ_1 and μ_2 are two contact forces between the peg and hole after the peg enters the hole. The dynamic equations can be presented as follows:

$$\begin{aligned} |F_{hy5}| &= |f_1| - |f_2| \\ |F_{hy5}| &= \mu(|f_1| + |f_2|) \\ |M_{hx5}| &= |f_1|(L_g - z_{d5}) - \mu|f_1|R_p - |f_2|L_g + \mu|f_2|R_p \end{aligned} \tag{211}$$

From this, the two contact forces between the peg and hole can be obtained and

presented as follows:

$$|f_1| = \frac{\mu|F_{hy5}| + |F_{hz5}|}{2\mu} \tag{212}$$

and

$$|f_2| = \frac{|F_{hz5}| - \mu|F_{hy5}|}{2\mu} \tag{213}$$

To make the contact forces positive, F_{hy5} and F_{hz5} must satisfy that:

$$|F_{hy5}| < \frac{|F_{hz5}|}{\mu} \tag{214}$$

To rotate the peg, the moment around the X_h axis must satisfy:

$$|M_{hx5}| = |F_{hy5}|\frac{2L_g - z_{d5} - 2\mu R_p}{2} - |F_{hz5}|\frac{z_{d5}}{2\mu} \tag{215}$$

If the forces and moments applied to the peg are kept as constants before and after insertion, they must be in the range illustrated in Fig. 133.

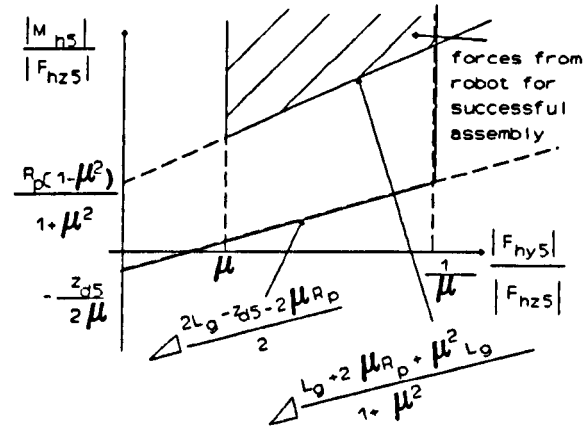

Fig. 133 Forces from the robot for the insertion adjustment

APPENDIX 5

THE FORWARD PROJECTION OF THE PEG WHEN $M_{SY}^{*}=0$

If O_p is on the Y_h axis and the direction of θ is along the X_h axis, the peg-hole system is with two contact points. The projection of the centre of these two contact points is along Y_p axis. In this case the projections of the end-surface of the peg and upper-surface of the hole can be presented as follows:

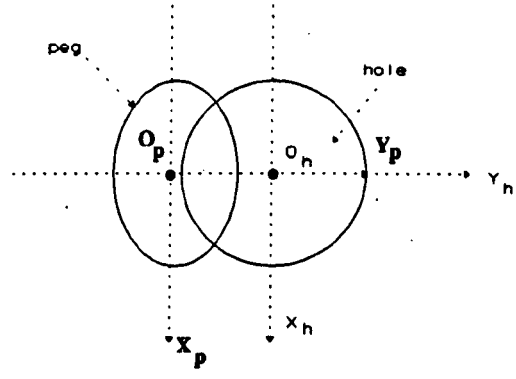

Fig. 133 Projections of contact surfaces on $X_hO_hY_h$ plane when O_p is along Y_h axis and θ is along X_h axis

At this time, the measured moment is along the X_h axis. If the moment around the force sensor is along the X_h axis and $|\theta_{hx}| >> |\theta_{hy}|$, the possible projection of O_p on $X_hO_hY_h$ plane can be presented as follows:

$$\pi\{F_s^{*}|M_s^{*}=M_{hx}\} \cap \pi(|\theta_{hx}| < |\theta_{hy}|) = \{O_p,\theta|(O_hO_p)_{hx} = 0,\ \pi/2 > |\theta_{hx}| > |\theta_{hy}| \cup \pi/2 > |\theta_{hx}| > |\theta_{hy}|\} \tag{216}$$

where

$$\{O_p,\theta|(|(O_hO_p|>R_h),\ \frac{\pi}{2} > |\theta_{hx}| > |\theta_{hy}|\} = \{O_p,\theta|\textit{the lowwest point the peg is out} \tag{217}$$

If the projection of initial area for the centre of the end-surface of the peg on the $X_hO_hY_h$ plane is in a circle:

$$R_n = \{O_p,\theta|\ |O_hO_p| < \frac{R_h}{2}\} \tag{218}$$

then the forward projection with the movement R_h /2 along the -X_h axis can be presented as follows:

$$R_{n-1} = F_{\theta,n}(R_n) = \{O_p,\theta|((O_p)_{hx})^2 + ((O_p)_{hy} + \frac{1}{2}R_h)^2 \le R_h^2\} \tag{219}$$

In this case, the lowest point of the peg is in the hole, i.e.

$$R_{n-1} = F_{\theta,n}(R_n) = \{O_p,\theta|(O_{p_{hx}})^2 + (O_{p_{hy}} + \frac{1}{2}R_h)^2 \le R_h^2, \textit{the lowwest point of the peg is below the top surface of the hole}\}$$

so,

$$\pi\{F_s^*|M_s^* = M_{sx}\} \cap \{O_p,\theta|\frac{\pi}{2} > |\theta_{hx}| > |\theta_{hy}|\} \cap R_{n-1} = \{O_p,\theta|(O_hO_p)_{hx} = 0, \frac{\pi}{2} > |\theta_{hx}| > |\theta_{hy}|\} \tag{221}$$

furthermore,

$$R_{n-1} \cap \pi\{F_s^*|M_s^* = M_{sx}\} = \{O_p,\theta|(O_hO_p)_{hx} = 0, \frac{\pi}{2} > |\theta_{hx}| > |\theta_{hy}|\} \tag{222}$$

That means that combined with the range of the forward projection of the initial area, when M^{*s} is only along the X_h axis, O_p touches Y_h axis.

PAGE/PAGES EXCLUDED UNDER INSTRUCTION FROM THE UNIVERSITY